

Project No.: GOCE-CT-2003-505488

LESSLOSS

**Risk Mitigation for Earthquakes and Landslides
Integrated Project**

Sixth Framework Programme
Priority 1.1.6.3 Global Change and Ecosystems

Deliverable Report

Deliverable 57 – Methodology of analysis for underground structures in soft soils

Sub-Project 7 – Techniques and methods for vulnerability reduction

Deliverable/Task Leader: IST (n°19)

Revision: Draft/Final

February, 2006

Project co-funded by the European Commission within the Sixth Framework Programme (2002-2006)	
Dissemination Level	
PU	Public
PP	Restricted to other programme participants (including the Commission Services)

RE	Restricted to a group specified by the consortium (including the Commission Services)	
CO	Confidential, only for members of the consortium (including the Commission Services)	

PREFACE

TABLE OF CONTENTS

PREFACE.....	i
TABLE OF CONTENTS	iii
LIST OF TABLES	vii
LIST OF FIGURES.....	ix
LIST OF SYMBOLS AND ABBREVIATIONS.....	xiii
1. INTRODUCTION.....	1
2. SOIL STRUCTURE INTERACTION	3
2.1 INTRODUCTION.....	3
2.2 LESSONS FROM PAST EARTHQUAKES.....	3
2.3 QUALITATIVE ANALYSIS OF SEISMIC VULNERABILITY.....	5
2.4 USUAL ANALYSIS METHODOLOGY	7
2.5 ANALYSIS OF RESULTS.....	17
2.5.1 Model with thick soil cover.....	17
2.5.2 Model with thin soil cover	24
2.5.3 Comparisons of results. Influence of the stiffness of the structure	27
3. DESCRIPTION OF THE ANALYSIS PROGRAM.....	35
3.1 OBJECTIVES.....	35
3.2 METHODOLOGY.....	35
3.3 INPUT DATA.....	36

3.3.1	Nodes	36
3.3.2	Cross-sections	37
3.3.3	Beams	38
3.3.4	Concentrated loads.....	39
3.3.5	Distributed loads	39
3.3.6	Imposed displacements	40
3.4	EVALUATION OF THE SECANT STIFFNESS MATRIX ANF FIXED END FORCES AND MOMENTS	40
3.4.1	Section level.....	40
3.5	OUTPUT	59
4.	SEISMIC CONCEPTION AND METHODOLOGY OF ANALYSIS	63
4.1	INTRODUCTION.....	63
4.2	BEHAVIOUR OF REINFORCED CONCRETE ELEMENTS UNDER IMPOSED DISPLACEMENTS....	64
4.2.1	Redefinition of Basic Concepts	64
4.2.2	Factors That Influence Ductility	76
4.3	CONCEPTION.....	95
4.4	DESIGN METHODOLOGY.....	102
5.	PRACTICAL APPLICATION EXAMPLE	108
5.1	STRUCTURE DESIGNED ACCORDING TO CURRENT CODE CONCEPTS	109
5.2	STRUCTURE DESIGNED ACCORDING TO THE PROPOSED METHODOLOGY.....	113
5.2.1	Choice of deformation mechanism.....	113
5.2.2	Design of reinforcement	116
5.2.3	Results	120
6.	SUMMARY AND CONCLUSIONS	122

REFERENCES.....123

LIST OF TABLES

Table 2.1. Moments at the middle of the arch, at top of the columns and relative horizontal displacements between top and bottom of the structure.....	21
Table 2.2 – Ratio between horizontal displacement in the structure and in the free-field	31
Table 2.3 – Frequencies and horizontal displacements for the column of soil and models 1sl and 1sl -	31
Table 3.1. Coefficients for the decomposition of the rational function.....	46
Table 4.1. Material properties	69
Table 4.2. Amounts of tensile reinforcement	70
Table 4.3. Results at yielding and rupture.....	71
Table 4.4. Maximum compressive strains at the top and base sections ($\times 10^{-3}$).....	75
Table 4.5. T section reinforcement.....	78
Table 4.6. Results for T section at yielding and rupture.....	78
Table 4.7. Results for enlarged rectangular and circular sections at yielding and rupture.....	81
Table 4.8. Results for square section with web reinforcement at yielding and rupture.....	84
Table 4.9. Results for the T section with web reinforcement at yielding and rupture	86
Table 4.10. Results with high axial force at yielding and rupture.....	88
Table 4.11. Curvatures at the base section with and without concrete tensile strength [$/1000\text{m}$]. (section A).....	90
Table 4.12. Curvatures at the base section with and without concrete tensile strength [$/1000\text{m}$]. (section B).....	90
Table 4.13. Maximum curvature at the base section (section A, $\delta=2.5\delta_y$)	92

Table 4.14. Maximum curvature demand at the base section (section A, $\delta=6\delta_0$)..... 93

LIST OF FIGURES

Figure 2.1. Collapse of the central columns of Dakai tube station, Kobe, Japan.....	4
Figure 2.2. Scheme of collapse and settlement over Dakai tube station, Kobe, Japan	4
Figure 2.3. Eventual three-dimensional soil flow near the extremities of the structure.....	5
Figure 2.4. Schematic identification of flexible and rigid alignments	6
Figure 2.5. Representation of soil deformations along rigid alignments	7
Figure 2.6. Design of tube station 1.....	12
Figure 2.7 – Soil/structure models	14
Figure 2.8 – Example of soil constitutive relationships [Ishibashi, I. & Zhang, X., 1993]	15
Figure 2.9 – Acceleration response spectrum for $\xi=5\%$ and soil type 1.....	16
Figure 2.10 – Stepped response spectrum to account for different viscous damping coefficients (ξ)	17
Figure 2.11. Configuration of modes 1, 2, 3, 4, 7, 12 and 21and respective frequencies and mass participation factors for model 1	20
Figure 2.12 – Cantilever model.....	22
Figure 2.13 – Soil only modes of vibration in cantilever model.....	22
Figure 2.14. Horizontal displacement field for model 1	24
Figure 2.15. Configuration, frequencies and mass participation factors for the first three and 5 th and 12 th modes for model 2.....	25
Figure 2.16. Horizontal displacement field for model 2	27
Figure 2.17. Horizontal displacement field for altered model 2.....	28

Figure 2.18. Evaluation of the structure distortional stiffness	29
Figure 2.19. Horizontal displacement fields for models 1 ^r and 1.....	30
Figure 2.20. Horizontal displacement fields for models 2 ^r , and 2.....	30
Figure 3.1. Example input data for nodes.....	37
Figure 3.2. Input window to define section geometry	38
Figure 3.3. Graphic visualisation of constitutive relationships.....	38
Figure 3.4 – Example input data for beams.....	39
Figure 3.5. Example input data for concentrated loads.....	39
Figure 3.6. Example input data for distributed loads.....	40
Figure 3.7. Example input data for imposed displacements	40
Figure 3.8. Secant stiffness	41
Figure 3.9. Cross sections.....	44
Figure 3.10 – Part of the cross section	45
Figure 3.11 – Linear bar finite element.....	47
Figure 3.12 – Internal forces and moments due to distributed loads	50
Figure 3.13. Distributed loads	51
Figure 3.14. Linear bar finite element, auxiliary bar and cross section (cinematic variables).....	52
Figure 3.15 – Linear bar finite element, auxiliary bar and cross section (static variables).....	53
Figure 3.16. Fixed end forces and moments.....	59
Figure 3.17. Example structure	60
Figure 3.18. Example of the output of the programme.....	61
Figure 4.1. Schematic representation of a built-in column subjected to imposed horizontal displacement.....	65
Figure 4.2. Evaluation of strains and stresses.....	65

Figure 4.3. Example cross-sections.....	68
Figure 4.4. Constitutive relationships for steel and concrete	69
Figure 4.5. Qualitative difference between the constitutive relationships for plain and confined concrete (adapted from CEB, [1983])	69
Figure 4.6. Moment-curvature relationships for example sections	70
Figure 4.7. Variation of the yield curvature with the depth of the compressive zone.....	72
Figure 4.8. Schematic representation of change in the yield moment and yield curvature by increasing the flexural reinforcement.....	72
Figure 4.9. Trilinear stress-strain relationship for steel	74
Figure 4.10. Maximum cross-section compressive strains.....	75
Figure 4.11. Definition of T shaped cross-section.....	77
Figure 4.12. Moment curvature relationships for T shaped section	78
Figure 4.13. Enlarged rectangular and circular sections.....	81
Figure 4.14. Moment curvature relationships for the enlarged circular and rectangular sections	81
Figure 4.15. Square section with flexural reinforcement only in the web.....	83
Figure 4.16. Moment curvature relationships for the square section with web reinforcement	84
Figure 4.17. Definition of T shaped section with web reinforcement.	85
Figure 4.18. Moment curvature relationships for the T section with web reinforcement.....	86
Figure 4.19. Moment curvature relationships for compressed sections.....	88
Figure 4.20. Curvature diagrams for sections A considering the concrete tensile strength.....	90
Figure 4.21. Moment-curvature diagrams for columns with different steel hardening stiffness and $\sigma_u/\sigma_y=1.3$	92
Figure 4.22. Curvature diagrams for columns with different steel hardening stiffness.....	93
Figure 4.23. Curvature diagrams for columns with different steel hardening stiffness.....	94
Figure 4.24. Plan of tube station of variable width	97

Figure 4.25. Division of short beam in two adjacent beams.....	98
Figure 4.26. Restriction to column deformation due to stairs and potential consequences	99
Figure 4.27. Restriction to deformation of the structure due to non structural masonry wall and possible solution.....	100
Figure 4.28. Restriction to column deformation due to stiff filling material and possible solution	101
Figure 4.29. Imposed displacements on a ductile structure	105
Figure 5.1. Example underground structure	108
Figure 5.2. Horizontal displacement profiles.....	109
Figure 5.3. Reinforcement for maximum displacement according to Direct Design	112
Figure 5.4. Curvature diagrams at maximum displacement – code design [/1000m]	113
Figure 5.5. Example structure: global mechanisms	114
Figure 5.6. Mechanism with unavoidable hinges at intermediate locations of walls and columns .	115
Figure 5.7. Details of design according to the proposed methodology	118
Figure 5.8. Material constitutive relationships and moment-curvature diagrams at the column base section	119
Figure 5.9. Curvatures at maximum displacement - proposed methodology [/1000m].....	120

LIST OF SYMBOLS AND ABBREVIATIONS

G	= Shear modulus
ζ	= Damping ratio
γ	= Distortion
η	= Behaviour factor
a_g	= Peak ground acceleration
f	= Frequency
M_x, M_z	= Mass participation factors
r_d	= Ratio between free-field and structural displacement
k_x	= Spring stiffness in the x direction
K_y	= Spring stiffness in y direction
K_r	= Rotational stiffness
U_x	= x displacement
U_y	= y displacement
U_r	= Rotation
F_x	= Force in x direction
F_y	= Force in y direction
M	= Moment
ε_G	= Strain of the section centre of gravity
χ	= Curvature
N	= Axial force
σ	= Axial stress

V	= Shear force
ϵ	= Strain
$d_1, d_2, d_3, d_4, d_5, d_6$	= Finite element independent displacements
u, w	= Longitudinal and transverse displacements
φ_n, φ_w	= Shape functions
K_s	= Cross section secant stiffness matrix
K_e	= Element secant stiffness matrix
X_{FIX}	= Vector of fixed end forces and moments
P_N, P_T	= Distributed forces
A	= Cross section area
E	= Elasticity modulus
Δy	= Distance between local and auxiliary axis
ϵ_{su}	= Ultimate steel strain
ϵ_{cu}	= Ultimate concrete strain
h	= Height of cross section
ϵ_{sy}	= Steel yield strain
σ_{sy}	= Steel yield stress
ϵ_{cy}	= Concrete strain at maximum stress
f_{ct}	= Maximum tensile stress of concrete
f_c	= Maximum compressive stress of concrete
f_{cu}	= Concrete compressive stress at failure
A_a	= Area of tensile reinforcement
EI_{sec}	= Secant flexural stiffness
M_y	= Yield moment
M_u	= Ultimate moment
c	= Depth of the compressive zone

E_b	= Steel hardening stiffness
E_s	= Steel young's modulus
χ_y	= Yield curvature
χ_u	= Ultimate curvature
c_y	= depth of the compressive zone at yielding
c_u	= depth of the compressive zone at rupture
A_w	= Area of distributed reinforcement in the web
A_f	= Area of distributed reinforcement in the flange
L	= Column length
δ	= Imposed displacement
δ_y	= Yield displacement
PHZ	= Plastic hinge zone
λ	= Shear ratio
δ_{ed}	= Design displacement
δ_u	= Ultimate column displacement
H	= Height of example structure
q	= q-factor
γ_o	= overstrength factor
M_{Sd}	= Design bending moment
M_{Rd}	= Flexural capacity

1. INTRODUCTION

This report is deliverable n°57 of the LESSLOSS project, and is integrated in sub-project n° 7 “Techniques and methods for vulnerability reduction” under task 8 “Underground structures”, and was elaborated by IST.

The report fulfils the objectives set out for task 8 of the subproject “Techniques and methods for vulnerability reduction”, and is subdivided in six chapters.

Chapter 1, “Introduction”, describes the contents of the report.

In chapter 2, “Qualitative analysis of the seismic behaviour of large underground structures”, are presented the reasons to perform the work, already included in the contract, the scope of the work is delimited, and the soil structure interaction under earthquake actions is studied by means of the linear dynamic analysis of some cases. The relative importance of different vibration modes is identified and it is concluded that the effect of the most relevant modes can be considered equivalent to the imposition to the structure of a horizontal displacement field along the height.

Chapter 3, “Description of the analysis program”, describes the program PIER used to perform the physical and geometrical nonlinear static analysis that is performed in chapter 4. The program aims at studying the behaviour of reinforced concrete plane frames under sets of applied forces and displacements. The program allows the definition of constitutive relationships for steel and concrete defined by sets of polynomial equations to the third degree. Since the deformation capacity can only be exhausted after yielding of the flexural reinforcement, the program allows accounting for the sources of nonlinear flexural behaviour in order to estimate the deformation capacity of reinforced concrete plane frames.

Chapter 4 “Seismic conception and methodology of analysis” presents a design methodology and seismic conception criteria for large reinforced concrete underground structures in soft soils.

Chapter 5 “Design Example” presents a plan model of an underground structure with appropriate seismic conception, as described in chapter 4. It also illustrates the

application of the proposed methodology and a comparison of the differences to an alternative design based on the extrapolation of EC8 part I prescriptions for buildings.

Chapter 6 summarizes the main conclusions of this work.

2. SOIL STRUCTURE INTERACTION

2.1 INTRODUCTION

The analysis of damage induced by earthquakes in large underground reinforced concrete structures in the past shows that in general these structures are less sensitive to earthquake actions than structures that develop above ground level. [Gomes, 1999; Hashash et al, 2000]. In fact if the soil deformability is reduced, underground structures are subjected to almost rigid body motions, which induce little internal forces in the structures. Therefore, no damage or collapse is observed in these conditions. The above facts and reasoning have contributed to the little attention that has been paid to the study of the seismic behaviour of underground structures. Therefore it has been common practice, even in many earthquake prone areas, not to design underground structures to withstand earthquake effects.

2.2 LESSONS FROM PAST EARTHQUAKES

However, the reality, in particular the recent reality, shows that this type of structure can also be vulnerable to seismic actions. During the Hyogoken-Nanbu earthquake, which hit the town of Kobe in Japan in 1995, a total of 6 out of 21 underground stations suffered strong damage [Iwatate et al, 2000].

As an example, it is presented the case of Dakai tube station, which collapsed due to rupture of the central columns, as shown in figure 2.1. The collapse of the columns triggered the collapse of the top slab, giving rise to 2,0m settlements at the surface, as shown in figure 2.2.



Figure 2.1. Collapse of the central columns of Dakai tube station, Kobe, Japan

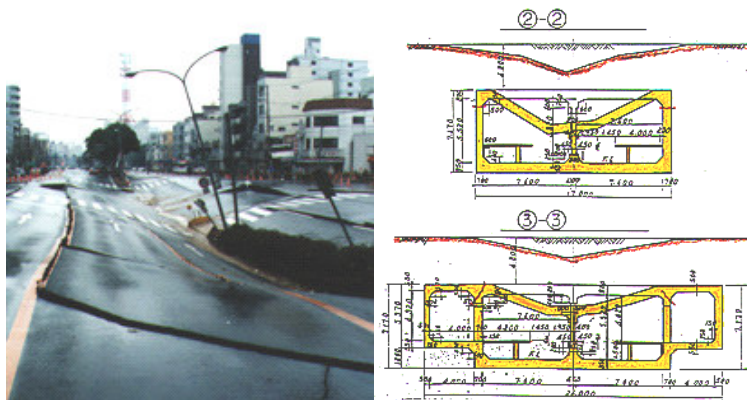


Figure 2.2. Scheme of collapse and settlement over Dakai tube station, Kobe, Japan

It should also be noted that in densely populated urban areas the collapse of underground tube stations may also trigger the collapse of neighbouring buildings if large soil movements take place. This would be the case if the collapse involves the perimeter walls, leading to the soil filling the previously empty volume occupied by the station.

It is therefore important to study the reasons for the collapse of underground structures when most cases of large underground structures show reduced seismic vulnerability.

2.3 QUALITATIVE ANALYSIS OF SEISMIC VULNERABILITY

Iwatate et al [2000], based on numerical studies and shake table tests of small scale models, attributed the cause of collapse of Dakai tube station to the distortion field imposed by the soil to the structure during the earthquake movement. It was also pointed out that the lack of ductility of the central columns also contributed to the collapse of several stations.

The configuration of the station in plan is similar to a rectangle 120m long and 17m wide in the narrowest zone and 26m in the largest zone (Yoshida et al, 1997). The perimeter walls are almost undeformable in their own plan, therefore with little capacity to accommodate significant relative displacements in this plan. However the available information is that collapse of the structure was not triggered by the collapse of the perimeter walls. This means that the stiffness of the structure in the longitudinal direction counteracts the displacements soil profile in the free-field, and may even lead to a three-dimensional soil flow in the vicinity of the extremities of the structure or lack of cinematic compatibility between soil and structure, as schematically represented in figure 2.3.

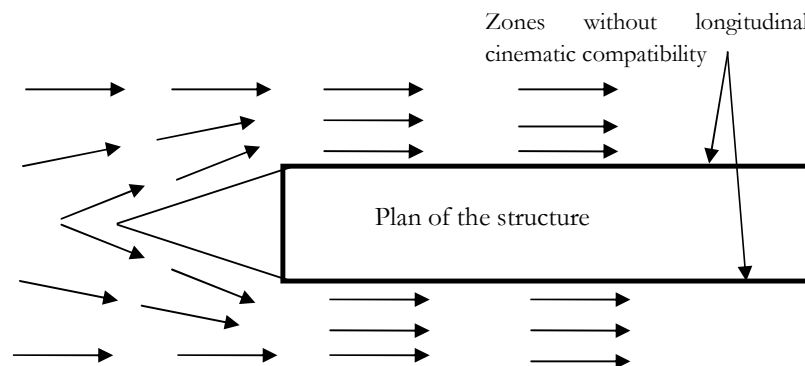


Figure 2.3. Eventual three-dimensional soil flow near the extremities of the structure

The collapse of the central columns of Dakai tube station occurred essentially due to deformations in the transversal direction of the station [Iwatate et al 2000], in particular in zones not near the extremities, where three-dimensional effects are not relevant and the structure tends to be more flexible than in the longitudinal direction.

In order to understand the observed behaviour two main situations regarding vertical cross sections of the global structure, to which correspond qualitatively different types of behaviour, can be identified:

- Rigid alignments – vertical cross sections of the global structure characterized by the proximity of very stiff structural elements parallel to the plan of the cross section (for instances perimeter walls in their own plan). This elements offer strong resistance to the soil inertia forces, therefore withstanding very small displacements in their own plan.
- Flexible alignments – vertical cross sections of the global structure located away from the zone of influence of the structural elements stiff in their own plan.

Figure 2.4 shows schematically the difference between flexible and rigid alignments.

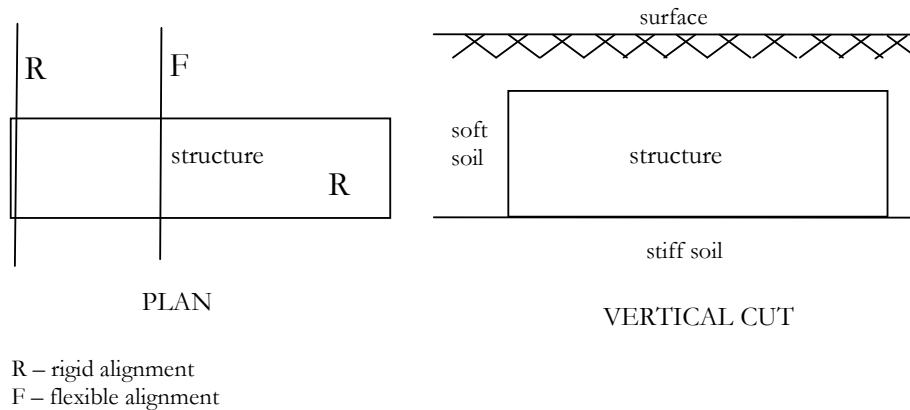


Figure 2.4. Schematic identification of flexible and rigid alignments

The dynamic behaviour of the soil/structure systems along flexible alignments is dominated by the soil inertia forces, which are dominant as compared to the inertia forces generated in the structure. The structure being flexible in these alignments does not oppose significant resistance to the soil deformations. Therefore there is cinematic compatibility in the vertical soil/structure interface and the structure is forced to deform along the height following the displacement field imposed by the soil on the interface. In the plan of rigid alignments the structure is stiff enough to do not follow the soil deformations in the free field, as represented in figure 2.5. This corresponds to the observed behaviour since the structure can not withstand those deformations but little or no damage is usually observed in those cases. Dakai tube station is an example, among others.

Dakai tube station was built in soft soils. In these soils the displacement soil profile along vertical lines in the free-field is large enough to exceed the structures deformation capacity. In stiff soils, the displacement profile in the free-field involves very little distortions along the height, which most structures accommodate without damage. This is the reason why underground structures are usually not sensitive to earthquake actions.

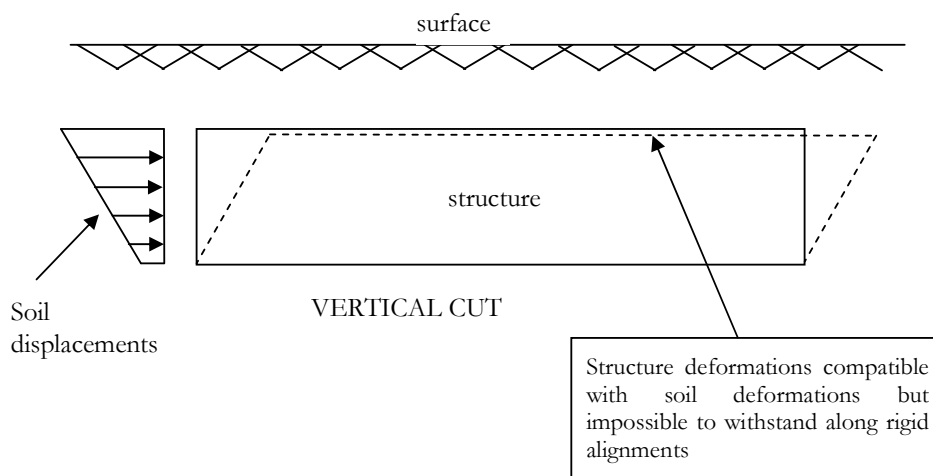


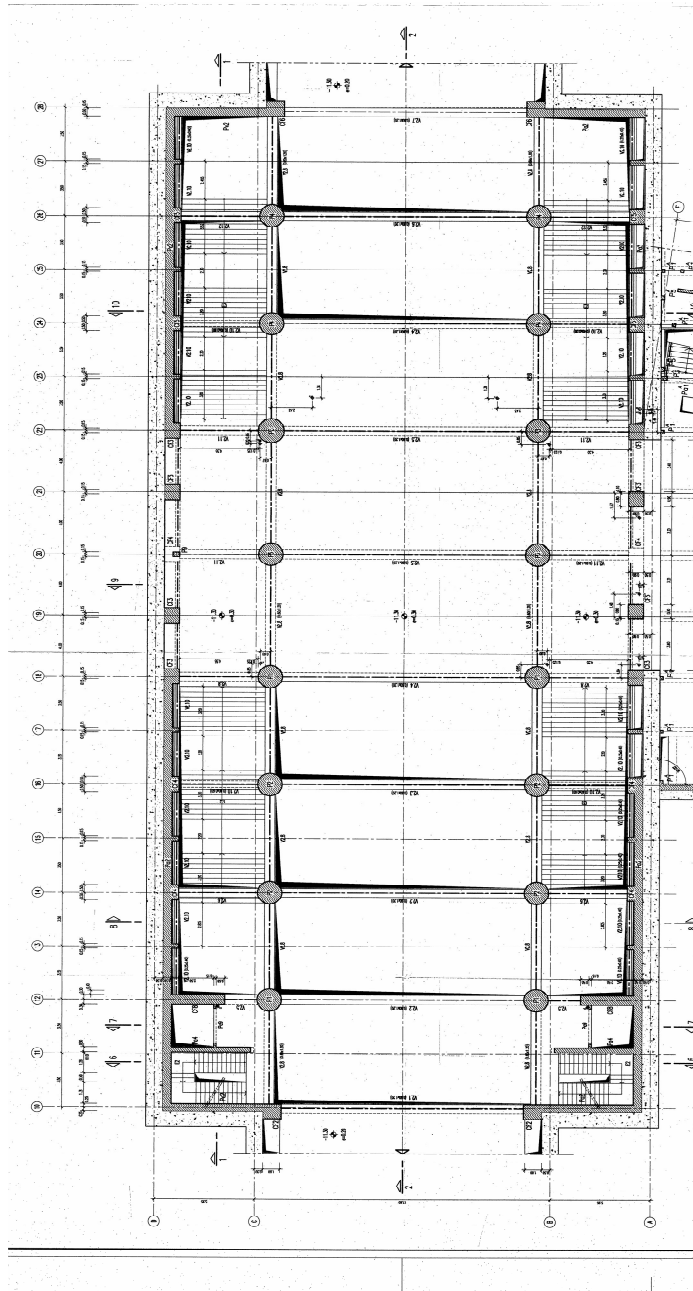
Figure 2.5. Representation of soil deformations along rigid alignments

The above explanation about the collapse of Dakai tube station also applies to the potential seismic behaviour of other underground structures with similar shape and dimensions in plan. Therefore, despite the fact that this work aimed essentially at the seismic analysis of underground tube stations in soft soils, it can also be applied to other large reinforced concrete underground structures with similar characteristics, such as car parks and other social and economic facilities.

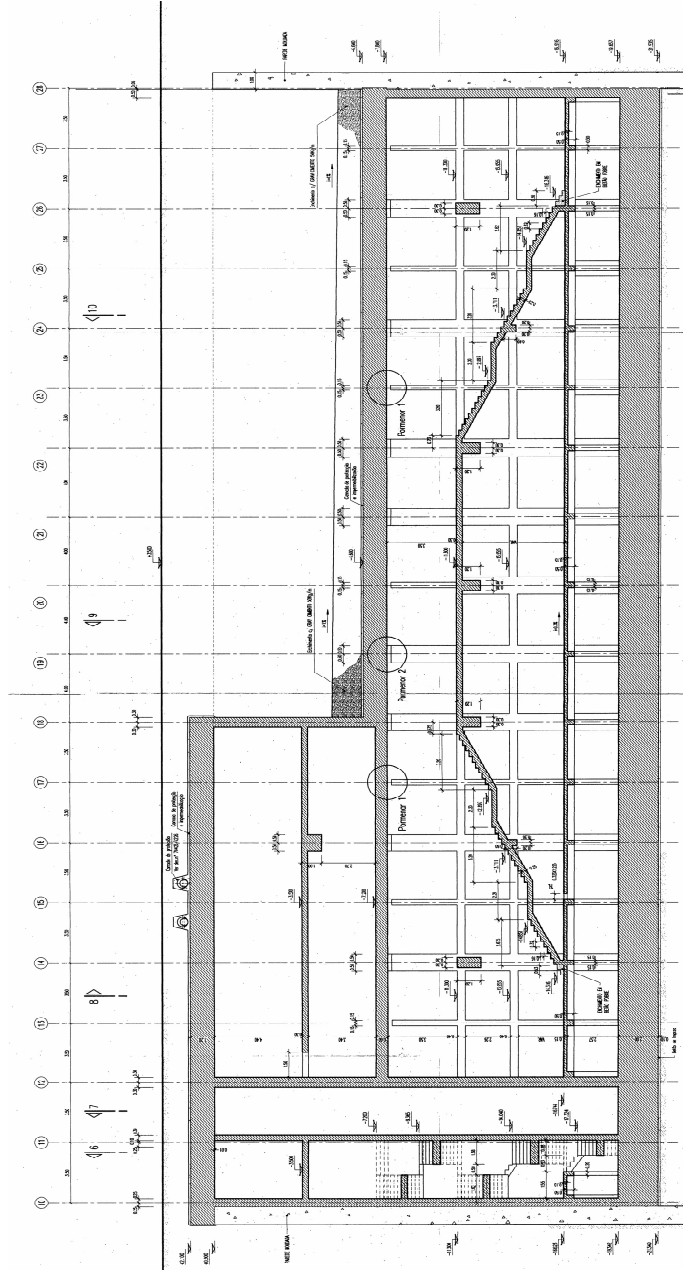
2.4 USUAL ANALYSIS METHODOLOGY

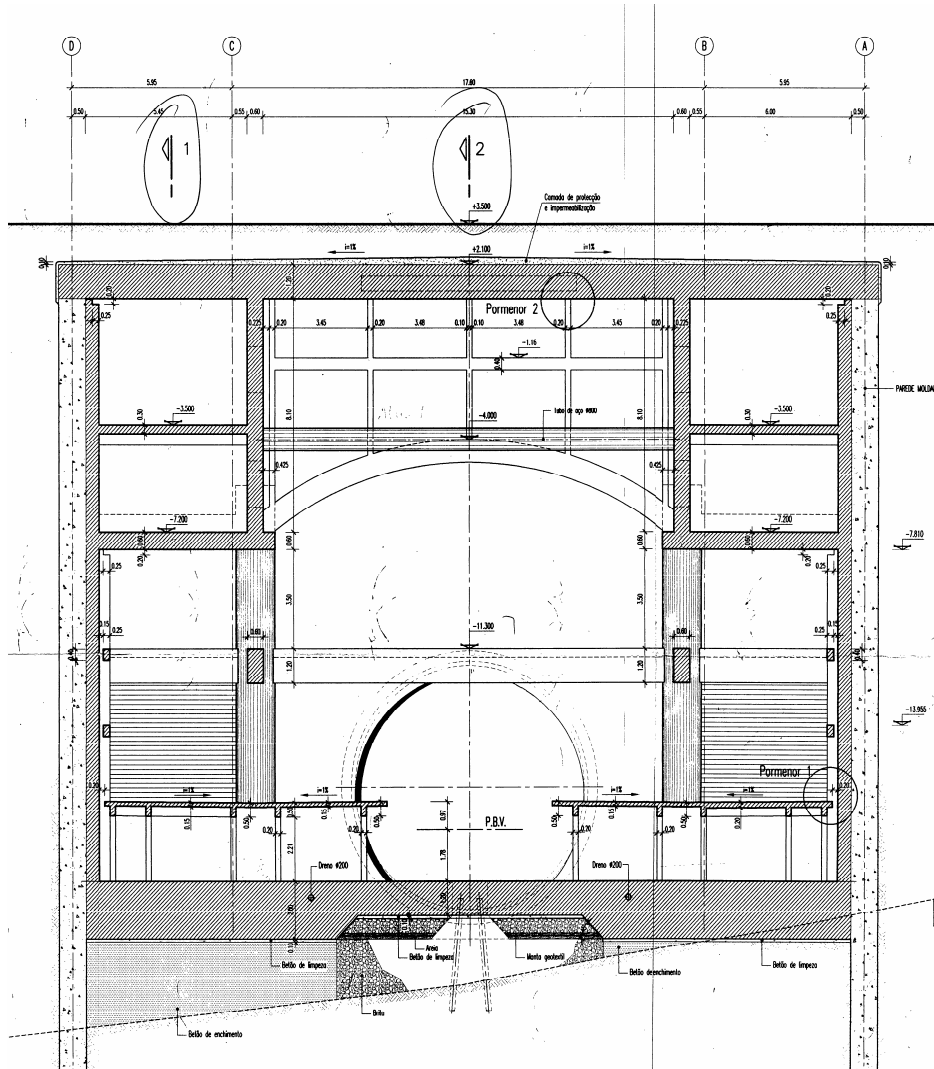
Figure 2.6 shows the plan, a longitudinal and two transversal cross-sections of the design of a tube station that will be used as an example. Usually in soft soils and urban areas the perimeter walls are vertical walls made with piles or built in slurry reinforced concrete walls. This derives of the lack of space due to the presence of neighbouring buildings and/or because it is the best constructive solution. This is due to the nature of the soils and/or the presence of the water associated to the need to isolate the interior of the

station during construction in order to avoid the water to go in. In the case the structure has no or little soil cover the top slab is flat. In the zone where there is a thick soil cover the top slab often comprises an arch in order to resist the vertical load partially by arch effect.

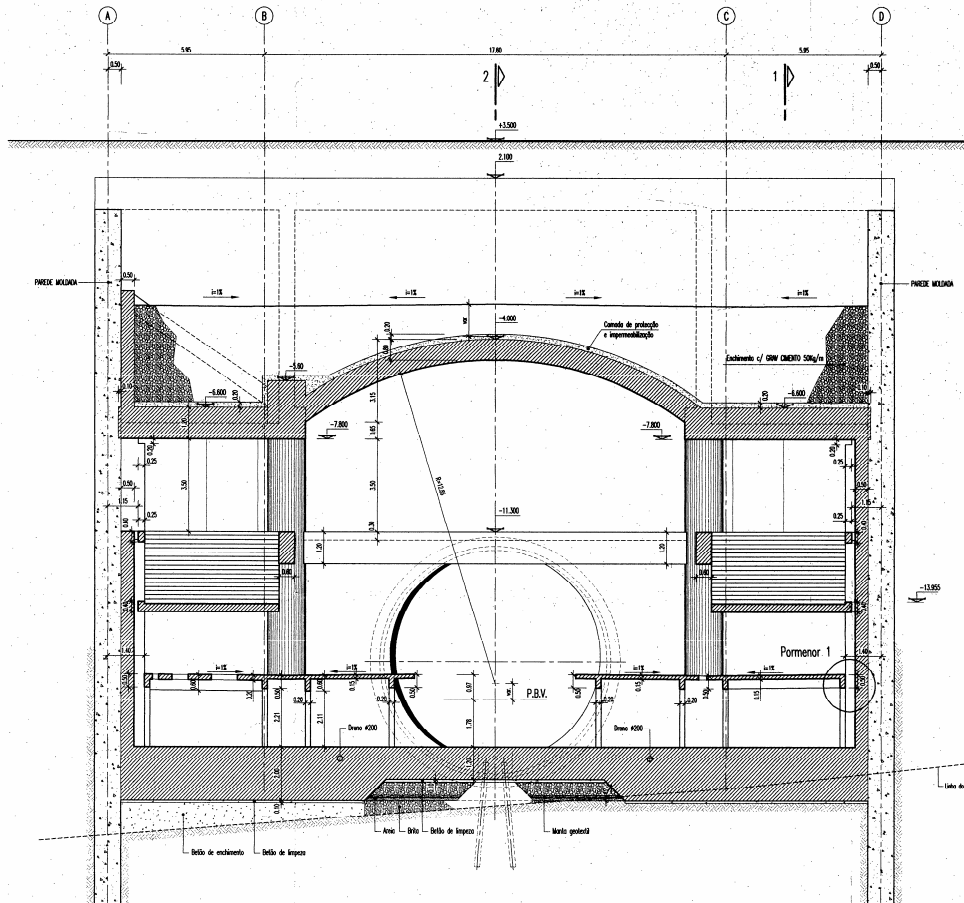


a) Station 1. Plan of 2nd level





c) Station 1. Transverse vertical cut 8-8



d) Station 1. Transverse vertical cut 10-10

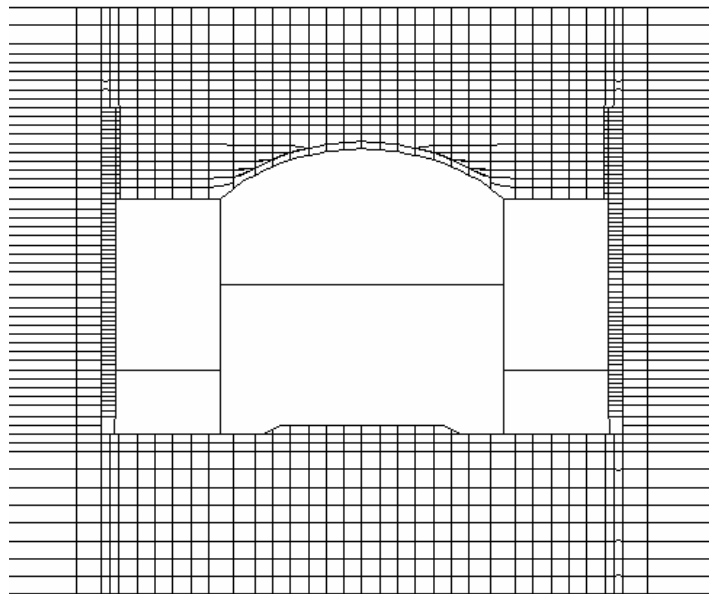
Figure 2.6. Design of tube station 1

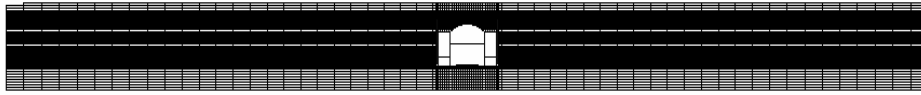
A common model of analysis of earthquake effects in underground structures represents both the structure and the soil along flexible alignments, yielding a plane model. All the height of soft soil is included in the model, until the depth where competent soil or the bed-rock is found. The seismic action in stiff soil is introduced at this level.

There may be some doubts regarding the distinction between flexible and rigid alignments in the transverse direction (the direction perpendicular to the largest

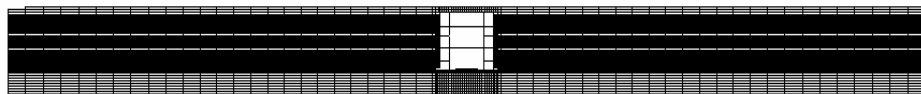
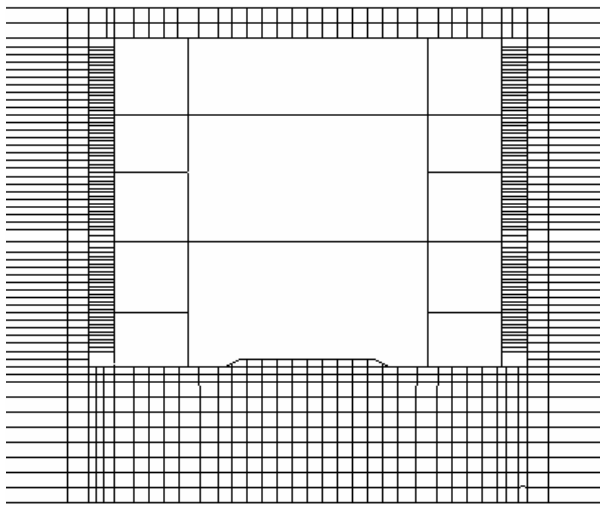
dimension in plan). Therefore a safe procedure would be to analyse all transversal cross-sections of the structure (identified as “F” in figure 2.4), except the extremity walls. The longitudinal alignments by the columns are close to the longitudinal perimeter walls and can be considered rigid if the shear deformation of the top and bottom slabs in their own plan can be disregarded, as it is usually accepted.

The design of the structure shows that essentially two different cross sections of the station can be distinguished: one by the zone where there is a significant concrete cover above the top slab and the other where the structure extends almost up to the surface. Variations of these two cross-sections may also exist, for instances due the removal of some beams due to the need to leave space for stairs. Figure 2.7 shows the respective soil/structure models, in which the soil is modelled by plane strain elements and the structure by linear bars. Each model intends to represent a band of soil and structure with the width equal to the distance between columns in the longitudinal direction of the station. In both models it is imposed that the soil elements on both sides of the model, in a large zone extending from the extremities, which represent the free-field, have the same horizontal displacements at all horizontal levels. The minimum dimension of this zone and the dimension of the zone between this and the structure were calibrated in such a way that if these dimensions are increased the results are not affected.





a) Model 1 - along a flexible alignment in the zone with large soil cover (vertical cut 10-10)



b) Model 2 - along flexible alignment in the zone with little soil cover (vertical cut 8-8)

Figure 2.7 – Soil/structure models

It is well known that soils exhibit shear stiffness degradation and increased energy dissipation capacity, usually accounted for by means of an equivalent viscous damping coefficient, as the amplitude of deformation increases. Figure 2.8 shows an example of such relationships that depend on the soil plasticity index.

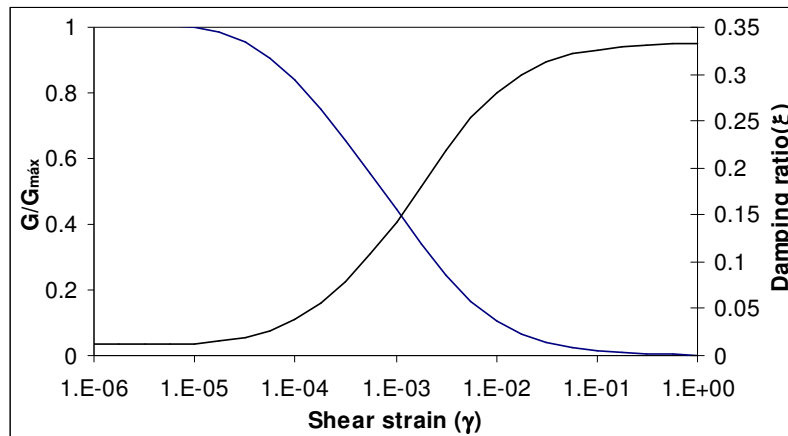


Figure 2.8 – Example of soil constitutive relationships [Ishibashi, I. & Zhang, X., 1993]

The nonlinear behaviour of the soil is usually studied separately considering a column of soil and the vertical propagation of shear waves. By adjusting the soil properties to the level of deformation experienced by the soil for a given seismic action, usually defined by a set of accelerograms, the values of the shear modulus G and of the equivalent viscous damping ζ for linear analysis can be obtained. This model, known as the linear equivalent model, allows the simulation of the soil in a global soil/structure model as a linear elastic material. However it should be mentioned that there are limits to the application of this methodology, whose scope of validity does not include extreme situations associated to very large soil deformations. In those situations a complete simulation of the soil nonlinear behaviour is necessary. Since this study focuses on the conception, analysis and design of the reinforced concrete structure, the soil properties for a given level of deformation in the free-field are treated as output of previous geotechnical studies and input for the design of the structure. Therefore the soil is treated in the soil/structure global models shown in figure 2.7 as a linear material.

The behaviour of the structure may be treated as linear if the amplitude of deformations is kept within certain limits. However the deformation capacity of reinforced concrete structures extends far beyond those limits if the structures exhibit ductile behaviour. Therefore there is no interest in restraining the field of analysis of the structure to the linear range. However this does not imply that the nonlinear behaviour has to be explicitly considered in the global soil/structure model, as it will be shown in this chapter.

In order to study this problem the first analysis of the soil/structure models will be performed considering the elastic properties of the reinforced concrete structure.

Therefore the model is linear, what allows representing the seismic action by means of response spectra. For the analysis that follows the acceleration response spectra defined in EC8 [2003] was used, considering the following parameters:

$$S=1 \quad T_B=0,15s \quad T_C=0,4s \quad T_D=2s \quad a_g=2,7 \text{ m/s}^2$$

The above values correspond to a spectrum associated with a far distance earthquake of large magnitude, duration of 30s and low frequency contents. The above corresponds to the horizontal component of the earthquake movement. The spectrum for the vertical direction was obtained multiplying the spectrum for the horizontal direction by 2/3. The acceleration response spectrum for the horizontal direction is shown in figure 2.9.

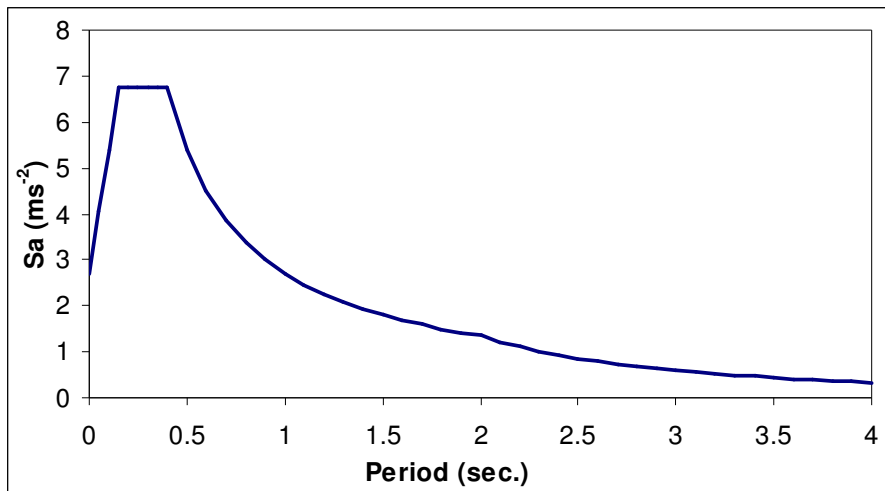


Figure 2.9 – Acceleration response spectrum for $\xi=5\%$ and soil type 1

However a problem arises in the analysis of this type of structural system, which is the choice of the viscous damping coefficient, since in general the soil and the structure exhibit different damping characteristics. One possible approximate solution for this problem is (i) to identify which is the material, soil or concrete, whose contribution is predominant to the energy dissipation in each mode shape and (ii) associate to the respective frequency (or period) the spectral acceleration obtained from the spectra evaluated with the viscous damping coefficient of that material. For the soil an average viscous damping coefficient must be chosen considering the results of the nonlinear analysis of the soil column. This was the procedure used and gives raise to a stepped response spectra, as schematically illustrated in figure 2.10.

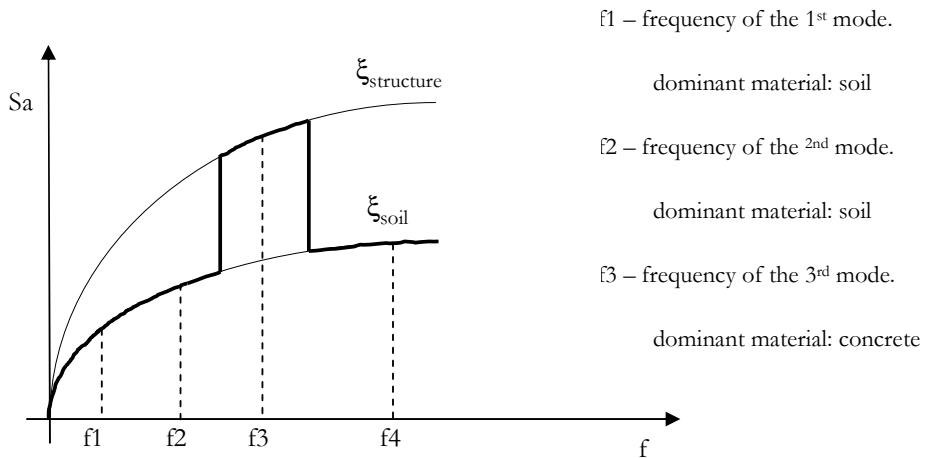
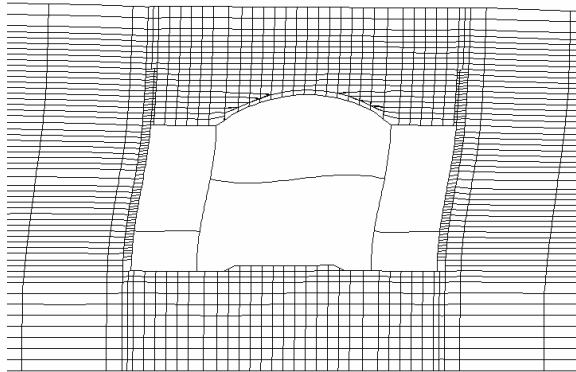


Figure 2.10 – Stepped response spectrum to account for different viscous damping coefficients (ξ)

2.5 ANALYSIS OF RESULTS

2.5.1 Model with thick soil cover

The configuration of the first four vibration modes and modes 7, 12 and 21 that exhibit large vertical displacements on the structure with the concrete cover (model 1) are shown in figure 2.11. The respective frequencies and mass participation factors are also shown.



Mode 1 $f_1 = 0,90$ Hz $M_{x1} = 64,5$ $M_{z1} = 0,0$



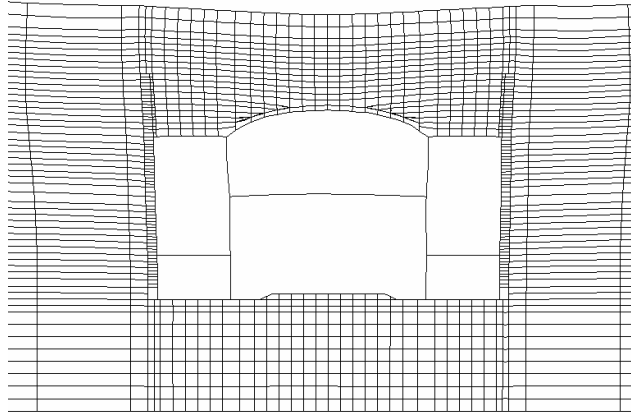
Mode 2 $f_2 = 1,51$ Hz $M_{x2} = 0,3$ $M_{z2} = 0,0$



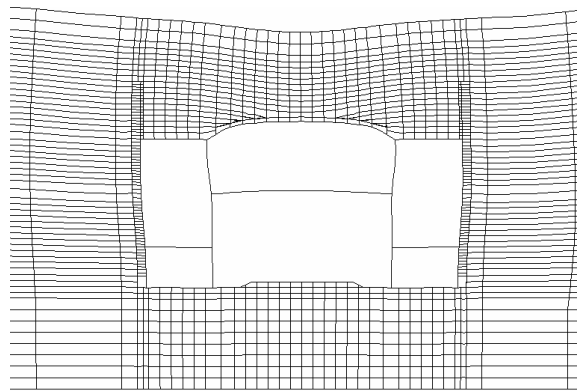
Mode 3 $f_3 = 1,85$ Hz $M_{x3} = 0,0$ $M_{z3} = 0,0$



Mode 4 $f_4 = 2,08$ Hz $M_{x4} = 0,0$ $M_{z4} = 0,0$



Mode 7 $f_7 = 2,86$ Hz $M_x7 = 0.8$ $M_z7 = 0.0$



Mode 12 $f_{12} = 3,77$ Hz $M_x12 = 0.0$ $M_z12 = 9.5$

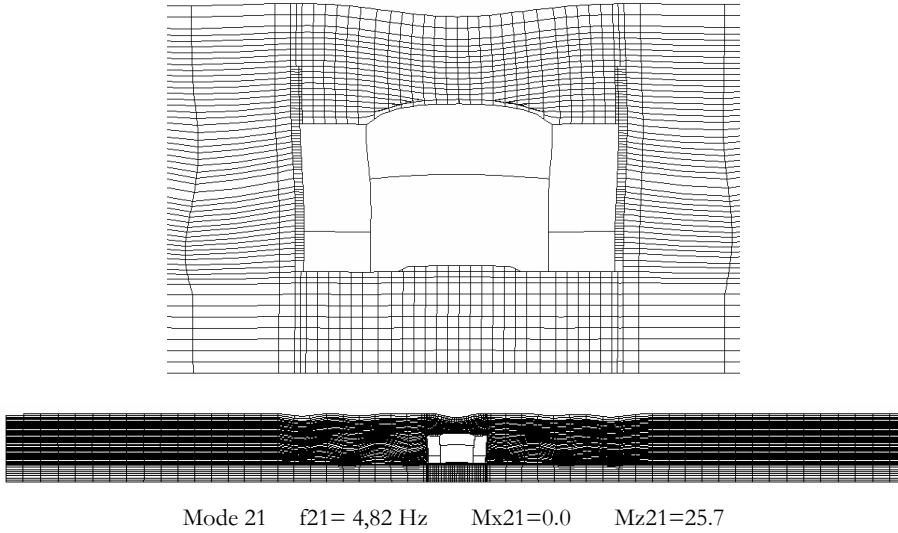


Figure 2.11. Configuration of modes 1, 2, 3, 4, 7, 12 and 21 and respective frequencies and mass participation factors for model 1

The relative importance of the different modes can not be evaluated as a function of their frequencies and mass participation factors only, since the mass participation factors depend essentially on soil displacement configurations. Therefore modes which induce relevant action-effects on the structure may not have large mass participation factors, as these only depend slightly on the structure deformed shape on the same mode. For instances the configuration of modes 7, 12 and 21 are associated essentially to deformations in the structure with less influence from the surrounding soil, as compared for instances with modes 1 and 2. In this situation the effects on the structure depend essentially on the behaviour of the structure itself and not of the surrounding soil. Therefore the damping coefficient associated with these modes should be the damping coefficient of the material of the structure.

The data on table 2.1 shows the relative importance of the different modes in what regards some action-effects: the bending moment at the middle of the arch, at the top of the columns and the difference of horizontal displacement between the top and bottom of the structure for each of the modes referred to in figure 2.11. The same results considering the effect of the 40 modes included in the analysis are also shown.

Table 2.1. Moments at the middle of the arch, at top of the columns and relative horizontal displacements between top and bottom of the structure

Modes	M_{arch} [kNm/m]	M_{column} [kNm/m]	d_{relative} [mm]
All	631	3050	59.59
1	0	2895	58.24
2	2	285	6.13
3	2	3	0.018
4	0	5	0.140
7	326	458	1.631
12	595	790	2.576
21	499	596	1.416

The results show that the first mode accounts for 97.5% of the total relative horizontal displacement along the height that the structure must withstand due to the seismic action. The second mode is also associated to considerable differences of horizontal displacements along the height of the structure, and also in the same direction on both sides of the structure. Since the joint mass of the structure and of the cover soil is much less than the mass of soil on both sides of the station, the inertia force generated in the soil on both sides of the structure is much larger than the inertia force generated in the structure and cover soil. This implies that the dynamic characteristics of these modes depend essentially on the soil dynamic characteristics. The effects on the structure also depend on the soil lateral displacements. In these configurations the overall energy dissipation depends essentially on the soil energy dissipation capacity. Therefore the damping coefficient associated with the frequency of these modes must be the soil damping coefficient.

In order to confirm the predominance of the influence of the soil in the dynamic characteristics of these modes it was analysed a cantilever structure only with shear deformation and the height, mass, stiffness and damping of a column of soil with the same characteristics considered in model 1. Figure 2.12 shows the discretization of the cantilever and figure 2.13 the respective frequencies and vibration modes.

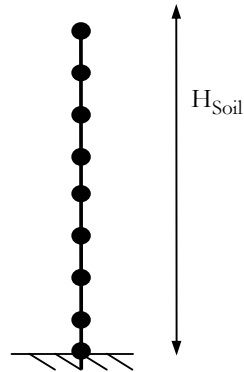


Figure 2.12 – Cantilever model



Figure 2.13 – Soil only modes of vibration in cantilever model

The zone with little deformation on the lower part of the model is the one that represents the competent soil where the structure is founded and that is much less deformable than the layers above.

As can be observed there is good correspondence between the first two modes of the soil only model, evaluated in the cantilever model and shown in figure 2.13, and the 1st and 7th modes of soil/structure model 1, which present similar soil deformations along the height. The frequency of the first mode of the structure with the cover soil, without any

soil on the sides would be 1.29 Hz. This value is higher than the first frequency of the model only with soil. Since the soil/structure model can be considered the result of the insertion of the structure and cover soil on a model just with soil, it can be concluded the higher stiffness of the model of the structure with cover soil only increases very slightly the frequency of the complete model. This increase is very low due to the fact that the influence of the structure in the main dynamic characteristics (frequency and damping) of the soil/structure system is also very low. The effect of the structure in the global soil/structure model is a localized one, in the vicinity of the structure, as it will be shown later in this report.

The results of table 1 show the influence of modes 7, 12 and 21. These modes are characterized by “opening” of the arch of the top slab, with vertical displacements at the centre of the arch as well as horizontal displacements in opposite directions at the extremities of the arch. This configuration is associated to some soil horizontal displacements on opposite directions on both sides of the structure which are accommodated by soil deformations in the vicinity of the structure. These are symmetric modes with a configuration qualitatively different of the first mode and more sensitive to vertical ground motion..

The strongest effects on the structure are clearly associated with the fundamental mode. The first modes associated essentially with inertia forces in the structure and cover soil are the 7th and 12th mode. Even though these modes may produce some relevant effects in some zones of the structure, for instances the bending moment in the middle of the arch of the top slab where the first mode has no relevant effects, in general the effects of these modes are much smaller than the ones associated with the first mode. For instances, according to the results shown in table 1, the bending moment on top of the columns, where both modes produce effects, is 2895kN.m for the 1st mode. This value is 5.1% below the value of 3050kN.m obtained considering the influence of all the modes included in the analysis. However in the section at the middle of the arch the situation is the opposite: the first mode has no contribution to the bending moment, due to the anti-symmetric deformed shape of the structure in the first mode, while influence of the modes with “opening” of the arch is predominant. It is therefore possible that higher order modes can have a strong influence on the seismic action-effects on some structural members. However this fact deserves the following comments: (i) the periods of modes 7,12 and 21 are still in the range of the spectrum where the highest accelerations take place. For far distance seismic events, to which correspond response spectrum shifted to higher periods, the periods of these modes could fall out of the range of the higher spectral accelerations, reducing the effects and relative importance of these modes; (ii) the design of the arch for the load combination in which the main variable action is the live load usually yields a considerable reserve strength compared to the permanent load effects that must be accounted for in the design for the load combination in which the

seismic action is the main variable action. Therefore this may not be the load combination that controls the design of the arch.

Another feature of behaviour can be observed in figure 2.14 in which the horizontal displacements along a horizontal reference level (at the level of the top of the columns of model 1) are plotted, considering only the effect of the first mode and the effect of all modes considered in the dynamic analysis.

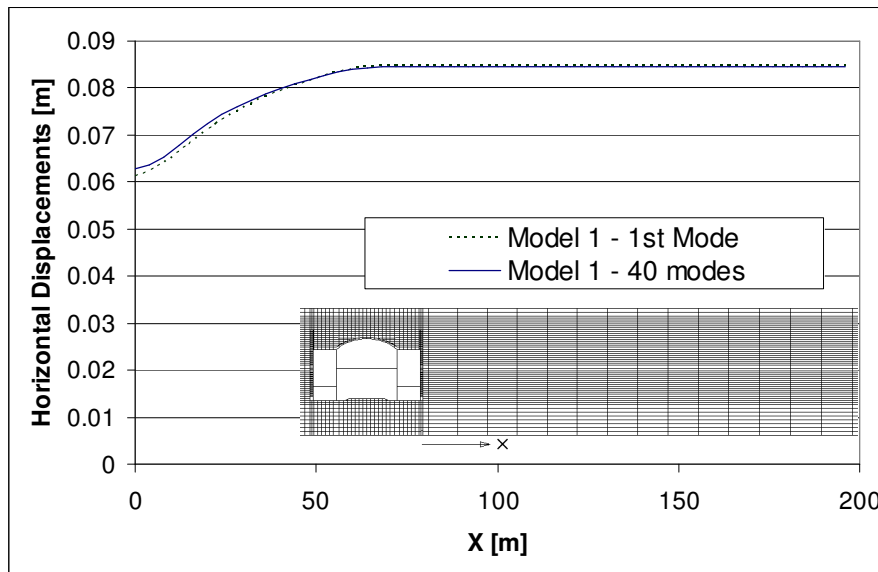


Figure 2.14. Horizontal displacement field for model 1

As it can be seen the 1st mode accounts for 97.5% of the total horizontal displacement in the structure and 100% of the total horizontal displacement in the free field. The reduction of displacements in the structure as compared to the displacements in the free-field, is due to the stiffness of the structure and deformations of the soil in the vicinity of the structure, and is 26%.

2.5.2 Model with thin soil cover

Figure 2.15 shows the frequencies and configurations of the first modes of model 2, with a flat top slab and 2.0m soil cover.

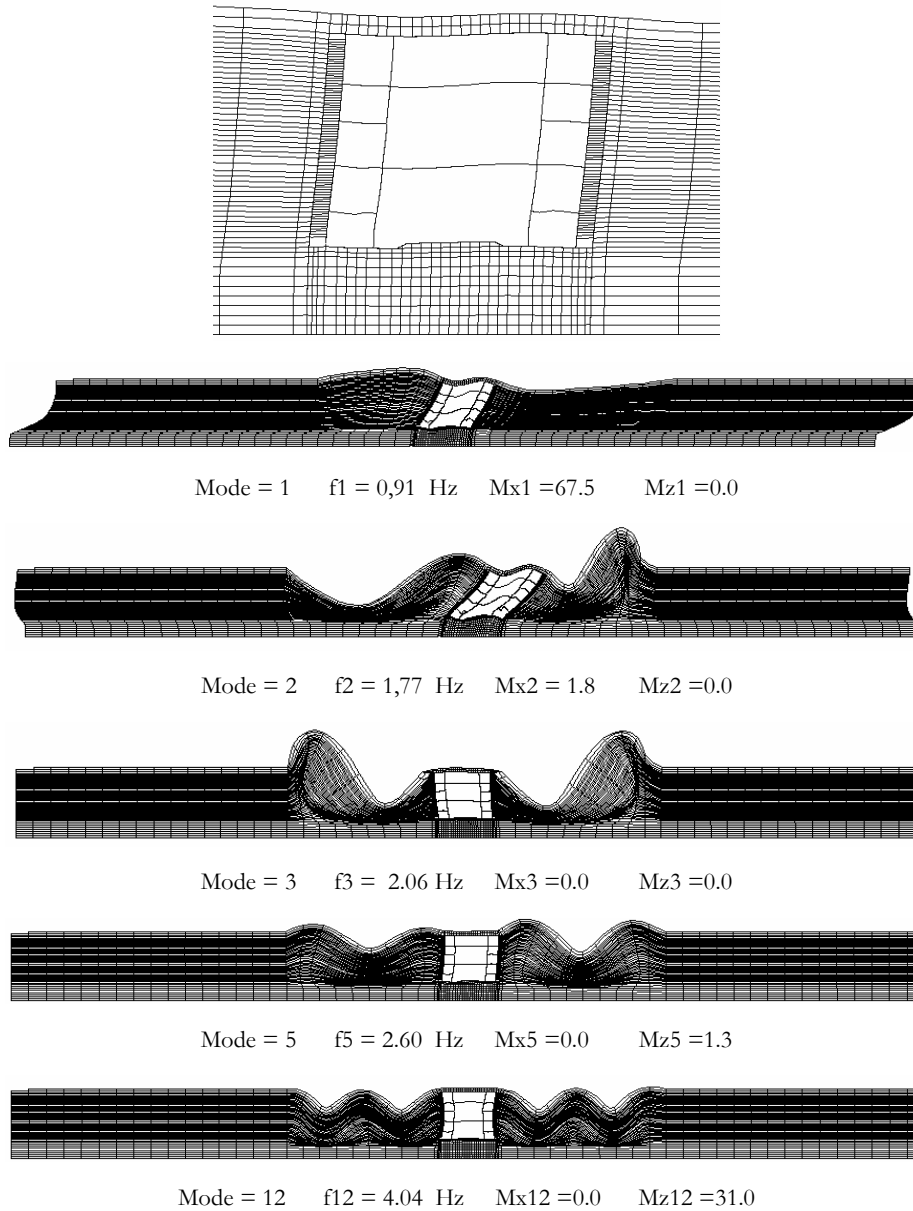


Figure 2.15. Configuration, frequencies and mass participation factors for the first three and 5th and 12th modes for model 2

As it can be observed the frequency and configuration of the first mode is similar to the one obtained for model 1, confirming that the dynamic characteristics of the first mode is essentially conditioned by the soil dynamic behaviour. The most relevant difference between both models is that in model 2 the first symmetric mode associated with relevant vertical displacements of the top slab is mode 56 with a frequency of $f=8.2\text{Hz}$. This and other modes with similar configurations induce a bending moment of 545kN.m in the middle of the top slab where the first mode has no effect. However this would be unlikely to condition the design of this section of the top slab, since the design for the load combination in which the live load is the main variable action would probably yield a higher bending moment. If the soil cover was completely removed there would be no mode with frequency below 10Hz with a configuration with relevant vertical displacement at the middle of the top slab or relevant bending moments at the middle section of the top slab. The main reason for this would be the inexistence of covering soil, therefore the vibrating mass in the modes with significant vertical displacements, such as modes 7th and 12th of model 1, is reduced, yielding modes with very high frequencies. Therefore all the modes in the range $f < 10\text{ Hz}$, including the first, are strongly influenced by the soil dynamic behaviour. Thus, it can be concluded that in underground stations with the configurations analysed, the relative importance of higher modes of vibration is associated mainly with the thickness of the soil cover, being more reduced for structures with little soil cover. This can also be illustrated by the ratio between the moment at the top of the columns due to the first mode and due to the first 100 modes, to which correspond frequencies close to 11Hz . This ratio is 94% for the structure of model 2 with 2m soil cover and 91% for the structure with no soil cover, showing the little importance of higher modes of vibration.

The horizontal displacements along the horizontal reference line (at the same level considered for model 1) for model 2 are plotted in figure 2.16, equivalent to figure 2.14 for model 1.

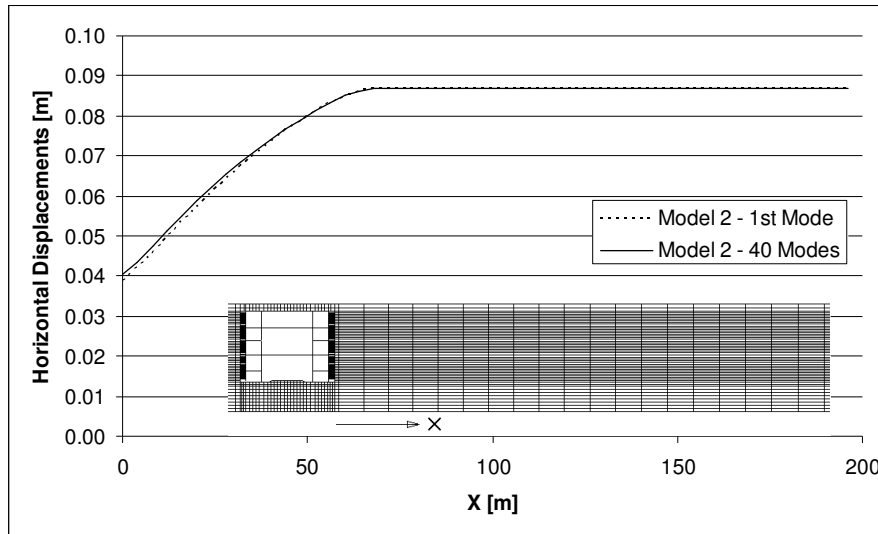


Figure 2.16. Horizontal displacement field for model 2

The figure shows there is a higher reduction of displacements from the free-field to the vicinity of the structure. This is associated with the fact that the fundamental frequency of model 2, corresponding to a model whose configuration is the horizontal displacement of the whole structure to the same side, is much higher than for model 1. The frequency of the structure and cover soil (without surrounding soil) for model 2 is 2.47 Hz, a value considerably higher than for model 1.

2.5.3 Comparisons of results. Influence of the stiffness of the structure

In order to separate the influence of the stiffness of the structure from the effect of the structural configuration, the stiffness of all vertical elements of the structure of model 2 were reduced in the same proportion in such a way that the frequency of both structures (the ones of model 1 and model 2) with the respective cover soil becomes equal. A new analysis of the full soil/structure model 2 with the new structure with less stiffness was performed and the horizontal displacements along the reference horizontal level are shown in figure 2.17. The displacements in the free-field for models 1 and 2 are similar but not exactly equal, due to differences in the soil characteristics of both models, which were derived from a real case. Since what matters in the analysis of the results is the reduction of horizontal displacements from the free field to the structure the displacement diagram for model 1 was scaled uniformly in order to yield the same displacement of model 2 for the free-field.

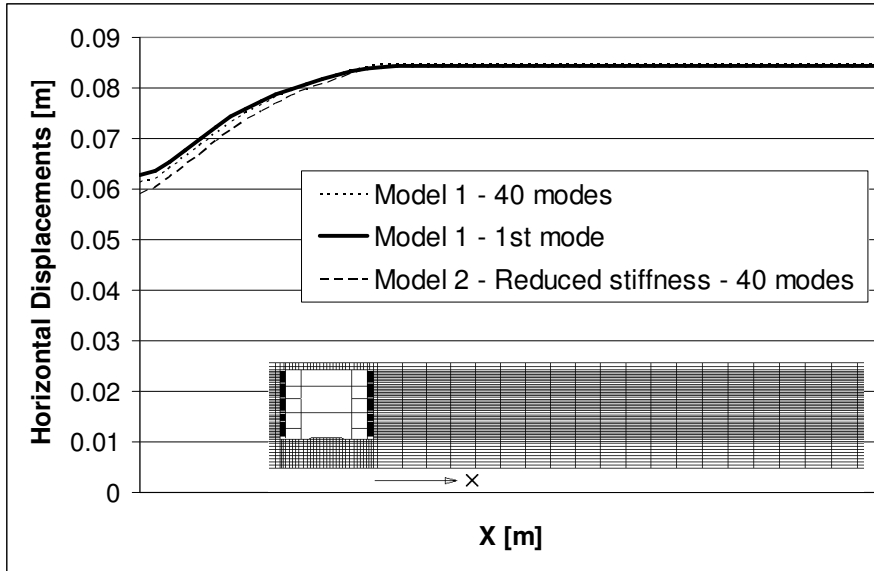


Figure 2.17. Horizontal displacement field for altered model 2

Figure 2.17 shows that the pattern of horizontal displacements of model 2 with less stiffness is the same as for model 1. This observation, coupled with the fact that both models (model 1 and model 2 altered) present similar stiffness to relative horizontal displacements along the height, means that the structural configuration had almost no influence on the variation of horizontal displacements between the vicinity of the structure and the free-field.

The stiffness to relative horizontal displacements along the height, which will be designated as distortional stiffness k_{dist} , can be quantified by applying an horizontal force at the top of each structural model (without soil); the stiffness, obtained by dividing the force by the average distortion along the height, as shown in figure 2.18, is:

$$\text{Structure 1} \quad k_{\text{dist}} = 654\,666 \text{ kN}$$

$$\text{Structure 2} \quad k_{\text{dist}} = 2751\,947 \text{ kN}$$

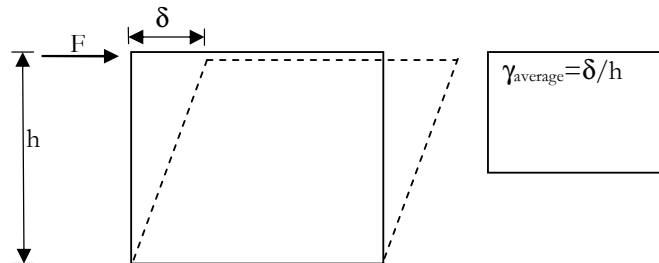


Figure 2.18. Evaluation of the structure distortional stiffness

It results from the previous discussion that the main factor that can influence the difference between the free-field horizontal displacements and the ones in the vicinity of the structure is the ratio between the distortional stiffness of the structure and the stiffness of the soil. For a given geotechnical scenario, as it is the case in real situations and in the analysis performed in this chapter, it is the stiffness of the structure the key parameter that influences the difference of horizontal displacements between the structure and the free-field. In order to study this issue, in each of the previous models the stiffness of all the vertical elements was decreased in such a way that the global distortional stiffness of the models, as defined in figure 2.18, was divided by 5 (models 1- and 2-).

Models 1- and 2- may be considered to represent the original structures after significant incursions in the nonlinear range, after cracking and yielding haven taken place.

The main results of the analysis of the new models are synthesized in figures 2.19 and 2.20 and table 2.2. Figure 2.19 shows the horizontal displacements for the models 1 (1- and 1) along the reference horizontal level, and figure 2.20 shows the same results for the 2 models 2. Table 2.2 shows the ratio between the value of the horizontal displacement in the structure and the displacement of the free-field (r_d) for the 4 case studies.

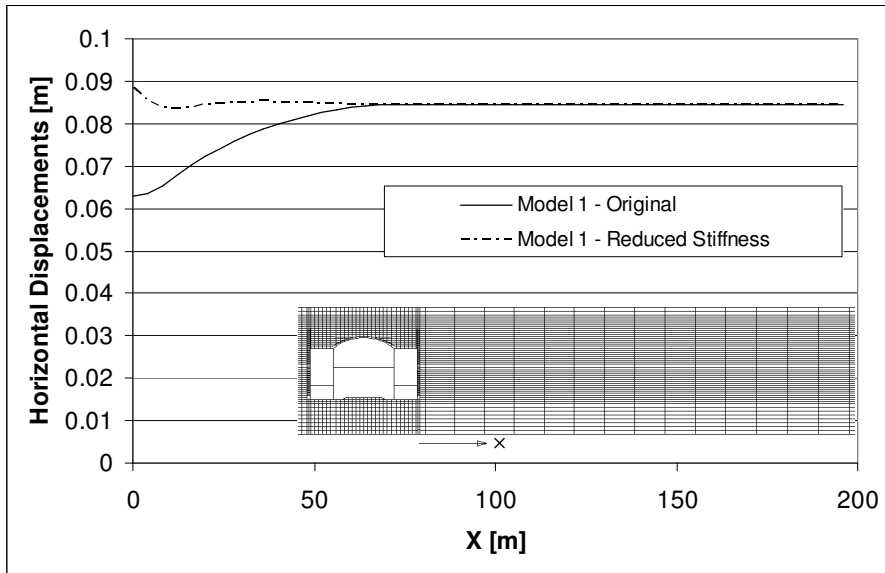


Figure 2.19. Horizontal displacement fields for models 1- and 1

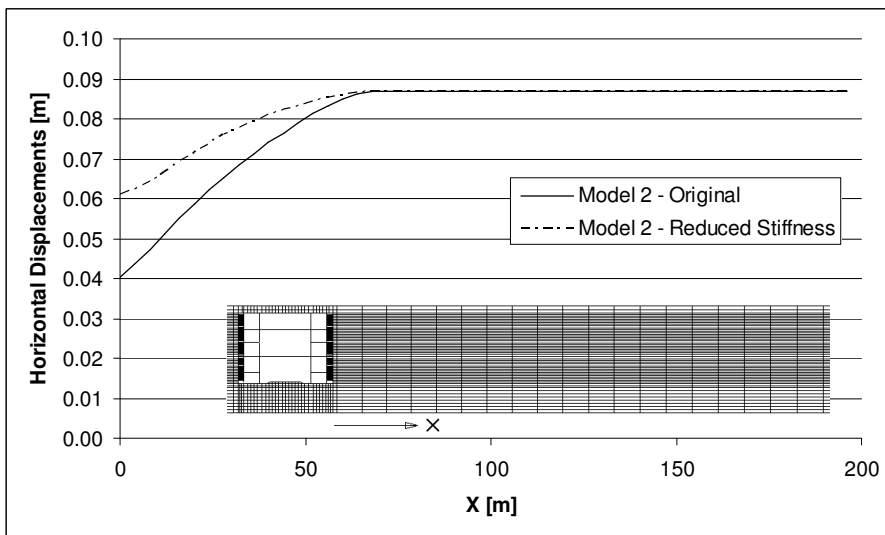


Figure 2.20. Horizontal displacement fields for models 2-; and 2

Table 2.2 – Ratio between horizontal displacement in the structure and in the free-field

r_d	Models 1	Models 2
1 ⁻ , 2 ⁻	1.046	0.700
1, 2	0.744	0.464

The results illustrate the influence of the reduction of the stiffness of the structure on the expected “reduction” of the displacement field along the height imposed to the structure. The results indicate that the nonlinear behaviour of reinforced concrete structures, being equivalent to a reduction of the stiffness of the structure, leads to the increase of structural horizontal displacements imposed to the structure. Therefore it is an unsafe procedure to evaluate the displacements imposed to the structure using a linear elastic model if the amplitude of imposed displacements is enough to force the structure to enter deeply in the nonlinear range.

The results also indicate that in some situations it may be unsafe to assume that there is a reduction of displacements in the vicinity of the structure, as compared to the displacements in the free-field. This can be observed in figure 2.19, which shows that for model 1⁻ the horizontal displacement in the structure at the reference level is higher than the displacement in the free-field at the same level. This can be understood if we consider again the model of the structure with cover soil but no soil on the sides of the structure. The analysis of the structures of models 1 and 1⁻ with no soil on the sides, that will be designated as models 1_{sl} and 1_{sl}⁻, and of a soil column, yield the frequencies for the first modes and horizontal displacement at reference horizontal level shown in table 2.3

Table 2.3 – Frequencies and horizontal displacements for the column of soil and models 1_{sl} and 1_{sl}⁻

	Soil column	1 _{sl}	1 _{sl} ⁻
f(Hz)	0.87	1.29	0.63
δ(mm)	86.3	48.5	108.0

It had already been shown that model 1_{sl} is stiffer than the soil column, therefore yields a higher frequency and a lower displacement under the prescribed seismic action. However the reduction in stiffness from model 1_{sl} to model 1_{sl}⁻ reduces the frequency of the first mode to f=0.63Hz, a value below the fundamental frequency of the soil only model. The horizontal displacement at the reference level is also higher for model 1_{sl}⁻ than the same displacement in the soil only model. Therefore model 1⁻ can be considered the result of

the insertion in the soil only model of a more flexible system, model 1_{st}. The fact that the dynamic behaviour of the system is dominated by the soil obviously makes the horizontal displacements in the structure more similar to the displacements in the soil. However the deformability of the soil in the vicinity of the structure allows for horizontal displacements in the structure slightly closer to the displacement that the structure would undergo without the soil on the sides, this is, a slightly higher displacement in this case. It should be pointed out that this situation is extremely unlikely if the structure has little or no soil cover, as in such a situation the horizontal inertia force in the structure with no soil on the sides would be rather small and the horizontal displacements in such a structural model would probably be smaller than the same displacements in the free field.

It should also be mentioned that in model 1_{st} the bending moment in the middle section of the arch due to the permanent loads would increase as compared to the same value evaluated with model 1. This would be due to the reduction of the arch effect associated to the lower restriction that the vertical elements would offer to the horizontal displacements at the extremities of the arch. It is also worth mentioning that if a different seismic action, richer in high frequencies for instances, was the input for analysis, the relative importance of the 7th, 12th and 21st modes of model 1 would increase and eventually could lead to higher bending moments at the arch.

The above analysis of results shows that the stiffer structure reduces the horizontal displacement field in its vicinity, as compared to the one in the free-field. Therefore if the structure is very stiff the displacements that it has to withstand can be much smaller than the ones in the soil away from the zone of influence of the structure. This effect may be enhanced if there is a three-dimensional soil flow or cinematic incompatibility at the soil structure interface, as already mentioned when discussing the difference between rigid and flexible alignments. For very flexible alignments, the structure offers almost no resistance to the soil deformation and is forced to accommodate a soil displacement profile along the height similar to the one that takes place at the free-field. For structures with little or no soil cover, on the flexible side of the range, it will be a safe procedure to impose to the structure the soil displacement on the free-field. In some cases of structures with large soil covers the horizontal displacements in the structure may even be superior to the ones in the free-field.

It may be impossible to apply the free-field displacements to structures on stiff side of the range, as these structures usually have low capacity to accommodate imposed deformations. Obviously this also depends on the value of those deformations that depend of other parameters such as the stiffness of the soil and the intensity of the seismic action. For the intermediate situations a soil/structure model such as the ones used in the previous analyses can be used to evaluate the displacement field imposed to the structure.

It results from the above that, under earthquake actions, underground structures have to withstand a horizontal displacement field along the height of flexible alignments that is essentially imposed externally by the surrounding soil. Since the configuration of the most important vibration modes depends essentially on the soil deformations and inertia forces, the energy dissipation in these modes depends essentially on the soil energy dissipation capacity. Therefore the energy dissipation capacity of the structure has little influence on the horizontal displacement field that the structure has to withstand.

For some structural configurations, such as the cross section of the example structure in the zone with thick soil cover, earthquakes may induce effects relevant for certain elements in the structure that are not associated with horizontal displacements imposed on the structure by the soil on the sides of the structure. These effects must also be considered in addition to the ones previously mentioned.

3. DESCRIPTION OF THE ANALYSIS PROGRAM

3.1 OBJECTIVES

This chapter describes the program PIER, that aim at the physic and geometric nonlinear monotonic analysis of reinforced concrete plane frames under concentrated and distributed loads, as well as applied displacements.

3.2 METHODOLOGY

The analytical formulation consists on an iterative procedure based on a secant stiffness approach and total actions, including applied loads and imposed displacements. The program is formulated to perform a linear elastic analysis by the displacement method at each step. The first iteration is performed considering the structure in its undeformed configuration and the initial tangent stiffness matrix. In all the next steps an updated secant stiffness matrix is used. If geometrical non-linear effects, whose consideration is optional, are considered, the location of the nodes is also updated in each iteration. At each step the new secant stiffness matrix is evaluated considering the coupled secant flexural and axial stiffness of each element, evaluated at each step as a function of the deformation state at the end of the last iteration. This is based on section analysis considering the different stress/strain states within the section, evaluated as a function of the control variables at section level. These are the curvature χ and the extension of the centre of gravity of the concrete cross-section ϵ_G . The stiffness of the concrete between cracks is disregarded. The iterative procedure stops if displacements and internal forces have only very little variations between iterations.

Since the analysis accounts for the physical nonlinear behaviour of reinforced concrete, cross-sections characteristics (geometry, constitutive relationships for plain and confined concrete, steel areas, location and constitutive relationship) need to be defined before the analysis. The program allows the definition of constitutive relationships (σ - ϵ curves) for steel and concrete by means of sets of branches, each one defined by a third degree polynomial equation, in such a way that the whole domain of possible strains is covered. In each section it is possible to define more than one type of concrete, especially to allow the definition of plain and confined concrete as two different materials with different constitutive relationships. Only linear bar elements are available in the program. Each element is characterized by cross sections of the extreme nodes and a finite length. The

stiffness is considered constant along the entire length of each element at each step, therefore the element's length is chosen as a function of the desired accuracy.

The stiffness matrix of each element is calculated considering flexural and axial deformations. Shear deformations are disregarded and transverse reinforcement does not need to be defined. The effect of confinement reinforcement is indirectly accounted for in the concrete constitutive relationships. Only deformations in the plan of the structure are considered. Therefore all cross sections analyses only consider bending around the axis perpendicular to the plan of the structure.

Since the analysis is plan, three degrees of freedom per node are considered and each element has six degrees of freedom, three in each extremity node. The evaluation of the stiffness matrix of each element is based on the cross-section secant stiffness matrix associated to the element, which is evaluated as the average of the stiffness matrices of the elements end sections. This is evaluated as a function of the characteristics and deformation state of the cross-section, accounted for by the curvature χ and the extension of the centre of gravity of the concrete cross-section ϵ_G . The process of evaluation of the stiffness matrix is described in section 3.4.

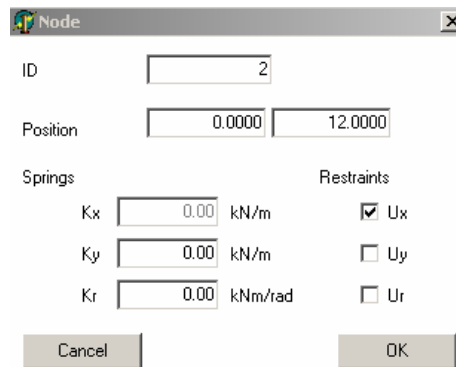
3.3 INPUT DATA

The structural model is defined by the items listed below.

- Nodes;
- Materials;
- Beams;
- Concentrated loads;
- Distributed loads
- Imposed displacements

3.3.1 Nodes

Each node references not only its position, but also the boundary conditions. Nodes can be free or have rigid or elastic restraints.



Node	
ID	2
Position	0.0000 12.0000
Ssprings	
Kx	0.00 kN/m
Ky	0.00 kN/m
Kr	0.00 kNm/rad
Restrains	
<input checked="" type="checkbox"/>	Ux
<input type="checkbox"/>	Uy
<input type="checkbox"/>	Ur
Cancel	OK

Figure 3.1. Example input data for nodes

3.3.2 Cross-sections

Cross sections are defined by the geometry of the unconfined concrete, confined concrete, amounts and location of reinforcement, and respective constitutive relationships. Since several members may have the same concrete geometry, and different elements will also have the same constitutive relationship, in order to avoid the need to provide the same data more than once, the geometry of the sections and the constitutive relationships are input separately. Therefore sets of constitutive relationships are defined, as well as several geometries for cross sections, including the amounts and location of reinforcement. Then each cross section is defined by the assigning to the materials associated with a given section geometry the corresponding constitutive relationships. The program also allows the graphic visualisation of section geometry as well as the constitutive relationships. Figure 3.2 shows an example of the input window for the definition of section geometry. Figure 3.3 shows a graphic visualization of material constitutive relationships.

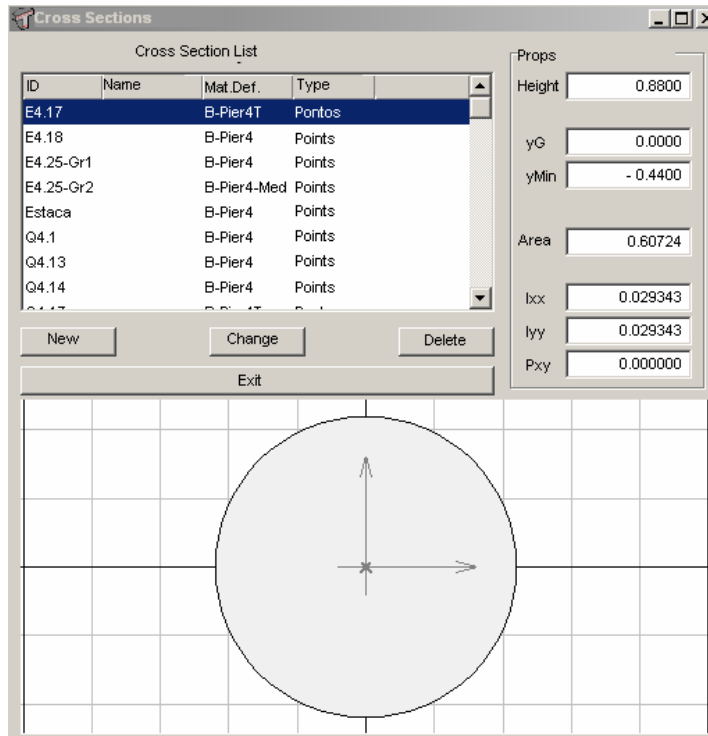


Figure 3.2. Input window to define section geometry

Figure 3.3. Graphic visualisation of constitutive relationships

3.3.3 Beams

The word beam is used here to characterize linear structural elements (that in reality may be other types of elements, columns for instances) with the same cross section along the length. As in general each beam will be too long to have a constant stiffness as the deformation state varies along the length of the beam, it will be necessary to subdivide it in smaller linear bar elements whose stiffness can be considered constant along the length.

Beams are characterized by the extremity nodes and respective cross section. The user has the option of dividing each beam in several smaller linear bar elements with the same cross-section as the accuracy of the results depends on the discretization. Figure 3.4 shows an example of the input window for beams.

Figure 3.4 – Example input data for beams

3.3.4 Concentrated loads

Concentrated loads may be applied at nodes or at intermediate sections of beams, as shown in Figure 3.5.

Figure 3.5. Example input data for concentrated loads

3.3.5 Distributed loads

Beams allow trapezoidal distributed loads to be applied in the directions parallel and perpendicular to the axis of the beam, as exemplified in figure 3.6.

The screenshot shows a dialog box titled "Distributed load". It has two main sections: "Location" and "Applied force".

- Location:** A dropdown menu for "Beam" is set to "1". Below it, "Distance to initial node" is set to "0.000".
- Applied force:** Two rows of input fields. The first row is "Horizontal" with a value of "0.000" and units "kN/m". The second row is "Vertical" with a value of "5.000" and units "kN/m".

At the bottom, there are "Cancel" and "OK" buttons, and a circular arrow icon in the center.

Figure 3.6. Example input data for distributed loads

3.3.6 Imposed displacements

It is possible to define the final displacement at each node, as follows:

The screenshot shows a dialog box titled "Imposed displacement". It has two main sections: "Location" and "Imposed displacement".

- Location:** A dropdown menu for "Node" is set to "2".
- Imposed displacement:** Three rows of input fields with checkboxes.
 - Ux: 0.156240 m
 - Uy: 0.000000 m
 - Rot: 0.000000 rad

At the bottom, there are "Cancel" and "OK" buttons.

Figure 3.7. Example input data for imposed displacements

3.4 EVALUATION OF THE SECANT STIFFNESS MATRIX ANF FIXED END FORCES AND MOMENTS

3.4.1 Section level

(a) **Equations.** The secant stiffness matrix is first evaluated at section level. Considering the deformation vector $\underline{\varepsilon} = \begin{bmatrix} \varepsilon_G \\ \chi \end{bmatrix}$ and the force vector $X = \begin{bmatrix} N \\ M \end{bmatrix}$, the stiffness matrix assumes the following shape:

$$K_s = \begin{bmatrix} \left(\frac{\partial N}{\partial \varepsilon_G} \right)_{\text{sec}} & \left(\frac{\partial N}{\partial \chi} \right)_{\text{sec}} \\ \left(\frac{\partial M}{\partial \varepsilon_G} \right)_{\text{sec}} & \left(\frac{\partial M}{\partial \chi} \right)_{\text{sec}} \end{bmatrix} \quad (3.1)$$

Each term is evaluated by applying the definition of the terms of the stiffness matrix and considering the secant stiffness of each steel bar and concrete fibre associated to the stress/strain state at the end of the last iteration, as shown in figure 3.10

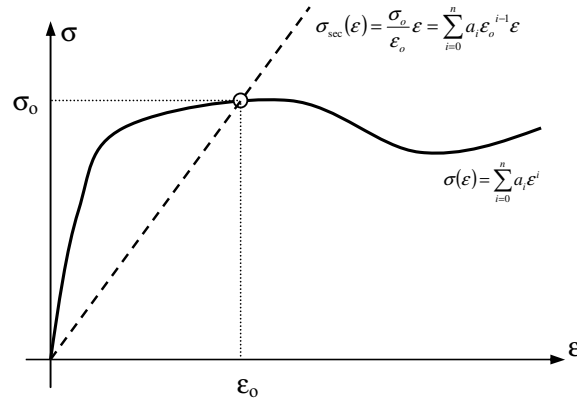


Figure 3.8. Secant stiffness

The expressions for the evaluation of the terms of the stiffness matrix are as follows:

$$\left(\frac{\partial N}{\partial \varepsilon_G} \right)_{\text{sec}} = \int_{\Omega} \sigma_{\text{sec}}(\varepsilon) d\Omega \quad \text{with} \quad \varepsilon_{G, \text{imposed}} = 1 \wedge \chi_{\text{imposed}} = 0 \quad (3.2)$$

$$\left(\frac{\partial M}{\partial \varepsilon_G} \right)_{\text{sec}} = \int_{\Omega} \sigma_{\text{sec}}(\varepsilon) \times y d\Omega \quad \text{with} \quad \varepsilon_{G, \text{imposed}} = 1 \wedge \chi_{\text{imposed}} = 0 \quad (3.3)$$

$$\left(\frac{\partial N}{\partial \chi} \right)_{\text{sec}} = \int_{\Omega} \sigma_{\text{sec}}(\varepsilon) d\Omega \quad \text{with} \quad \varepsilon_{G, \text{imposed}} = 0 \wedge \chi_{\text{imposed}} = 1 \quad (3.4)$$

$$\left(\frac{\partial M}{\partial \chi} \right)_{\text{sec}} = \int_{\Omega} \sigma_{\text{sec}}(\varepsilon) \times y \, d\Omega \quad \text{with} \quad \varepsilon_{G,\text{imposed}} = 0 \wedge \chi_{\text{imposed}} = 1 \quad (3.5)$$

The stiffness matrix is evaluated considering at each location and material of the cross section the secant stiffness associated with the respective stress/strain state, characterized by the extension of the centre of gravity of the gross concrete section ($\varepsilon_{G,o}$) and by the curvature around the axis perpendicular to the plan of the structure (χ_o). The associated strain field is given by:

$$\varepsilon_o(y) = \varepsilon_{G,o} + \chi_o \times y \quad (3.6)$$

The strain fields imposed for the purpose of deriving the terms of the stiffness matrix are given by:

$$\varepsilon_{\text{imposed}} = \varepsilon_{G,\text{imposed}} + \chi_{\text{imposed}} \times y \quad (3.7)$$

As $N_o = \int_{\Omega} \sigma_o \, d\Omega = \int_{\Omega} \sigma(\varepsilon_o) \, d\Omega$ and $M_o = \int_{\Omega} \sigma_o \times y \, d\Omega = \int_{\Omega} \sigma(\varepsilon_o) \times y \, d\Omega$ it can be

observed that:

$$\begin{bmatrix} \left(\frac{\partial N}{\partial \varepsilon_G} \right)_{\text{sec}} & \left(\frac{\partial N}{\partial \chi} \right)_{\text{sec}} \\ \left(\frac{\partial M}{\partial \varepsilon_G} \right)_{\text{sec}} & \left(\frac{\partial M}{\partial \chi} \right)_{\text{sec}} \end{bmatrix} \times \begin{bmatrix} \varepsilon_{G,o} \\ \chi_o \end{bmatrix} = \begin{bmatrix} N_o \\ M_o \end{bmatrix} \quad (3.8)$$

For instances for the case of the bending moment:

$$\begin{aligned} & \left(\frac{\partial M}{\partial \varepsilon_G} \right)_{\text{sec}} \times \varepsilon_{G,o} + \left(\frac{\partial M}{\partial \chi} \right)_{\text{sec}} \times \chi_o = \\ & = \left(\int_{\Omega} \sigma_{\text{sec}} \times y \, d\Omega \right)_{\varepsilon_{G,\text{imposed}}=1} \times \varepsilon_{G,o} + \left(\int_{\Omega} \sigma_{\text{sec}} \times y \, d\Omega \right)_{\chi_{\text{imposed}}=1} \times \chi_o = \\ & = \left(\int_{\Omega} \frac{\sigma_o}{\varepsilon_o} \times 1 \times y \, d\Omega \right) \times \varepsilon_{G,o} + \left(\int_{\Omega} \frac{\sigma_o}{\varepsilon_o} \times y \times y \, d\Omega \right) \times \chi_o = \end{aligned}$$

$$= \int_{\Omega} \frac{\sigma_o}{\epsilon_o} \times (\epsilon_{G,o} + \chi_o \times y) \times y \, d\Omega = \int_{\Omega} \frac{\sigma_o}{\epsilon_o} \times \epsilon_o \times y \, d\Omega = \int_{\Omega} \sigma_o \times y \, d\Omega = M_o \quad (3.9)$$

In general the terms of the stiffness matrix can be evaluated by means of expressions as follows:

$$K_{pq} = \int_{\Omega} \sigma_{\text{sec}}(\epsilon) \times y^j \, d\Omega = \int_{\Omega} \sum_{i=0}^n a_i (\epsilon_{G,o} + \chi_o y)^{i-1} \times y^k \times y^j \, d\Omega \quad (3.10)$$

$$K_{pq} = \int_{\Omega} \sum_{i=0}^n a_i (\epsilon_{G,o} + \chi_o y)^{i-1} \times y^{j+k} \, d\Omega \quad (3.11)$$

The symmetry of the stiffness matrix implies that the terms $\left(\frac{\partial M}{\partial \epsilon_G}\right)_{\text{sec}}$ and $\left(\frac{\partial N}{\partial \chi}\right)_{\text{sec}}$ are necessarily equal, what can be concluded from the fact that both correspond to the same strain state $(\epsilon_{G,o}, \chi_o)$ and the sum $j+k$ is 1 in both cases.

(b) Integration procedure. The terms K_{pq} can be subdivided in two parcels, a polynomial and a rational function as follows:

$$K_{pq} = \int_{\Omega} \sum_{i=0}^n a_i (\epsilon_{G,o} + \chi_o y)^{i-1} \times y^{j+k} \, d\Omega = \int_{\Omega} \sum_{i=1}^n a_i (\epsilon_{G,o} + \chi_o y)^{i-1} \times y^{j+k} \, d\Omega + \int_{\Omega} \frac{a_0 \times y^{j+k}}{\epsilon_{G,o} + \chi_o y} \, d\Omega \quad (3.12)$$

The polynomial parcel is a linear combination of parcels of the following type:

$$\int_{\Omega} y^j \, d\Omega \quad (3.13)$$

The area of the cross sections Ω is defined by one or several closed lines as shown in figure 3.9.

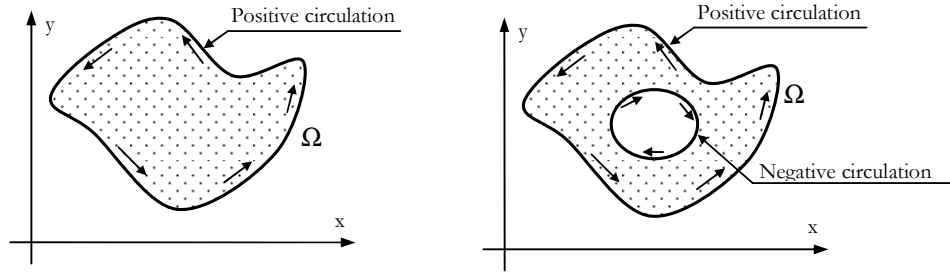


Figure 3.9. Cross sections

Each line can be considered as a sequence of arches described as a function of a single parameter, as follows:

$$\text{Arch } k: \begin{cases} x = x_k(s) \\ y = y_k(s) \end{cases} \quad s \in [s_{o,k}; s_{f,k}] \quad (3.14)$$

It is assumed that the arches are continuous and differentiable. In program PIER all arches are linear segments. Even though the cross sections perimeters may include circumference arches, each of these is treated as a set of linear segments for the purpose of defining the integration domain.

The integral of any function $f(y)$ on the region between the y axis and the line that limits the surface Ω in the interval $[a,b]$ of the parameter s is given by:

$$\int_{y=y(a)}^{y(b)} \int_{x=0}^{x(y)} f(y) dx dy \quad (3.15)$$

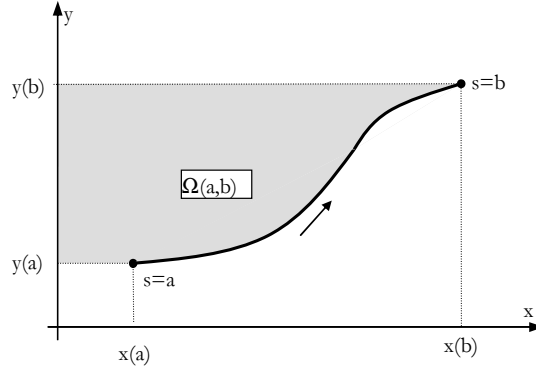


Figure 3.10 – Part of the cross section

For the function $f(y) = y^j$:

$$\int_{y=y(a)}^{y(b)} \int_{x=0}^{x(y)} y^j dx dy = \int_{y=y(a)}^{y(b)} x(y) \times y^j dy = \int_{s=a}^b x(s) \times y^j(s) \frac{dy}{ds} ds \quad (3.16)$$

In order to evaluate the integral of y^j over the area Ω it is enough to extend the integral between the initial and last point of each arch $[s_{o,k}; s_{f,k}]$ that constitutes the perimeter of the cross section and sum all the parcels.

$$\int_{\Omega} y^j d\Omega = \sum_k \int_{s=s_{o,k}}^{s_{f,k}} x(s) \times y^j(s) \frac{dy}{ds} ds \quad (3.17)$$

This allows transforming the integral over an area in a line integral. For the case the arches are straight lines, the functions $x(s)$ e $y(s)$ are linear functions:

$$\begin{cases} x = x_o + n_x s \\ y = y_o + n_y s \end{cases} \quad (3.18)$$

In this situation the integral assumes the following shape:

$$\int_{\Omega} y^j d\Omega = \int_{s=s_o}^{s_f} (x_o + n_x s) \times (y_o + n_y s)^j \times n_y ds \quad (3.19)$$

This expression represents the integral of a $j+1$ degree polynomial function which can be evaluated developing the above equation.

The rational parcel of the terms of the stiffness matrix can be transformed in the sum of a polynomial with a hyperbolic function (for instances by applying Ruffini's rule):

$$\int_{\Omega} \frac{a_0 \times y^{j+k}}{\varepsilon_{G,o} + \chi_o y} d\Omega = \int_{\Omega} \sum_{i=0}^{j+k-1} c_i y^i d\Omega + \int_{\Omega} \frac{K}{\varepsilon_{G,o} + \chi_o y} d\Omega \quad (3.20)$$

The coefficients c_1 , c_2 and K are shown in Table 3.1 for the different values of $j+k$.

Table 3.1. Coefficients for the decomposition of the rational function

$j+k$	c_1	c_0	K
0	--	--	a_0
1	--	$\frac{a_0}{\chi_o}$	$\frac{-a_0 \varepsilon_{G,o}}{\chi_o}$
2	$\frac{a_0}{\chi_o}$	$\frac{-a_0 \varepsilon_{G,o}}{\chi_o^2}$	$\frac{a_0 \varepsilon_{G,o}^2}{\chi_o^2}$

The first parcel of the second term can be integrated as described before because it is a polynomial function, while the hyperbole (S_{HH}) requires extra care, as it may be not be well defined.

$$S_{HH} = \int_{\Omega} \frac{K}{\varepsilon_{G,o} + \chi_o y} d\Omega = \int_{y=y_o}^{y_f} \int_{x=0}^{x(y)} \frac{K}{\varepsilon_{G,o} + \chi_o y} dx dy = \int_{y=y_o}^{y_f} \frac{Kx}{\varepsilon_{G,o} + \chi_o y} dy = \int_{s=s_o}^{s_f} \frac{Kx}{\varepsilon_{G,o} + \chi_o y} \times \frac{dy}{ds} ds \quad (3.21)$$

This situation may arise in the points where $\varepsilon_{G,o} + \chi_o \times y = 0$. However it should be noted that at this points the term a_0 of the constitutive relationships is always zero, as all stress-strain relationships are monotonic and $\varepsilon=0 \Rightarrow \sigma=0$. Therefore the hyperbolic function does not exist in these zones, as $a_0=0 \Rightarrow K=0$.

The value of S_{HH} can be evaluated as follows.

$$S_{HH} = \int_{s=s_o}^{s_f} \frac{Kx}{\varepsilon_{G,o} + \chi_o y} \times \frac{dy}{ds} ds = \int_{s=s_o}^{s_f} \frac{K \times (x_o + n_x s)}{\varepsilon_{G,o} + \chi_o \times (y_o + n_y s)} \times n_y ds \quad (3.22)$$

In practical terms it is necessary to integrate a function with a constant term and another term function of s^{-1} , this is:

$$S_{HH} = \int_{s=s_o}^{s_f} k_c ds + \int_{s=s_o}^{s_f} \frac{k_s}{v + w \times s} ds = k_c \times (s_f - s_o) + \frac{k_s}{w} \times \ln \left| \frac{v + w s_f}{v + w s_o} \right| \quad (3.23)$$

The values of the coefficients k_c , k_s , v e w are the following:

$$k_c = \frac{K n_x}{\chi_o} \quad (3.24)$$

$$k_s = \frac{K x_o}{\chi_o} - \frac{K n_x}{\chi_o} \times \frac{\varepsilon_{G,o} + \chi_o y_o}{\chi_o n_y} \quad (3.25)$$

$$v = \frac{\varepsilon_{G,o} + \chi_o y_o}{\chi_o n_y} \quad (3.26)$$

$$w = 1 \quad (3.27)$$

3.4.2 Element level

The linear bar finite element considered in program PIER is shown in figure 3.11.

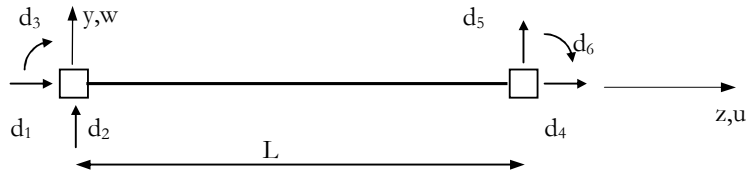


Figure 3.11 – Linear bar finite element

Designating the axial and transversal displacements by u and w respectively, and bearing in mind that the rotations θ are the first derivatives of the transversal displacements, the displacement vector at any location can be written as a function of the shape functions (φ_u e φ_w) and of the nodal displacements as follows:

$$\begin{bmatrix} u \\ w \\ \theta \end{bmatrix} = \begin{bmatrix} \varphi_{u1} & \varphi_{u2} & \varphi_{u3} & \varphi_{u4} & \varphi_{u5} & \varphi_{u6} \\ \varphi_{w1} & \varphi_{w2} & \varphi_{w3} & \varphi_{w4} & \varphi_{w5} & \varphi_{w6} \\ -\dot{\varphi}_{w1} & -\dot{\varphi}_{w2} & -\dot{\varphi}_{w3} & -\dot{\varphi}_{w4} & -\dot{\varphi}_{w5} & -\dot{\varphi}_{w6} \end{bmatrix} \times \begin{bmatrix} d_1 \\ d_2 \\ d_3 \\ d_4 \\ d_5 \\ d_6 \end{bmatrix} \quad (3.28)$$

$$\underline{\underline{u}} = \underline{\underline{\varphi}} \underline{\underline{d}} \quad (3.29)$$

The deformation vector at section level can be obtained from the displacement vector by means of cinematic relationships:

$$\begin{bmatrix} \varepsilon_G \\ \chi \end{bmatrix} = \begin{bmatrix} \frac{\partial u}{\partial z} \\ \frac{\partial^2 w}{\partial z^2} \\ -\frac{\partial^2 w}{\partial z^2} \end{bmatrix} = \begin{bmatrix} \frac{\partial}{\partial z} & \bullet & \bullet \\ \bullet & -\frac{\partial^2}{\partial z^2} & \bullet \end{bmatrix} \times \begin{bmatrix} u \\ w \\ \theta \end{bmatrix} \quad (3.30)$$

$$\underline{\underline{\varepsilon}} = \underline{\underline{L}} \underline{\underline{u}} \quad (3.31)$$

The vector of internal forces and moments (N,M) at the cross sections can be obtained by multiplying the secant stiffness matrix by the vector of the deformations of the cross section.

$$\begin{bmatrix} N \\ M \end{bmatrix} = \begin{bmatrix} K_{s,\varepsilon\varepsilon} & K_{s,\varepsilon\chi} \\ K_{s,\chi\varepsilon} & K_{s,\chi\chi} \end{bmatrix} \times \begin{bmatrix} \varepsilon_G \\ \chi \end{bmatrix} \quad (3.32)$$

$$\underline{\underline{X}} = \underline{\underline{K}}_s \times \underline{\underline{\varepsilon}} \quad (3.33)$$

Therefore the linear bar stiffness matrix can be obtained as follows:

$$\underline{\underline{K}}_e = \int \left(\underline{\underline{L}} \underline{\underline{\varphi}} \right)^T \times \underline{\underline{K}}_s \times \underline{\underline{L}} \underline{\underline{\varphi}} \quad (3.34)$$

while the fixed end forces and moments ($\underline{\underline{X}}_{\text{FIX}}$) for distributed axial loads ($\underline{\underline{p}}_N$) and distributed transversal loads ($\underline{\underline{p}}_T$) are given by:

$$X_{FIX} = -\int \underline{\underline{\phi}}^T \times \underline{\underline{p}} = -\int \begin{bmatrix} \varphi_{u1} & \varphi_{w1} & -\dot{\varphi}_{w1} \\ \varphi_{u2} & \varphi_{w2} & -\dot{\varphi}_{w2} \\ \varphi_{u3} & \varphi_{w3} & -\dot{\varphi}_{w3} \\ \varphi_{u4} & \varphi_{w4} & -\dot{\varphi}_{w4} \\ \varphi_{u5} & \varphi_{w5} & -\dot{\varphi}_{w5} \\ \varphi_{u6} & \varphi_{w6} & -\dot{\varphi}_{w6} \end{bmatrix} \times \begin{bmatrix} p_N \\ p_T \\ \bullet \end{bmatrix} \quad (3.35)$$

Therefore:

$$\underline{\underline{L}} \underline{\underline{\phi}} = \begin{bmatrix} \frac{\partial}{\partial z} & \bullet & \bullet \\ \bullet & -\frac{\partial^2}{\partial z^2} & \bullet \end{bmatrix} \times \begin{bmatrix} \varphi_{u1} & \varphi_{u2} & \varphi_{u3} & \varphi_{u4} & \varphi_{u5} & \varphi_{u6} \\ \varphi_{w1} & \varphi_{w2} & \varphi_{w3} & \varphi_{w4} & \varphi_{w5} & \varphi_{w6} \\ -\dot{\varphi}_{w1} & -\dot{\varphi}_{w2} & -\dot{\varphi}_{w3} & -\dot{\varphi}_{w4} & -\dot{\varphi}_{w5} & -\dot{\varphi}_{w6} \end{bmatrix} \quad (3.36)$$

$$\underline{\underline{L}} \underline{\underline{\phi}} = \begin{bmatrix} \frac{\partial \varphi_{u1}}{\partial z} & \frac{\partial \varphi_{u2}}{\partial z} & \frac{\partial \varphi_{u3}}{\partial z} & \frac{\partial \varphi_{u4}}{\partial z} & \frac{\partial \varphi_{u5}}{\partial z} & \frac{\partial \varphi_{u6}}{\partial z} \\ \frac{\partial^2 \varphi_{w1}}{\partial z^2} & \frac{\partial^2 \varphi_{w2}}{\partial z^2} & \frac{\partial^2 \varphi_{w3}}{\partial z^2} & \frac{\partial^2 \varphi_{w4}}{\partial z^2} & \frac{\partial^2 \varphi_{w5}}{\partial z^2} & \frac{\partial^2 \varphi_{w6}}{\partial z^2} \\ -\dot{\varphi}_{w1} & -\dot{\varphi}_{w2} & -\dot{\varphi}_{w3} & -\dot{\varphi}_{w4} & -\dot{\varphi}_{w5} & -\dot{\varphi}_{w6} \end{bmatrix} \quad (3.37)$$

$$\underline{\underline{K}}_e = \int \begin{bmatrix} \dot{\varphi}_{u1} & -\ddot{\varphi}_{w1} \\ \dot{\varphi}_{u2} & -\ddot{\varphi}_{w2} \\ \dot{\varphi}_{u3} & -\ddot{\varphi}_{w3} \\ \dot{\varphi}_{u4} & -\ddot{\varphi}_{w4} \\ \dot{\varphi}_{u5} & -\ddot{\varphi}_{w5} \\ \dot{\varphi}_{u6} & -\ddot{\varphi}_{w6} \end{bmatrix} \times \begin{bmatrix} K_{s,\varepsilon\varepsilon} & K_{s,\varepsilon\chi} \\ K_{s,\chi\varepsilon} & K_{s,\chi\chi} \end{bmatrix} \times \begin{bmatrix} \dot{\varphi}_{u1} & \dot{\varphi}_{u2} & \dot{\varphi}_{u3} & \dot{\varphi}_{u4} & \dot{\varphi}_{u5} & \dot{\varphi}_{u6} \\ -\ddot{\varphi}_{w1} & -\ddot{\varphi}_{w2} & -\ddot{\varphi}_{w3} & -\ddot{\varphi}_{w4} & -\ddot{\varphi}_{w5} & -\ddot{\varphi}_{w6} \end{bmatrix} \quad (3.38)$$

$$K_{-e,ij} = \int (K_{s,\varepsilon\varepsilon} \dot{\varphi}_{ui} - K_{s,\chi\varepsilon} \ddot{\varphi}_{wi}) \dot{\varphi}_{uj} - (K_{s,\varepsilon\chi} \dot{\varphi}_{ui} - K_{s,\chi\chi} \ddot{\varphi}_{wi}) \ddot{\varphi}_{wj} \quad (3.39)$$

$$X_{FIX,j} = -\int (p_N \varphi_{uj} + p_T \varphi_{wj}) \quad (3.40)$$

It can be concluded that being the section stiffness matrix $\underline{\underline{K}}_s$ symmetric, the linear bar stiffness matrix is also symmetric.

The internal forces at any section (M,N,and V) can be considered the sum of two parcels. The first is due to the nodal displacements and the second is due to the distributed loads along the span :

$$\underline{X} = \underline{X}_{nodal} + \underline{X}_{span} \quad (3.41)$$

The internal forces M and N due to the nodal displacements can be evaluated as follows:

$$\underline{X}_{nodal} = \underline{K}_s \times \underline{L} \times \underline{\varphi} \times \underline{d} \quad (3.42)$$

The shear force due to the nodal displacements must be evaluated by means of equilibrating the finite element:

$$V_{nodal} = \frac{dM_{nodal}}{dz} = K_{\chi^e} \frac{d\varepsilon_G}{dz} + K_{\chi^x} \frac{d\chi}{dz} \quad (3.43)$$

The forces due to the distributed loads are given by the sum of two parcels:

$$\underline{X}_{span} = \underline{X}_{span}^o + \Delta \underline{X}_{span} \quad (3.44)$$

The first parcel refers to the fixed end forces and moments on the first node and the second parcel can be obtained by equilibrium equations obtained using a model as shown in figure 3.12.

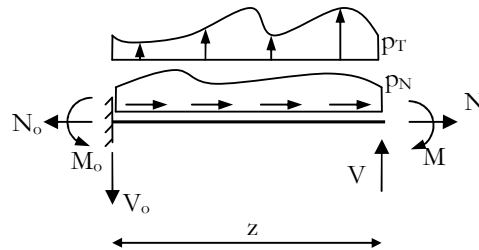


Figure 3.12 – Internal forces and moments due to distributed loads

$$N = N_o - \int p_N = N_o + \Delta N \quad (3.45)$$

$$\Delta N = - \int p_N \quad (3.46)$$

$$V = V_o - \int p_T = V_o + \Delta V \quad (3.47)$$

$$\Delta V = - \int p_T \quad (3.48)$$

$$M = M_o + \int V = M_o + \Delta M \quad (3.49)$$

$$\Delta M = \int V \quad (3.50)$$

The forces N_o , V_o e M_o are the fixed end forces and moments on the first node.

The variations of internal forces for the cases of uniform and triangular distributed loading, represented in figure 3.13, are as follows:

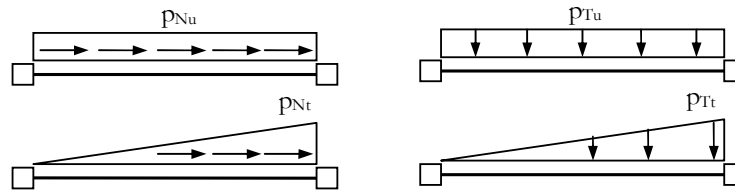


Figure 3.13. Distributed loads

$$\Delta N = -p_{Nu}z - \frac{p_{Nt}z^2}{2L} \quad (3.51)$$

$$\Delta V = +p_{Tu}z + \frac{p_{Tt}z^2}{2L} \quad (3.52)$$

$$\Delta M = V_o z + \frac{p_{Tu}z^2}{2} + \frac{p_{Tt}z^3}{6L} \quad (3.53)$$

The evaluation of each element stiffness matrix and fixed end forces and moments requires the definition of the shape functions for the axial and transversal displacement. Since the cross sections stiffness matrix was assumed constant along the length of each element, it is possible to use the exact solutions from the Strength of Materials using an auxiliary system of axis where the cross section stiffness matrix is diagonal.

Figure 3.14 shows both finite elements, the real bar centred in point P and the auxiliary bar, which has a diagonal stiffness matrix, centred in point G.

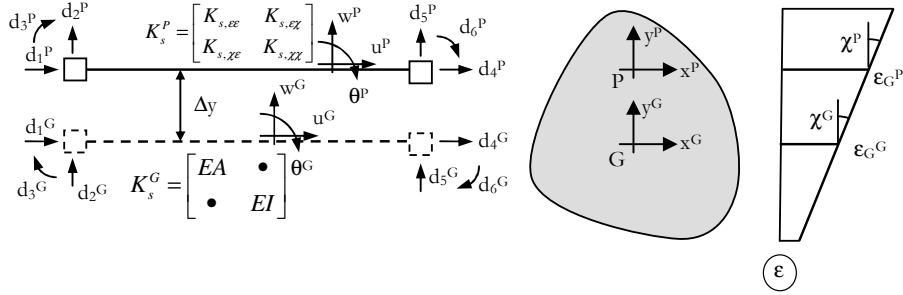


Figure 3.14. Linear bar finite element, auxiliary bar and cross section (cinematic variables)

The cinematic variables of the main and auxiliary bars can be related as follows:

$$\boldsymbol{\varepsilon}^G = \mathbf{B}_s \boldsymbol{\varepsilon}^P \quad (3.54)$$

$$\begin{bmatrix} \boldsymbol{\varepsilon}_G^G \\ \boldsymbol{\chi}^G \end{bmatrix} = \begin{bmatrix} 1 & -\Delta y \\ \bullet & 1 \end{bmatrix} \begin{bmatrix} \boldsymbol{\varepsilon}_G^P \\ \boldsymbol{\chi}^P \end{bmatrix} \quad (3.55)$$

$$\mathbf{d}^G = \mathbf{B}_e \mathbf{d}^P \quad (3.56)$$

$$\begin{bmatrix} d_1^G \\ d_2^G \\ d_3^G \\ d_4^G \\ d_5^G \\ d_6^G \end{bmatrix} = \begin{bmatrix} 1 & \bullet & -\Delta y & \bullet & \bullet & \bullet \\ \bullet & 1 & \bullet & \bullet & \bullet & \bullet \\ \bullet & \bullet & 1 & \bullet & \bullet & \bullet \\ \bullet & \bullet & \bullet & 1 & \bullet & -\Delta y \\ \bullet & \bullet & \bullet & \bullet & 1 & \bullet \\ \bullet & \bullet & \bullet & \bullet & \bullet & 1 \end{bmatrix} \begin{bmatrix} d_1^P \\ d_2^P \\ d_3^P \\ d_4^P \\ d_5^P \\ d_6^P \end{bmatrix} \quad (3.57)$$

$$\mathbf{u}^G = \mathbf{B}_u \mathbf{u}^P \quad (3.58)$$

$$\begin{bmatrix} u^G \\ w^G \\ \theta^G \end{bmatrix} = \begin{bmatrix} 1 & \bullet & -\Delta y \\ \bullet & 1 & \bullet \\ \bullet & \bullet & 1 \end{bmatrix} \begin{bmatrix} u^P \\ w^P \\ \theta^P \end{bmatrix} \quad (3.59)$$

Figure 3.15 shows both bars, the local and the auxiliary systems of axis on the cross section and the respective static variables.

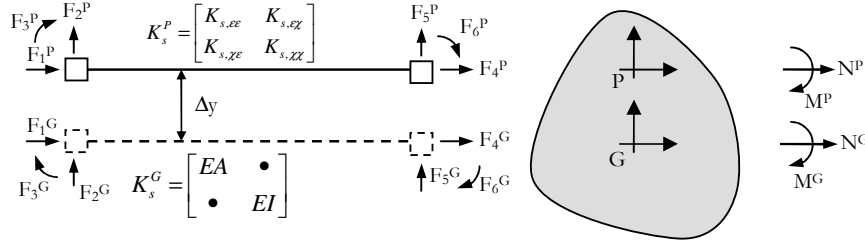


Figure 3.15 – Linear bar finite element, auxiliary bar and cross section (static variables)

The static variables of the main and auxiliary bars can be related as follows:

$$X^P = B_s^T X^G \quad (3.60)$$

$$\begin{bmatrix} N^P \\ M^P \end{bmatrix} = \begin{bmatrix} 1 & \bullet \\ -\Delta y & 1 \end{bmatrix} \begin{bmatrix} N^G \\ M^G \end{bmatrix} \quad (3.61)$$

$$F^P = B_e^T F^G \quad (3.62)$$

$$\begin{bmatrix} F_1^P \\ F_2^P \\ F_3^P \\ F_4^P \\ F_5^P \\ F_6^P \end{bmatrix} = \begin{bmatrix} 1 & \bullet & \bullet & \bullet & \bullet & \bullet \\ \bullet & 1 & \bullet & \bullet & \bullet & \bullet \\ -\Delta y & \bullet & 1 & \bullet & \bullet & \bullet \\ \bullet & \bullet & \bullet & 1 & \bullet & \bullet \\ \bullet & \bullet & \bullet & \bullet & 1 & \bullet \\ \bullet & \bullet & \bullet & -\Delta y & \bullet & 1 \end{bmatrix} \begin{bmatrix} F_1^G \\ F_2^G \\ F_3^G \\ F_4^G \\ F_5^G \\ F_6^G \end{bmatrix} \quad (3.63)$$

Considering the transformations of coordinates between both systems, the stiffness matrices at section level in both systems of axis can be related as follows:

$$X^G = K_s^G \epsilon^G \quad (3.64)$$

$$B_s^T X^G = B_s^T K_s^G B_s \epsilon^P \quad (3.65)$$

$$X^P = B_s^T K_s^G B_s \epsilon^P \quad (3.66)$$

$$K_s^P = B_s^T K_s^G B_s \quad (3.67)$$

A similar relationship can be established at the level of the finite element as follows:

$$K_e^P = B_e^T K_e^G B_e \quad (3.68)$$

The compatibility relationships allow relating the shape functions of both systems of axis as follows:

$$u^G = \varphi^G d^G \quad (3.69)$$

$$B_u u^P = \varphi^G B_e d^P \quad (3.70)$$

$$u^P = B_u^{-1} \varphi^G B_e d^P \quad (3.71)$$

$$\varphi^P = B_u^{-1} \varphi^G B_e \quad (3.72)$$

$$\varphi^P = \begin{bmatrix} 1 & \bullet & \Delta y \\ \bullet & 1 & \bullet \\ \bullet & \bullet & 1 \end{bmatrix} \begin{bmatrix} \varphi_{u1}^G & \varphi_{u2}^G & \varphi_{u3}^G & \varphi_{u4}^G & \varphi_{u5}^G & \varphi_{u6}^G \\ \varphi_{w1}^G & \varphi_{w2}^G & \varphi_{w3}^G & \varphi_{w4}^G & \varphi_{w5}^G & \varphi_{w6}^G \\ \dot{\varphi}_{w1}^G & \dot{\varphi}_{w2}^G & \dot{\varphi}_{w3}^G & \dot{\varphi}_{w4}^G & \dot{\varphi}_{w5}^G & \dot{\varphi}_{w6}^G \end{bmatrix} \begin{bmatrix} 1 & \bullet & -\Delta y & \bullet & \bullet & \bullet \\ \bullet & 1 & \bullet & \bullet & \bullet & \bullet \\ \bullet & \bullet & 1 & \bullet & \bullet & \bullet \\ \bullet & \bullet & \bullet & 1 & \bullet & -\Delta y \\ \bullet & \bullet & \bullet & \bullet & 1 & \bullet \\ \bullet & \bullet & \bullet & \bullet & \bullet & 1 \end{bmatrix} \quad (3.73)$$

For the auxiliary bar (G) the shape function, referred to the respective nodal displacements, are the exact solutions of the differential equation of linear bars:

$$\varphi_{u1}^G(z) = 1 - \frac{z}{L} = 1 - \zeta \quad (3.74)$$

$$\varphi_{u2}^G(z) = \varphi_{u3}^G(z) = 0 \quad (3.75)$$

$$\varphi_{u4}^G(x) = \frac{z}{L} = \zeta \quad (3.76)$$

$$\varphi_{u5}^G(z) = \varphi_{u6}^G(z) = 0 \quad (3.77)$$

$$\varphi_{w1}^G(z) = 0 \quad (3.78)$$

$$\varphi_{w2}^G(z) = 1 - 3\left(\frac{z}{L}\right)^2 + 2\left(\frac{z}{L}\right)^3 = 1 - 3\zeta^2 + 2\zeta^3 \quad (3.79)$$

$$\varphi_{w3}^G(z) = L \times \left[-\left(\frac{z}{L}\right) + 2\left(\frac{z}{L}\right)^2 - \left(\frac{z}{L}\right)^3 \right] = [-\zeta + 2\zeta^2 - \zeta^3] \times L \quad (3.80)$$

$$\varphi_{w5}^G(z) = 3\left(\frac{z}{L}\right)^2 - 2\left(\frac{z}{L}\right)^3 = 3\zeta^2 - 2\zeta^3 \quad (3.81)$$

$$\varphi_{w6}^G(z) = L \times \left[\left(\frac{z}{L}\right)^2 - \left(\frac{z}{L}\right)^3 \right] = [\zeta^2 - \zeta^3] \times L \quad (3.82)$$

$$\varphi^P = \begin{bmatrix} 1 & \bullet & \Delta y \\ \bullet & 1 & \bullet \\ \bullet & \bullet & 1 \end{bmatrix} \begin{bmatrix} \varphi_{u1}^G & \bullet & \bullet & \varphi_{u4}^G & \bullet & \bullet \\ \bullet & \varphi_{w2}^G & \varphi_{w3}^G & \bullet & \varphi_{w5}^G & \varphi_{w6}^G \\ \bullet & -\dot{\varphi}_{w2}^G & -\dot{\varphi}_{w3}^G & \bullet & -\dot{\varphi}_{w5}^G & -\dot{\varphi}_{w6}^G \end{bmatrix} \begin{bmatrix} 1 & \bullet & -\Delta y & \bullet & \bullet & \bullet \\ \bullet & 1 & \bullet & \bullet & \bullet & \bullet \\ \bullet & \bullet & 1 & \bullet & \bullet & \bullet \\ \bullet & \bullet & \bullet & 1 & \bullet & -\Delta y \\ \bullet & \bullet & \bullet & \bullet & 1 & \bullet \\ \bullet & \bullet & \bullet & \bullet & \bullet & 1 \end{bmatrix} \quad (3.83)$$

$$\varphi^P = \begin{bmatrix} \varphi_{u1}^G & -\Delta y \dot{\varphi}_{w2}^G & -\Delta y \varphi_{u1}^G - \Delta y \dot{\varphi}_{w3}^G & \varphi_{u4}^G & -\Delta y \dot{\varphi}_{w5}^G & -\Delta y \varphi_{u4}^G - \Delta y \dot{\varphi}_{w6}^G \\ \bullet & \varphi_{w2}^G & \varphi_{w3}^G & \bullet & \varphi_{w5}^G & \varphi_{w6}^G \\ \bullet & -\dot{\varphi}_{w2}^G & -\dot{\varphi}_{w3}^G & \bullet & -\dot{\varphi}_{w5}^G & -\dot{\varphi}_{w6}^G \end{bmatrix} \quad (3.84)$$

It can be observed that the difference between the shape functions of both systems of axis lies on the axial displacements.

$$\varphi_{u1}^P(z) = 1 - \frac{z}{L} = 1 - \zeta \quad (3.85)$$

$$\varphi_{u2}^P(z) = -\Delta y \dot{\varphi}_{w2}^G = \frac{\Delta y}{L} \times (6\zeta - 6\zeta^2) \quad (3.86)$$

$$\varphi_{u3}^P(z) = -\Delta y \varphi_{u1}^G - \Delta y \dot{\varphi}_{w3}^G = \Delta y \times (-3\zeta + 3\zeta^2) \quad (3.87)$$

$$\varphi_{u4}^P(z) = \frac{z}{L} = \zeta \quad (3.88)$$

$$\varphi_{u5}^P(z) = -\Delta y \dot{\varphi}_{w5}^G = \frac{\Delta y}{L} \times (-6\zeta + 6\zeta^2) \quad (3.89)$$

$$\varphi_{u6}^P(z) = -\Delta y \varphi_{u3}^G - \Delta y \dot{\varphi}_{w6}^G = \Delta y \times (-3\zeta + 3\zeta^2) \quad (3.90)$$

Once obtained the shape functions it is possible to evaluate the stiffness matrix and fixed end forces and moments in the local system of axis (P) The only variable not evaluated yet is the distance between both bars. This can be easily performed considering the respective cross section stiffness matrices, as follows:

$$K_s^P = B_s^T K_s^G B_s \quad (3.91)$$

$$\begin{bmatrix} K_{s,\epsilon\epsilon} & K_{s,\epsilon\chi} \\ K_{s,\chi\epsilon} & K_{s,\chi\chi} \end{bmatrix} = \begin{bmatrix} 1 & \bullet \\ -\Delta y & 1 \end{bmatrix} \begin{bmatrix} EA & \bullet \\ \bullet & EI \end{bmatrix} \begin{bmatrix} 1 & -\Delta y \\ \bullet & 1 \end{bmatrix} = \begin{bmatrix} EA & -\Delta y EA \\ -\Delta y EA & EI + \Delta y^2 EA \end{bmatrix} \quad (3.92)$$

Therefore it can be concluded that:

$$\begin{cases} EA = K_{s,\epsilon\epsilon} \\ -\Delta y EA = K_{s,\epsilon\chi} = K_{s,\chi\epsilon} \\ EI + \Delta y^2 EA = K_{s,\chi\chi} \end{cases} \quad (3.93)$$

The distance between both bars can be obtained as

$$\Delta y = \frac{-K_{s,\epsilon\chi}}{K_{s,\epsilon\epsilon}} \quad (3.94)$$

The flexural stiffness in the auxiliary system of axis is obtained in a manner similar to the application of the theorem of Lagrange-Steiner:

$$EI = K_{s,\chi\chi} - \Delta y^2 EA \quad (3.95)$$

It is therefore possible to evaluate the stiffness matrix for the finite element as well as the fixed end forces and moments and internal forces along the length of the bar. The main results and sequence of calculation are the following:

1. Distance to the auxiliary system of axis and respective axial and flexural stiffness:

- a. $\Delta y = \frac{-K_{s,\epsilon\chi}}{K_{s,\epsilon\epsilon}}; \quad EA = K_{s,\epsilon\epsilon}; \quad EI = K_{s,\chi\chi} - \Delta y^2 EA;$

2. Stiffness matrix:

$$\begin{aligned}
 \text{a. } K_e^G &= \begin{bmatrix} \frac{EA}{L} & \bullet & \bullet & -\frac{EA}{L} & \bullet & \bullet \\ \bullet & \frac{12EI}{L^3} & \frac{-6EI}{L^2} & \bullet & \frac{-12EI}{L^3} & \frac{-6EI}{L^2} \\ \bullet & \frac{-6EI}{L^2} & \frac{4EI}{L} & \bullet & \frac{6EI}{L^2} & \frac{2EI}{L} \\ -\frac{EA}{L} & \bullet & \bullet & \frac{EA}{L} & \bullet & \bullet \\ \bullet & \frac{-12EI}{L^3} & \frac{6EI}{L^2} & \bullet & \frac{12EI}{L^3} & \frac{6EI}{L^2} \\ \bullet & \frac{-6EI}{L^2} & \frac{2EI}{L} & \bullet & \frac{6EI}{L^2} & \frac{4EI}{L} \end{bmatrix} \\
 \text{b. } K_e^P = B_e^T K_e^G B_e &= \begin{bmatrix} \frac{EA}{L} & \bullet & -\Delta y \frac{EA}{L} & -\frac{EA}{L} & \bullet & \Delta y \frac{EA}{L} \\ \bullet & \frac{12EI}{L^3} & \frac{-6EI}{L^2} & \bullet & \frac{-12EI}{L^3} & \frac{-6EI}{L^2} \\ -\Delta y \frac{EA}{L} & \frac{-6EI}{L^2} & \frac{4EI}{L} + \Delta y^2 \frac{EA}{L} & \Delta y \frac{EA}{L} & \frac{6EI}{L^2} & \frac{2EI}{L} - \Delta y^2 \frac{EA}{L} \\ -\frac{EA}{L} & \bullet & \Delta y \frac{EA}{L} & \frac{EA}{L} & \bullet & -\Delta y \frac{EA}{L} \\ \bullet & \frac{-12EI}{L^3} & \frac{6EI}{L^2} & \bullet & \frac{12EI}{L^3} & \frac{6EI}{L^2} \\ \Delta y \frac{EA}{L} & \frac{-6EI}{L^2} & \frac{2EI}{L} - \Delta y^2 \frac{EA}{L} & -\Delta y \frac{EA}{L} & \frac{6EI}{L^2} & \frac{4EI}{L} + \Delta y^2 \frac{EA}{L} \end{bmatrix}
 \end{aligned}$$

3. Fixed end forces and moments (obtained by direct integration – see figure 3.16):

$$\text{a. } X^{FIX} = \begin{bmatrix} -\frac{p_{Nu}L}{2} \\ -p_{Nu}\Delta y \\ \frac{p_{Nu}\Delta yL}{2} \\ -\frac{p_{Nu}L}{2} \\ \frac{p_{Nu}\Delta y}{2} \\ \frac{p_{Nu}\Delta yL}{2} \\ 2 \end{bmatrix} + \begin{bmatrix} -\frac{p_{Nt}L}{6} \\ -\frac{p_{Nt}\Delta y}{2} \\ \frac{p_{Nt}\Delta yL}{4} \\ -\frac{p_{Nt}L}{3} \\ \frac{p_{Nt}\Delta y}{2} \\ \frac{p_{Nt}\Delta yL}{4} \\ 4 \end{bmatrix} + \begin{bmatrix} \bullet \\ \frac{p_{Tu}L}{2} \\ -\frac{p_{Tu}L^2}{12} \\ \bullet \\ \frac{p_{Tu}L}{2} \\ \frac{p_{Tu}L^2}{12} \\ 12 \end{bmatrix} + \begin{bmatrix} \bullet \\ \frac{3p_{Tt}L}{20} \\ -\frac{p_{Tt}L^2}{30} \\ \bullet \\ \frac{7p_{Tt}L}{20} \\ \frac{p_{Tt}L^2}{20} \\ 20 \end{bmatrix}$$

4. Deformations:

$$a. \quad \underline{\underline{\mathcal{E}}}_{nodal}^P = \underline{\underline{L}} \underline{\underline{\varphi}}^P \underline{\underline{d}}^P$$

$$b. \quad \underline{\underline{L}} \underline{\underline{\varphi}}^P = \begin{bmatrix} \frac{\partial}{\partial z} & \bullet & \bullet \\ \bullet & -\frac{\partial^2}{\partial z^2} & \bullet \end{bmatrix} \times \begin{bmatrix} \varphi_{u1}^G & -\Delta y \dot{\varphi}_{w2}^G & -\Delta y \dot{\varphi}_{u1}^G - \Delta y \dot{\varphi}_{w3}^G & \varphi_{u4}^G & -\Delta y \dot{\varphi}_{w5}^G & -\Delta y \dot{\varphi}_{u4}^G - \Delta y \dot{\varphi}_{w6}^G \\ \bullet & \varphi_{w2}^G & \varphi_{w3}^G & \bullet & \varphi_{w5}^G & \varphi_{w6}^G \\ \bullet & -\dot{\varphi}_{w2}^G & -\dot{\varphi}_{w3}^G & \bullet & -\dot{\varphi}_{w5}^G & -\dot{\varphi}_{w6}^G \end{bmatrix}$$

$$c. \quad \underline{\underline{L}} \underline{\underline{\varphi}}^P = \begin{bmatrix} \dot{\varphi}_{u1}^G & -\Delta y \ddot{\varphi}_{w2}^G & -\Delta y \dot{\varphi}_{u1}^G - \Delta y \ddot{\varphi}_{w3}^G & \varphi_{u4}^G & -\Delta y \ddot{\varphi}_{w5}^G & -\Delta y \dot{\varphi}_{u4}^G - \Delta y \ddot{\varphi}_{w6}^G \\ & -\ddot{\varphi}_{w2}^G & -\ddot{\varphi}_{w3}^G & & -\ddot{\varphi}_{w5}^G & -\ddot{\varphi}_{w6}^G \end{bmatrix}$$

$$d. \quad \underline{\underline{\mathcal{E}}}_{nodal}^P = \begin{bmatrix} \dot{\varphi}_{u1}^G d_1^P - \Delta y \ddot{\varphi}_{w2}^G d_2^P + (-\Delta y \dot{\varphi}_{u1}^G - \Delta y \ddot{\varphi}_{w3}^G) d_3^P + \varphi_{u4}^G d_4^P - \Delta y \ddot{\varphi}_{w5}^G d_5^P + (-\Delta y \dot{\varphi}_{u4}^G - \Delta y \ddot{\varphi}_{w6}^G) d_6^P \\ -\ddot{\varphi}_{w2}^G d_2^P - \ddot{\varphi}_{w3}^G d_3^P - \ddot{\varphi}_{w5}^G d_5^P - \ddot{\varphi}_{w6}^G d_6^P \end{bmatrix}$$

$$e. \quad \underline{\underline{\mathcal{E}}}_{nodal}^P = \begin{bmatrix} \underline{\underline{\mathcal{E}}}_G^P \\ \underline{\underline{\mathcal{X}}}_P^P \end{bmatrix}_{nodal} = \begin{bmatrix} \frac{-1}{L} d_1^P + \frac{\Delta y(6-12\zeta)}{L^2} d_2^P + \frac{\Delta y(-3+6\zeta)}{L} d_3^P + \frac{1}{L} d_4^P + \frac{\Delta y(-6+12\zeta)}{L^2} d_5^P + \frac{\Delta y(-3+6\zeta)}{L} d_6^P \\ \frac{6-12\zeta}{L^2} d_2^P + \frac{-4+6\zeta}{L} d_3^P + \frac{-6+12\zeta}{L^2} d_5^P + \frac{-2+6\zeta}{L} d_6^P \end{bmatrix}$$

5. Internal forces and moments:

$$a. \quad \underline{\underline{X}}_{nodal} = \underline{\underline{K}}_s \times \underline{\underline{L}} \times \underline{\underline{\varphi}} \times \underline{\underline{d}} = \underline{\underline{K}}_s \times \underline{\underline{\mathcal{E}}}_{nodal}$$

$$b. \quad \begin{bmatrix} N \\ M \end{bmatrix}_{nodal} = \begin{bmatrix} K_{s,\varepsilon\varepsilon} & K_{s,\varepsilon\chi} \\ K_{s,\chi\varepsilon} & K_{s,\chi\chi} \end{bmatrix} \times \begin{bmatrix} \underline{\underline{\mathcal{E}}}_G^P \\ \underline{\underline{\mathcal{X}}}_P^P \end{bmatrix}_{nodal}$$

$$c. \quad V_{nodal} = \frac{dM_{nodal}}{dz} = K_{\chi\varepsilon} \frac{d\underline{\underline{\mathcal{E}}}_G^P}{dz} + K_{\chi\chi} \frac{d\underline{\underline{\mathcal{X}}}_P^P}{dz}$$

$$d. \quad \frac{d\underline{\underline{\mathcal{X}}}_P^P}{dz} = -\frac{12}{L^3} d_2^P + \frac{6}{L^2} d_3^P + \frac{12}{L^3} d_5^P + \frac{6}{L^2} d_6^P$$

$$e. \frac{d\varepsilon_G^p}{dz} = \frac{-12\Delta y}{L^3}d_2^p + \frac{6\Delta y}{L^2}d_3^p + \frac{12\Delta y}{L^3}d_5^p + \frac{6\Delta y}{L^2}d_6^p = \frac{d\chi^p}{dz}\Delta y$$

$$f. N_o = \frac{p_{Nu}L}{2} + \frac{p_{Nt}L}{6}$$

$$g. V_o = p_{Nu}\Delta y + \frac{p_{Nt}\Delta y}{2} - \frac{p_{Tu}L}{2} - \frac{3p_{Tt}L}{20}$$

$$h. M_o = \frac{-p_{Nu}\Delta yL}{2} - \frac{p_{Nt}\Delta yL}{4} + \frac{p_{Tu}L^2}{12} + \frac{p_{Tt}L^2}{30}$$

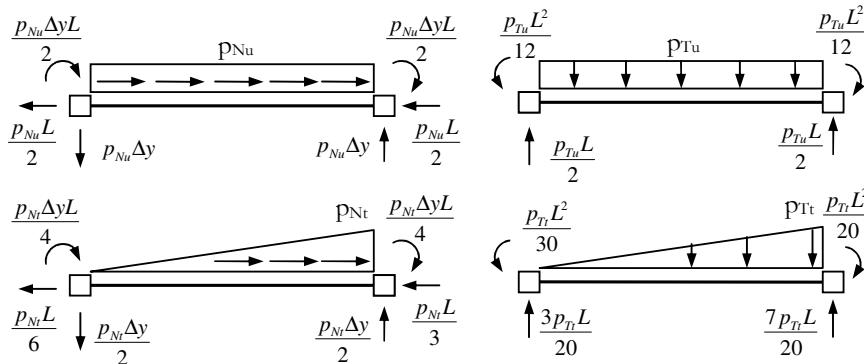


Figure 3.16. Fixed end forces and moments

3.5 OUTPUT

The output of the program comprises the deformed shape of the structure, diagrams of bending moments, curvatures and extensions of the centre of gravity of gross concrete sections. The following figures show an example, in which some plastic hinges developed at the extremities of a column.

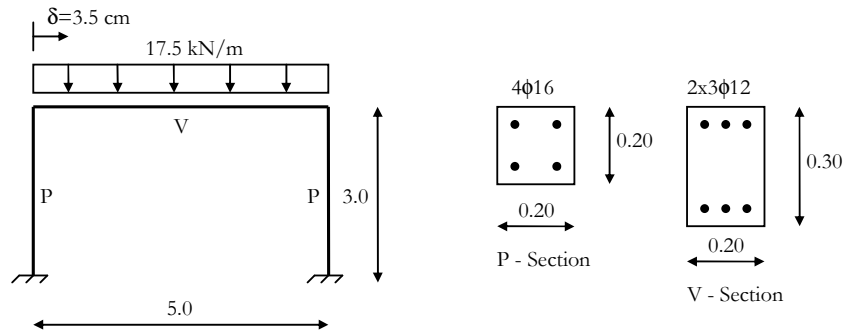
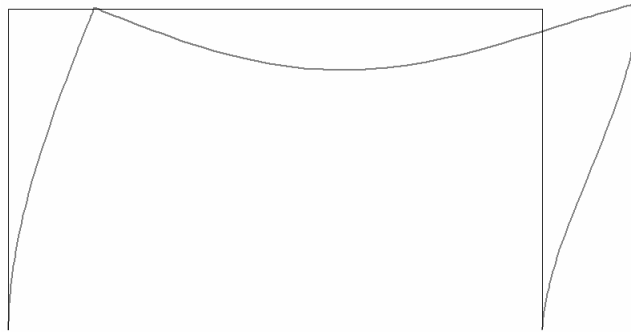
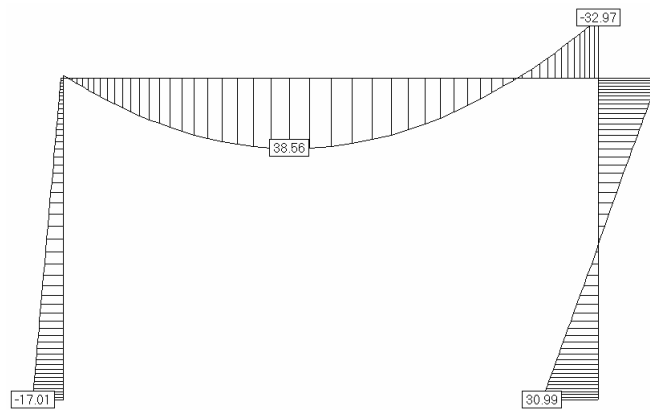


Figure 3.17. Example structure



Deformed shape



Bending moment diagram (kNm)

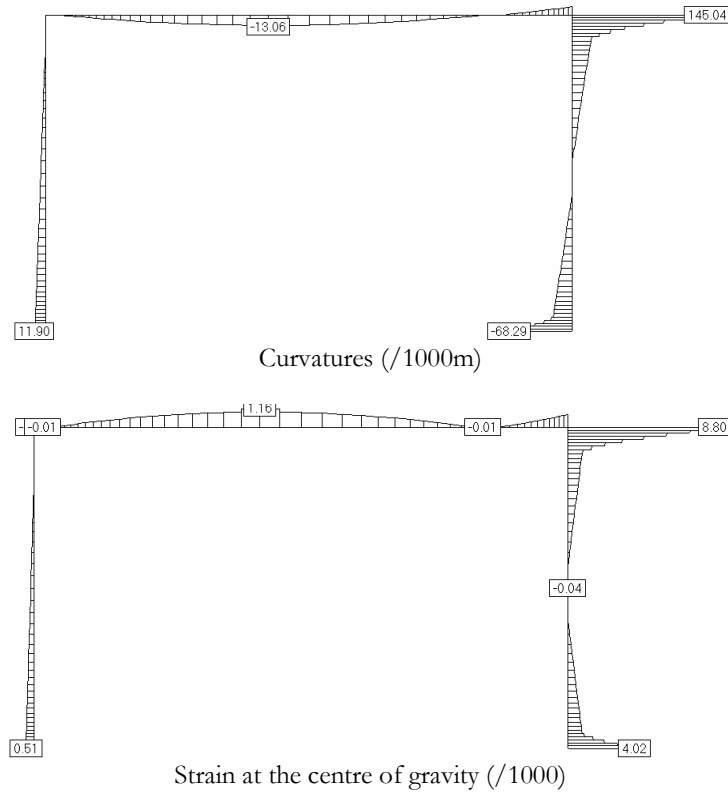


Figure 3.18. Example of the output of the programme

4. SEISMIC CONCEPTION AND METHODOLOGY OF ANALYSIS

4.1 INTRODUCTION

In this chapter a design methodology and seismic conception criteria for large reinforced concrete underground structures in soft soils are presented. The dynamic analysis of the soil/structure system allowed identifying two qualitatively different types of configurations of vibration modes:

1. those associated with horizontal displacements of the structure to the same side at each horizontal level and which are strongly conditioned by the dynamic behaviour of the soil
2. those associated with vertical displacements of the structure, eventually associated with small horizontal displacements of the perimeter walls to opposite sides.

The soil on the sides of the structure has very little influence on the configuration and frequency of the second group of modes, therefore it does not contribute to the resistance to the inertia forces these modes generate on the structure that must be resisted by the structure itself. Therefore the effects of these modes must be evaluated by the usual design procedures. The situation with the first group of modes is exactly the opposite: the configuration and frequency of the first group of modes is very strongly determined by the soil dynamic behaviour, and the inertia forces generated in the structure by these modes, essentially in the horizontal direction, can be directly transferred to the surrounding soil at the same level. The effect of these modes is qualitatively different and is equivalent to the imposition of horizontal displacements fields along the height of the structure by the surrounding soil. The effect of these modes is the most relevant and led to the observed damage in tube stations during the Kobe earthquake.

The discussion of chapter 2 has shown that, in general, the seismic design of large underground structures in soft soils must consist essentially on providing relative horizontal deformation capacity along the height to the flexible alignments of the structure, while maintaining the resistance to permanent loads. A possible alternative solution to protect underground structures from externally imposed soil deformations would be by means of treating the soil on a reasonable extension on both sides of the

structure in order to avoid that soil deformations in zones more far away from the station are transferred to the structure. For this purpose it would be necessary to treat the soil on a reasonable extension on both sides of the station, a solution almost equivalent to build a dam on either side of the station. This solution, besides being costly, would in general not be feasible in urban areas. However if the structure is not able to withstand the imposed displacements, it may be necessary to treat the soil to reduce (not avoid) soil displacements in the vicinity of the structure, leading to a solution that couples both solutions to the problem. This may be feasible within some limits.

This work aims at the study of the first approach, the provision of deformation capacity to the structure.

4.2 BEHAVIOUR OF REINFORCED CONCRETE ELEMENTS UNDER IMPOSED DISPLACEMENTS

4.2.1 Redefinition of Basic Concepts

According to current design procedures, as embodied in most codes of practice, structural designers would analyse an elastic soil/structure model in which soil properties were previously calibrated for the expected soil deformations to account for the soil stiffness degradation associated with increases in the amplitude of deformation. The evaluation of seismic internal action-effects in the structure would be done by dividing the respective values obtained from the linear analysis by the chosen q-factor. Alternatively a linear elastic model of the structure, without the surrounding soil, would be analysed imposing the free-field soil profile of horizontal displacements along the height to the structure, followed by the evaluation of the internal seismic action-effects by dividing the respective results by the q-factor. Both situations are equivalent to design the structure to resist (transfer to the foundations) the horizontal forces that would be necessary to impose the prescribed displacement field in the linear elastic model divided by the q-factor.

However this is not what happens in the real structure that does not need to transfer any inertia forces to the foundations. The reason for this contradiction lies on the fact that the internal action-effects obtained from the linear elastic analysis divided by the q-factor may not exist because there may not exist a constant ratio between internal forces and deformations, for instances between bending moments and curvatures, as assumed in the linear analysis. Even though the assumption of that constant ratio may be a reasonable approximation for structures working at stresses reasonably below the yield limits, it is not the case for ductile reinforced concrete structures under extreme actions that force the elements to go well into the post-yield range. This can be easily understood if we consider the simple example column built-in at both extremities subjected to a relative

horizontal displacement between both extremities, δ , as schematically represented in figure 4.1.

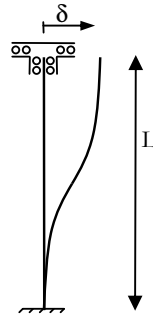


Figure 4.1. Schematic representation of a built-in column subjected to imposed horizontal displacement

If a given distribution of curvatures along the height of the column is assumed, it is possible to relate the curvatures at the end sections with the imposed displacement. Thus, the curvatures at those sections can also be considered to be externally imposed on the column cross-sections. Assuming for instances that there is no axial force and a given distribution of flexural reinforcement, it is possible to make an estimation of the curvature at yielding, as its variation with the amount of flexural reinforcement is reduced (this will be confirmed later in this chapter). Knowing the curvature and the neutral axis depth and, the strain diagram on the cross-section can be directly determined, as shown in figure 4.2. Therefore, knowing the constitutive relationships for steel and concrete, the stress state in the steel and concrete can be easily evaluated, as schematically shown in figure 4.2.

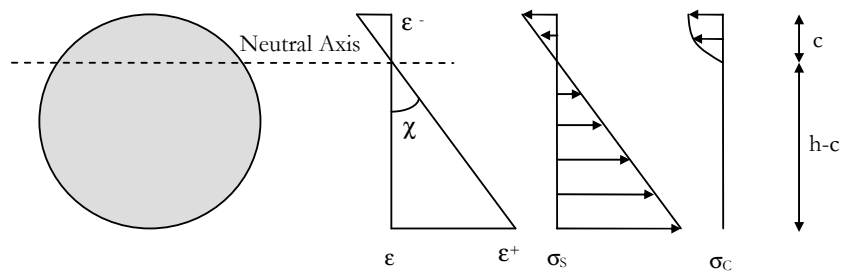


Figure 4.2. Evaluation of strains and stresses

It is therefore possible, for a given amount of flexural reinforcement, to evaluate the bending moment at the cross-section with simple static procedures, using equation 4.1.

$$M = \int_{\Omega} \sigma y d\Omega \quad (4.1)$$

Even though the above considerations are an approximation to real reinforced concrete behaviour, several main features of the above situation should be emphasized:

1. the maximum cross section strains at yielding depend essentially on the section dimension on the bending plane (perpendicular to the neutral axis);
2. as a result of the previous point, the strains at yielding do not vary significantly with the amount of flexural reinforcement;
3. the yield curvature and strain diagram are almost independent of the amount of flexural reinforcement (for $N=0$);
4. the yield bending moment at the cross section is output and not input of section analysis (under imposed displacements).

Note that the mentioned features are qualitatively different of current design procedures, in which:

1. the bending moment is input for section analysis;
2. the amount of flexural reinforcement is evaluated in order to provide the necessary flexural strength;
3. the curvature and strains are a function of the applied bending moment and amount of flexural reinforcement.

If the curvature ductility demand does not exceed the available curvature ductility, the amount of flexural reinforcement necessary to resist the imposed displacement is arbitrary, and can be set equal to zero, regardless of the imposed curvature. In this situation the design of the example column to withstand imposed horizontal displacements would not require to add any flexural reinforcement to the one that would be necessary to resist other actions. The linear analysis, by wrongly associate a not nil bending moment to an imposed curvature would lead to the design of the cross-sections for a bending moment that in fact is not acting on the cross-section.

Current code procedures for structures that develop above ground are in general inadequate to deal with this type of problem. This is related with the origins of modern earthquake engineering. At the early stages of modern earthquake engineering it was necessary to adopt a way of modelling seismic actions that civil engineers would know how to deal with at the time. Since civil engineers were used to design structures to resist

applied forces, the first codes to consider the effects of seismic actions modelled this action on buildings and bridges essentially by sets of horizontal forces equivalent to the inertia forces induced by earthquakes. Safety checkings were performed essentially by ensuring that the resisting static internal forces (bending and torsion moments, shear and axial forces) were superior to the correspondent action-effects, a safety checking format still embodied in codes of practice. Other relevant features of structural behaviour known to be important for the seismic response, as the structures ductility and energy dissipation capacity, were accounted for indirectly. At the initial stages these effects could be considered implicit in the seismic coefficients used to evaluate earthquake equivalent inertia forces, and, at a later stage, by means of global factors used to reduce earthquake static action-effects obtained by means of linear analysis, the behaviour factors (q-factor in EC8). These procedures allowed maintaining the safety checking format in terms of comparing resisting static effects with the same effects induced by the applied actions, which was very convenient for practical purposes. However it had a negative effect as structural designers continued till today to look at structural design on the optic of evaluating amounts of reinforcement to resist static action-effects. This practice contributed to hide the importance of other relevant design parameters and to avoid that designers would get an adequate perception of what really is at stake.

In the case of underground structures the factor that is really the most important for the seismic performance of the structure is the deformation capacity, which is strongly associated with the ductility in the case of reinforced concrete structures. This renders current code procedures completely inadequate, because there are no inertia forces to be transferred to the foundations and because comparing static action-effects with the corresponding resistances is also an inadequate safety verification format. This needs to be done explicitly in terms of comparing the available ductility with the ductility demand. Even recently developed displacement based design procedures are not adequate for this purpose, as to a given displacement level that a structure must undergo associate a given stiffness and inertia forces. Underground structures do not need to have any stiffness to withstand, or control, the displacements that may be forced to undergo under seismic actions. Those displacements are essentially imposed and restricted by the surrounding soil and therefore do not need to be controlled by the structure. And even though to increase the stiffness of the structure may contribute to reduce the displacements, it is inefficient to increase the structural stiffness for this purpose. This is because the reduction on the imposed displacements will in general be smaller than the reduction of the structure deformation capacity that results from the increase in dimensions necessary to increase stiffness.

Therefore underground structures do not need to be provided with stiffness and resistance to horizontal forces, as above ground structures need. This is mathematically equivalent to allow the q-factor for underground structures to be infinite. Obviously the

concept of infinite behaviour factor does not make sense. It only highlights the inadequacy of current code methodologies derived for structures that develop above ground, based on comparing action-effects with and resisting static internal forces, for the safety evaluation of underground structures under earthquake actions.

The example of the built-in column can be used to illustrate most of the concepts just discussed. Two compact cross-sections are considered, as shown in figure 4.3. The main difference is that in section A the flexural reinforcement is distributed between the extreme fibres and the centre of gravity of the section but with more area of reinforcement near the extreme fibres, while in section B all the flexural reinforcement is concentrated near the extreme fibres (for bending around the X axis). The constitutive relationships considered for steel and concrete, are shown in figure 4.4. The steel ultimate strain was assigned a value higher than average in order to avoid triggering fracture of the steel, very seldom observed. The remaining numerical values of the variables that define the steel and concrete constitutive relationships are plausible design values of those variables and do not intend to represent any particular situation. Table 4.1 presents the values of these variables. The concrete tensile strength and the concrete cover were disregarded. The concrete cover was considered to be 6cm thick, measured from the concrete face to the axis of the closest layer of steel bars. The areas of the steel bars were considered concentrated at the centre of the respective sections. The concrete constitutive relationship for concrete simulates confined concrete. It is widely known that confined concrete possesses more ductility than plain concrete, which is essentially a brittle material. These features are qualitatively highlighted in figure 4.5 that shows the qualitative difference between the stress-strain curves for plain concrete and concrete confined in several ways. The steel hardening stiffness was disregarded, as indicated in table 4.1, and its influence will be discussed in more detail later in this chapter.

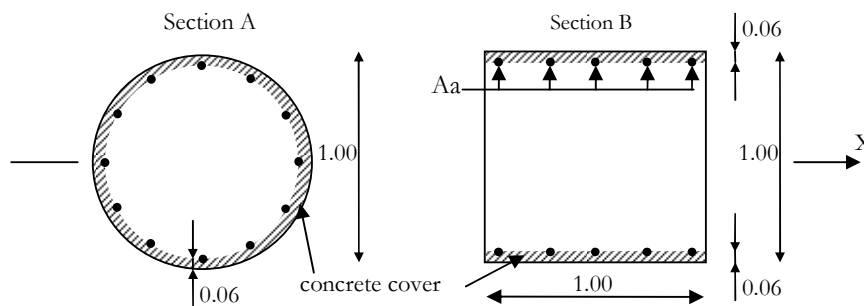


Figure 4.3. Example cross-sections

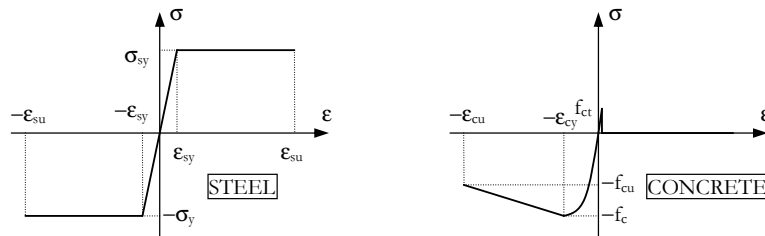


Figure 4.4. Constitutive relationships for steel and concrete

Table 4.1. Material properties

Steel

ϵ_{sy} (‰)	ϵ_{su} (‰)	σ_{sy} [MPa]
2.175	200	435

Concrete

ϵ_{cy} (‰)	ϵ_{cu} (‰)	f_c [MPa]	f_{cu} [MPa]	f_{ct} [MPa]
2.0	15.0	35	25	0

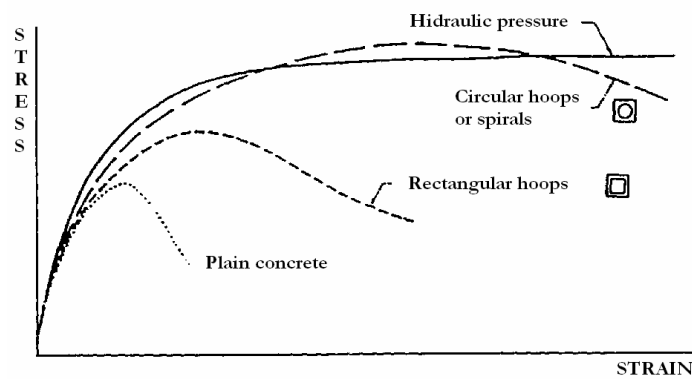


Figure 4.5. Qualitative difference between the constitutive relationships for plain and confined concrete (adapted from CEB, [1983])

For each section three different cases regarding the amounts of flexural reinforcement were considered corresponding to the amounts of tensile reinforcement (A_a in figure 4.3) for section B indicated in table 4.2

Table 4.2. Amounts of tensile reinforcement

	Case 1	Case 2	Case 3
A_a (cm ²)	20	50	125

For the circular section (A) A_a represents half the total reinforcement. Figure 4.6 shows the monotonic moment-curvature relationships for both sections and different amounts of flexural reinforcement, considering there is no axial force.

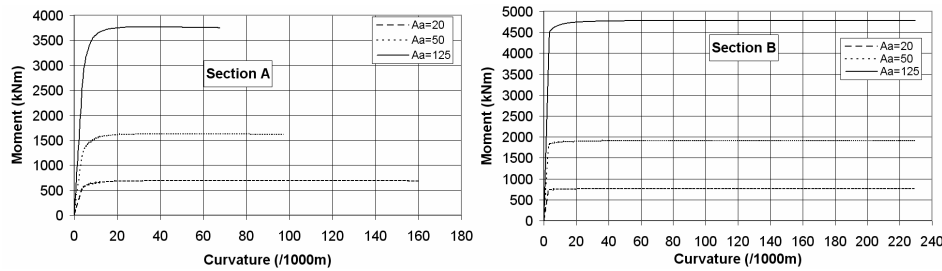


Figure 4.6. Moment-curvature relationships for example sections

In sections where yielding is progressive, as section A, yielding is defined as the point of first yielding of the flexural reinforcement. Rupture is defined as the attainment of the ultimate strain at any point of the section (excluding unconfined concrete) in either material. Since ϵ_{cu} is much inferior to ϵ_{su} , in general rupture is triggered at the concrete in compression. However that is not the case for section B, as the depth of the compressive zone is very small due to the concentration of compressive flexural reinforcement near the edge of the section. Thus, the length of the part of the cross section under tensile axial strains is similar in all the three cases and sufficiently higher than the depth of the compressive zone to trigger rupture by fracture of the steel. Therefore, the ultimate curvature is very similar for the three cases. However it should be emphasized that this situation is not very common as the design of section B represents an extreme situation in terms of design practice. Therefore section A will be used as the standard one in this study. Table 4.3 summarises the values of some variables at the yield and rupture points for both sections.

Table 4.3. Results at yielding and rupture.

Circular section A

Aa (cm ²)	χ_y (/1000m)	χ_u (/1000m)	c_y (m)	c_u (m)	M_y (kNm)	M_u (kNm)	$\frac{EI_{sec}}{A_a}$ (MN)	$\frac{M_y}{A_a}$ (kN/m)	$\frac{M_u}{A_a}$ (kN/m)
20	3.104	160.535	0.179	0.093	472.24	685.89	76.07	236 120	342 945
50	3.391	97.238	0.239	0.154	1108.90	1615.89	65.40	221 780	323 178
125	3.772	67.577	0.303	0.221	2604.85	3751.29	55.25	208 388	300 103

Square section B

Aa (cm ²)	χ_y (/1000m)	χ_u (/1000m)	c_y (m)	c_u (m)	M_y (kNm)	M_u (kNm)	$\frac{EI_{sec}}{A_a}$ (MN)	$\frac{M_y}{A_a}$ (kN/m)	$\frac{M_u}{A_a}$ (kN/m)
20	2.870	229.029	0.122	0.008	716.28	765.36	124.78	358 140	382 680
50	3.105	229.335	0.179	0.009	1789.92	1914.05	115.29	357 984	382 810
125	3.444	229.641	0.248	0.009	4415.22	4785.02	102.56	353 218	382 802

c – depth of the compressive zone

The results indicate that despite the large differences on the amounts of flexural reinforcement, and therefore on the flexural capacity, the differences on the yield curvature are reduced. For instances to an increase of 525% on the amount of flexural reinforcement from case 1 to case 3 (associated with similar increases in flexural capacity) correspond increases of only 21% on the yield curvatures. These variations are due to the increase in the depth of the compressive zone at yielding for the sections with more flexural reinforcement. This leads to an equal reduction of the depth of the zone under axial tensile strains (a reduction much smaller in relative terms, as the depth of the compressive zone is smaller) and therefore to a small increases of the yield curvature, as shown in figure 4.7.

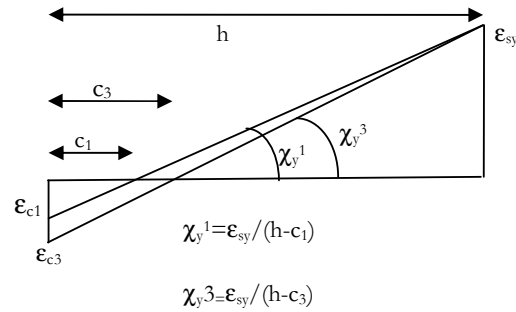


Figure 4.7. Variation of the yield curvature with the depth of the compressive zone

Therefore it can then be concluded that in the absence of axial force the yield curvature is essentially a function of the steel yield strain and section geometry, and is almost independent of the amount of flexural reinforcement. However, table 4.3 indicates that the bending moments (M_y and M_u) as well as the secant flexural stiffness at yielding (EI_y) vary almost proportionally with the amount of flexural reinforcement. This is schematically explained in figure 4.8.

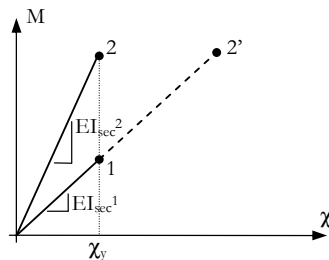


Figure 4.8. Schematic representation of change in the yield moment and yield curvature by increasing the flexural reinforcement

Point 1 represents a section yield point. If for instances the flexural reinforcement was duplicated, the flexural capacity would increase in such a way that, if the flexural stiffness was constant as assumed in linear analysis, the new situation would be represented by point 2'. In fact what happens is that the flexural capacity increases but the curvature almost does not increase and the point representative of the new situation is point 2 and not 2'. This clearly contradicts the concept of a constant stiffness independent of the amount of flexural reinforcement assumed in linear analysis.

The results also indicate that the ultimate curvature of section A is reasonably influenced by the amount of flexural reinforcement, while for section B the ultimate curvature is almost independent of the amount of flexural reinforcement. This difference is due to the fact that the types of rupture of both sections are qualitatively different, and to the different distribution of flexural reinforcement. In fact section B suffers rupture by the steel, and therefore the ultimate curvature is equal to $\chi_u = \epsilon_{su} / (h - c_u)$, with “h” being the length of the cross section (as defined in figure 4.7) and “c” the depth of the compressive zone. Due to the symmetry, the concentration of the compressive reinforcement near the edge of the section and the inexistence of compressive axial force, almost all the compressive force is taken by the steel. Therefore the depth of the compressive zone is very small and varies very little at rupture, leading to low concrete strains and rupture by the steel at similar ultimate curvatures for the three cases. The yield curvature varies more than the ultimate curvature for the same sections (B) due to the fact that at the initiation of flexural yielding (in tension) the compressive reinforcement has not yielded yet and its maximum capacity is not mobilized. This leads to a higher part of the compressive force to be taken by the concrete in compression, yielding higher depths of the compressive zone than the ones registered at rupture. Regarding section A, the variations in the yield curvature are also due to the variations on the depth of the compressive zone. However these are higher than for section B due to the higher contribution of concrete to resist the compressive force associated to the lower concentration of flexural reinforcement near the compressive edge of the section. The different amounts of flexural reinforcement also have an influence on the depth of the compressive zone at rupture, with an higher effect on the ultimate curvature χ_u . This is because $\chi_u = \epsilon_{cu} / c_u$ if failure is triggered by crushing of the concrete. Therefore, since $c < h - c$ a certain variation in the depth of the compressive zone has an higher influence on the ultimate curvature than on the yield curvature, leading to larger variations on the ultimate curvature between the three cases considered for section A. If the rupture of section B was not triggered by steel fracture and would take place by crushing of concrete the ultimate curvature would vary due to variations on the position of the neutral axis. However these variations would be lower than for section A, as the concentration of reinforcement near the compressive edge of the section would increase the contribution of steel to take the compressive force, decreasing the depth of the compressive zone. Anyway the concentration of the compressive reinforcement close to the edge of the section would always be a positive factor in what regards the section ultimate deformation capacity.

In a structure that develops above ground the extension of flexural yielding, one of the factors that influences damage, varies as a function of the adopted q-factor. The designer may even avoid yielding, designing the structure to withstand earthquake effects in the linear range by adopting $q=1$. However that is impossible for a structure in which the curvatures are imposed by external causes, as in the absence of axial force, the yield curvatures are almost independent of the amount of flexural reinforcement. Figure 4.8

clearly shows that if a curvature higher than the yield curvature is imposed on a section, it is not the increase of its flexural capacity (that could result from adopting q -factor equal to 1, lower than in a previous analysis) that will avoid yielding.

The example columns, represented in figure 4.1, with constant-cross section and a length “ L ” of 12m, were subjected to three levels of imposed relative horizontal displacement (δ) between its extremities: the yield displacement for case 1 (the lowest of the three), δ_y , $2.5\delta_y$ and $6\delta_y$, to which correspond displacements of 74.4mm, 186.0mm and 446.4mm respectively. The only difference to the previous analysis was the steel constitutive relationship: the hardening stiffness E_h was considered to be 2% of the elastic stiffness E_s , in order to allow for the spread of plasticity, and an upper limit for the steel stress of $\sigma_u=1.3\sigma_y$ was established, after which the steel tangent stiffness drops to zero. This yielded a trilinear stress-strain relationship for steel, as shown in figure 4.9. It is assumed that shear capacity is always superior to the shear demand and shear deformations can be disregarded as compared to flexural deformations.

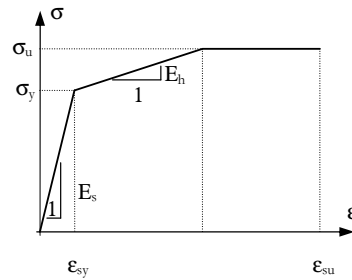
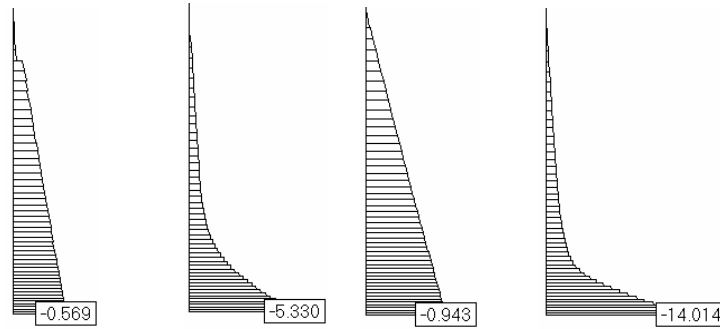


Figure 4.9. Trilinear stress-strain relationship for steel

Figure 4.10 shows the maximum concrete compressive strain ϵ_{max}^c in the cross sections of the column along the bottom half of the columns with section A, defined in figure 4.3 for the limit situations in terms of flexural reinforcement and imposed displacement: case 1 ($A_a=20\text{cm}^2$) and case 3 ($A_a=125\text{cm}^2$) and imposed displacement δ with values δ_y and $6\delta_y$.



(Column A – $A_a=20\text{cm}^2$; δ_y ; $6.0\delta_y$; $A_a=125\text{cm}^2$; δ_y , $6.0\delta_y$)

Figure 4.10. Maximum cross-section compressive strains

Table 4.4 shows the maximum compressive strain ϵ_c^{\max} at the top and base sections for the three cases of area of flexural reinforcement and the three imposed displacements.

Table 4.4. Maximum compressive strains at the top and base sections (x10-3).

Section A				Section B			
ϵ_c^{\max}	$\delta=\delta_y$	$\delta=2.5\delta_y$	$\delta=6\delta_y$	ϵ_c^{\max}	$\delta=\delta_y$	$\delta=2.5\delta_y$	$\delta=6\delta_y$
$A_a=20\text{cm}^2$	0.57	2.15	5.33	$A_a=20\text{cm}^2$	0.48	1.05	2.34
$A_a=50\text{cm}^2$	0.75	2.85	8.99	$A_a=50\text{cm}^2$	0.57	1.41	2.94
$A_a=125\text{cm}^2$	0.94	3.87	14.01	$A_a=125\text{cm}^2$	0.79	1.79	3.18

If the available ductility was the same for the three cases, it would be possible to evaluate the ability of the columns to withstand imposed displacements without knowledge of the amount of flexural reinforcement. In that situation the amount of flexural reinforcement that would necessary to add to resist imposed displacements could be arbitrarily chosen by the designer, as already referred to, leading to the possibility it could be set equal to zero. However the results indicate that the columns with more flexural reinforcement are less ductile, despite the fact that the maximum compressive strain is less sensitive to the amount of flexural reinforcement than to the imposed displacement. This strengthens the above choice of adding zero flexural reinforcement (to the reinforcement necessary to resist to the effects of other actions) to resist imposed displacements, as the most adequate option to maximize the element's deformation capacity. A third factor that strengthens this option is that by minimizing the flexural reinforcement, the flexural

capacity is minimized and therefore the shear demand, evaluated according to Capacity Design principles in order to avoid brittle behaviour, is also minimized.

Therefore the parameters a designer can change to increase the element deformation capacity (once the geometry and materials are chosen, and the flexural reinforcement necessary to resist to other actions is evaluated) in reinforced concrete symmetric elements without axial force as the ones studied, are (i) the maximum acceptable concrete compressive strain, ϵ_{cu} , which can be increased by providing confinement reinforcement and (ii) the depth of the compressive zone at failure, that can be reduced by not adding flexural reinforcement to the reinforcement necessary to resist to other actions (assuming this is a reasonable amount, as it will be shown is the natural situation in well conceived structures).

4.2.2 Factors That Influence Ductility

The previous discussion has omitted the analysis of the influence of some relevant factors on the deformation capacity of reinforced concrete members:

1. shape and dimensions of the cross-section,
2. material strength,
3. distribution of flexural reinforcement and ratio between compressive and tensile reinforcement,
4. level of axial force,
5. concrete tensile strength,
6. steel ultimate to yield stress ratio and steel hardening stiffness,
7. shear forces
8. slope of the post ultimate stress descending branch of the constitutive relationship of confined concrete.

The potential influence of the first three factors on the deformation capacity can be analysed at section level, while for the other factors it is relevant to study the influence of the parameters on the distribution of deformations along the length of the member. Therefore the influence of these parameters will be studied analysing the entire example columns. The influence of shear and of the slope of the descending branch of the constitutive relationship of confined concrete will be discussed qualitatively.

In order to analyse the results it is useful to revise some basic concepts. The deformation capacity of the cross section χ_u essentially is a function of the maximum compressive strain in the confined concrete core. The main parameter that controls the maximum

compressive strain demand, for a given curvature the section must withstand, is the depth of the compressive zone. If we look at figure 4.2 it is easy to establish

$$\varepsilon = c \cdot \chi \quad (4.2)$$

The depth of the compressive zone “c” depends essentially on the part of the compressive force taken by concrete. In the absence of an axial force acting on the section, this results from the division of the bending moment by the internal lever arm “d” minus the part of the compressive force taken by the compressive reinforcement, as follows:

$$F_{c, \text{concrete}} = M/d - F_{c, \text{steel}} \quad (4.3)$$

M – applied bending moment

(a) Shape and Dimensions of the Cross-section. In order to study the influence of the cross-section shape, a cross-section qualitatively different of the ones previously considered was analysed: a T shaped section, that in an underground structure may be useful for instances to strengthen the perimeter walls for the purpose of resisting external soil and water pressures. In order to compare results with one of the previously studied sections, let's consider the rectangular $3.0 \times 1.0 \text{ m}^2$ cross section shown on the left-hand side of figure 4.11, which can be considered equivalent to three side-by-side B sections. The amounts of flexural reinforcement of the T section were adjusted in order that it has similar flexural capacity to the rectangular $3.0 \times 1.0 \text{ m}^2$ section. In order to allow a direct comparison of results, the strain hardening stiffness of the steel of the T section was also set to zero. The steel areas A_{sup} and A_{inf} assume the values shown in table 4.5.

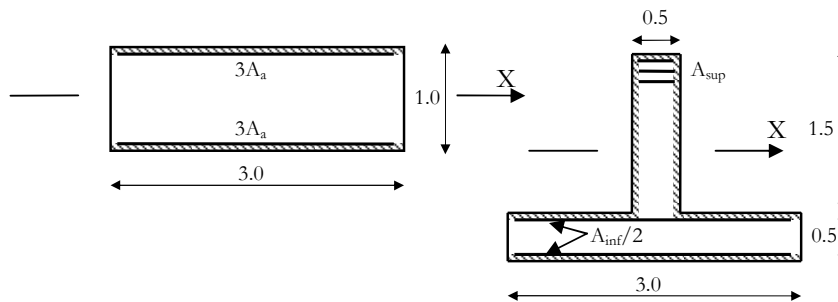


Figure 4.11. Definition of T shaped cross-section

Table 4.5. T section reinforcement

	Case 1	Case 2	Case 3
A_{sup} (cm ²)	25.56	64.17	162.51
A_{inf} (cm ²)	31.76	80.80	204.62

Figure 4.12 shows the positive and negative moment-curvatures relationships around the X axis for the T section and table 4.6 summarises the main results at yield and rupture points. As the T section is equivalent to three B sections, the moments in figure 4.12 and table 4.6 are divided by three for easiness of direct comparison with the results of section B, shown in figure 4.6 and table 4.3.

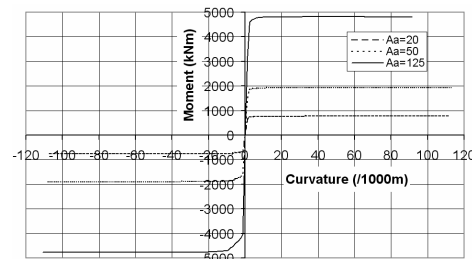


Figure 4.12. Moment curvature relationships for T shaped section

Table 4.6. Results for T section at yielding and rupture

Positive moments

Aa (cm ²)	χ_y (/1000m)	χ_u (/1000m)	c_y (m)	c_u (m)	M_y (kNm)	M_u (kNm)
20	1.41	111.61	0.340	0.088	645.4	771.8
50	1.56	113.98	0.483	0.125	1556.7	1921.5
125	1.77	91.53	0.650	0.164	3877.2	4811.5

Negative moments

Aa (cm ²)	χ_y (/1000m)	χ_u (/1000m)	c_y (m)	c_u (m)	M_y (kNm)	M_u (kNm)
20	1.24	107.39	0.130	0.018	622.2	759.6
50	1.29	108.28	0.199	0.033	1539.4	1903.0
125	1.38	110.97	0.301	0.078	3900.4	4763.1

For positive moments the web is under axial compression. Due to the fact that the web is six times thinner than the flange and the compressive reinforcement is spread by three layers, the neutral axis depth at yielding is more than the double of the corresponding value for section B. However the total length of the effective section is more than the double than for section B due to the fact that the thickness of the concrete cover, that was disregarded, was the same as for section B. Both factors resulted in the fact that the length of the zone under tensile axial strains is approximately the double of what it was for section B, leading to the reduction of the yield curvature to approximately half in the T section.

For negative moments the compressive side of the section is the side of the flange. Since the neutral axis crosses the flange, it is partially under compression and part in tension. The results show that the yield curvatures are less than half the yield curvatures of section B. This results from the increase of the length of the part of the section under tensile axial strains to more than the double of the correspondent value for section B. This derives from the fact that the depth of the compressive zone is much lower than for positive moments. This is due essentially to the fact that the width of the compressive zone, the flange, is much larger than the width of the web. The depth of the compressive zone also depends on other factors, such as the fact that the tensile and compressive forces due to bending are smaller than for section B as the internal lever arm is larger and the fact that there is less compressive reinforcement than for section B. However, in this case, these factors do not change the general tendency.

The relative difference between positive and negative ultimate curvatures is lower than the relative difference between the positive and negative yield curvatures, with the exception of case 3 for positive moments. That is due to the fact that the depth of the compressive zone varies less at rupture, as from yielding to rupture the neutral axis tends to move to the compressive side. This leads to lower variations in the zone under axial tensile strains that is the key parameter that conditions the ultimate curvature in these cases in which rupture takes place by fracture of the steel. Since this parameter has little

variations, the ultimate curvature only varies slightly with the amount of flexural reinforcement. Case 3 for positive moments represents a qualitatively different case as rupture is triggered by concrete crushing, leading to a lower ultimate curvature than for the other cases. Therefore the comparison with the results of section B clearly indicates that the analysed T section has much less deformation capacity than compact sections if the flexural capacity is similar in both cases.

In most of the above cases rupture was triggered by the steel. This is not a typical situation in design practice, as referred before. However if rupture was triggered by concrete crushing, as would be more likely in most practical cases in which there can be axial compression or asymmetric reinforcement, the conclusion would be qualitatively similar. In this cases the ultimate curvature χ_u would be $\chi_u = \epsilon_{cu}/c_u$, this is, the section deformation capacity would vary in the inverse proportion of the depth of the compressive zone. A qualitative comparison of the deformation capacity of a T section and a rectangular section, both with similar width and flexural capacity, would be as follows. For negative moments the situation of the T section would not be too different of the situation in compact sections, as the compressive force would be smaller, and due to the division of the reinforcement of the flange between both faces, there could be less compressive reinforcement. These factors, coupled with the large width of the flange, would eventually lead to situations in which the depth of the compressive zone would not be excessively different of the one in a compact section. In fact other factors as the thickness of the flange or an uneven distribution of reinforcement between the flange faces could have more influence. The main difference is for positive moments, in which the web is under compression. Even if the compressive force decreases due to the increase of the internal lever arm, as compared with the compact section, in general the decrease in the web thickness would be higher, leading to an increase in the neutral axis depth and to a reduction on the section deformation capacity. In the above studied cases only for case 3, that corresponds to the higher amount of flexural reinforcement and for positive moments, is that rupture took place on the concrete, reducing the ultimate curvature. This will be highlighted later in this chapter in the study of T sections with web reinforcement.

For the purpose of studying the effect of section dimensions, another two sections are studied: a square and a circular sections with the double of the side and diameter of the previously studied sections (defined in figure 4.3), as shown in figure 4.13. For a given geometry the dimension perpendicular to the plane of bending (direction of the X axis) is not important, as it does not changes the state of stress and strain in the plane of bending. The amount of reinforcement was four times more in order to maintain the same percentage of reinforcement with regard to the cross-section area.

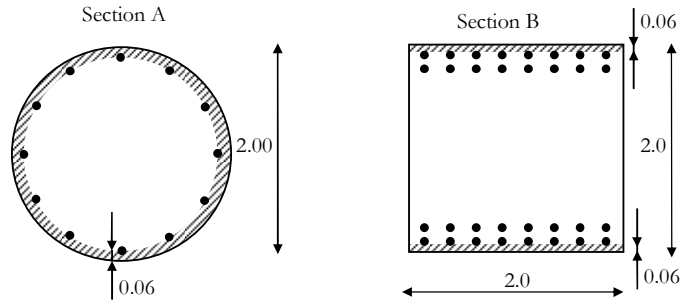


Figure 4.13. Enlarged rectangular and circular sections

Figure 4.14 shows the moment-curvature relationships for both sections and the three amounts of flexural reinforcement considered and table 4.7 shows the main results at yielding and rupture.

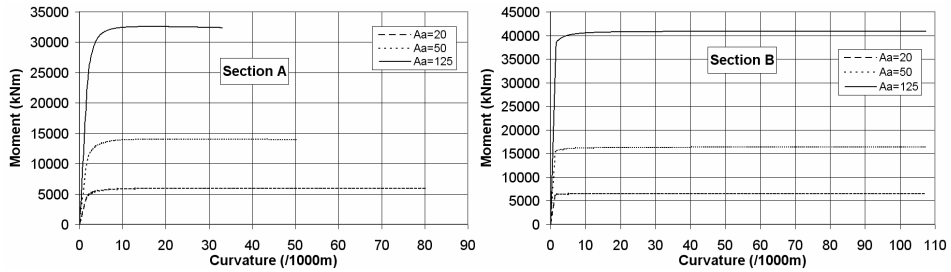


Figure 4.14. Moment curvature relationships for the enlarged circular and rectangular sections

Table 4.7. Results for enlarged rectangular and circular sections at yielding and rupture

Circular section (A)						
Aa (cm ²)	χ_y (/1000m)	χ_u (/1000m)	c_y (m)	c_u (m)	M_y (kNm)	M_u (kNm)
80	1.44	80.20	0.367	0.187	4085.1	5905.5
200	1.57	50.28	0.490	0.298	9612.4	13948.9
500	1.74	33.17	0.628	0.452	22491.8	32387.1

Rectangular section (B)

Aa (cm ²)	χ_y (/1000m)	χ_u (/1000m)	c_y (m)	c_u (m)	M_y (kNm)	M_u (kNm)
80	1.34	107.31	0.254	0.016	6131.3	6538.2
200	1.445	107.43	0.374	0.018	15370.6	16344.3
500	1.60	107.49	0.521	0.019	37893.5	40883.3

As expected, the results show a clear increase in the flexural capacity, as compared to the A and B sections. Regarding the comparison of the square sections, it can be observed that the distribution of flexural reinforcement is similar, leading to the same rupture mode by the steel. The increase in section dimension in the bending plane led to an almost proportional increase in the length of the section under tensile axial strains, reducing to slightly less than half both the yield and ultimate curvatures. The new circular section is an enlarged image of section A in which all dimensions duplicated and all areas increased four times. This resulted in the approximate duplication of all relevant dimensions, such as the length of the section under tension at yielding and the depth of the compressive zone at rupture. Since this section, such as section A, fails by crushing of concrete, this resulted in the decrease of the yield and ultimate curvatures approximately in the inverse proportion of the increase in dimensions.

The above means that unless there are strong variations in the percentage or distribution of flexural reinforcement, the deformation capacity varies almost inversely with the dimension of the cross-section in the bending plane.

(b) Material Strength. It results from the above that to resist imposed deformations structural elements should be as slender as possible. But obviously there are limits, which derive from the need to resist to the internal action-effects induced by other actions but the seismic action (essentially permanent and live loads). To resist to those effects and simultaneously minimize to element's dimensions in the plane of deformation, material with high strength should be used. Regarding the concrete it is known that higher strength concrete is more brittle than low strength concrete as this fails by the mortar and the former by the aggregates. However the difference is not significant (EC2 does not even distinguish the ultimate strains of concretes with $f_{ck} < 55\text{MPa}$) and is clearly compensated by the reduction of the depth of the compressive zone (within the element's cross-section) that can be obtained with higher strength concrete. In the case of steel, the use of higher strength steel contributes to the minimization of the element's dimensions necessary to resist the effects of permanent and live loads, which is obviously positive. However, the use of higher strength steel means that larger tensile forces can be

generated, which in turn leads to higher compressive forces due to bending. This can be negative if a poor strength concrete is used, leading to higher depths for the compressive zone. It is therefore necessary to avoid coupling higher strength steels with poor concrete. The opposite situation, strong concrete and weaker steel, is not so negative, but the best option is clearly to have high strength steel and concrete. For instances the use of concretes with $f_{ck} < 35\text{MPa}$ should be discouraged.

(c) Distribution of Flexural Reinforcement and Ratio Between Compressive and Tensile Reinforcement. The comparison of results between sections A and B, shown in figure 4.6, already highlighted some differences due to the distribution of flexural reinforcement. However, as the difference of results is not due exclusively to the difference in the distribution of flexural reinforcement, another section, with the shape and dimensions of section B, but with a different distribution of flexural reinforcement is studied. The section, shown in figure 4.15, has all the flexural reinforcement distributed along the faces perpendicular to the bending axis instead of having it near the faces parallel to the bending axis, the X axis. Three cases with different amounts of flexural reinforcement were considered. In all cases the total amount of flexural reinforcement was increased to maintain the ultimate flexural capacity, case by case.

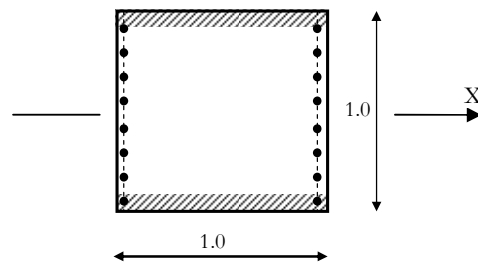


Figure 4.15. Square section with flexural reinforcement only in the web

The moment curvatures and the main results at yielding and rupture are shown in figure 4.16 and table 4.8

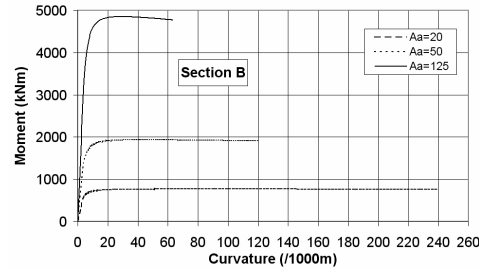


Figure 4.16. Moment curvature relationships for the square section with web reinforcement

Table 4.8. Results for square section with web reinforcement at yielding and rupture

A_s (cm ²) (half total reinf.)	χ_y (/1000m)	χ_u (/1000m)	c_y (m)	c_u (m)	M_y (kNm)	M_u (kNm)
21.2	2.89	242.25	0.127	0.054	463.9	762.6
58.1	3.16	120.68	0.191	0.124	1156.5	1906.6
171.9	3.61	63.08	0.277	0.238	2963.7	4772.4

With this distribution of reinforcement rupture by the steel only takes place in case 1, the one with a very small amount of reinforcement. This means that in general rupture will take place in the concrete, a qualitative difference of behaviour to section B, where the reinforcement is concentrated near the edges.

The yield curvatures are similar, only slightly more, than for section B. This is associated to a small increase in the depth of the compressive zone at yielding. It could be expected that, due to the lack of compressive reinforcement, the increase in the depth of the compressive zone would be higher than observed. The fact that the increase is small, is due to the fact that most of the tensile reinforcement has not yielded, leading to lower tensile and compressive forces at yielding, what is clearly reflected on the lower values of the yield moments.

The results show that at rupture the depth of the compressive zone clearly increases in all cases when compared with the same section with the flexural reinforcement further away from the neutral axis. This effect increases with the area of reinforcement. It leads to a clear reduction of the deformation capacity in cases 2 and 3 in which rupture is triggered by crushing of the concrete. The increase of the depth of the compressive zone is due to (i) the fact that at large curvatures almost all the tensile reinforcement has yielded and most of the reinforcement is under tensile axial stresses due to the fact that the length of

the tensile zone is higher than the length of the compressive zone. This means that at rupture the tensile force is higher than in the section with the tensile reinforcement concentrated in the zone more far away from the neutral axis, and (ii) on the compressive side a larger area of concrete needs to be mobilized to resist the compressive force because there is less compressive reinforcement in the zones more far away from the neutral axis. This effect is accentuated at large curvatures by the strength degradation of confined concrete at high strains, which is associated with the negative slope of the post-ultimate stress descending branch, shown in figure 4.4. This effect increases quantitatively with the increase in the area of reinforcement. Therefore it is clearly better to concentrate the flexural reinforcement as close as possible in the zones near the edges of the section.

The effect of the shape of the section, already studied, is coupled with the effect of the type of distribution of flexural reinforcement. In order to evaluate the effect of the section shape considering a uniform distribution of reinforcement along the faces perpendicular to the bending axis, the sections with the geometry shown in figure 4.11 were considered. The rectangular section intends to represent three side by side sections as the one represented in figure 4.15. The reinforcement of the T section was evaluated in order that the minor of its ultimate positive and negative moments is similar to the ultimate moment of the enlarged rectangular section with web reinforcement. The T section is shown in figure 4.17.

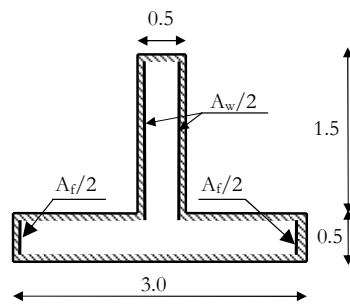


Figure 4.17. Definition of T shaped section with web reinforcement.

Figure 4.18 shows the positive and negative moment-curvature diagrams for the T section and Table 4.9 shows the main results. The bending moments are divided by three to allow direct comparison with the results of figure 4.16 and table 4.8.

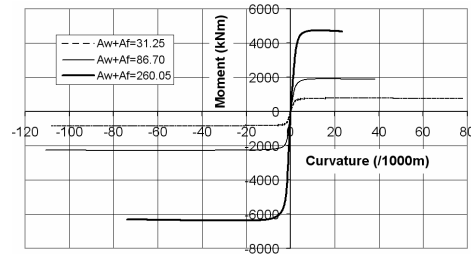


Figure 4.18. Moment curvature relationships for the T section with web reinforcement

Table 4.9. Results for the T section with web reinforcement at yielding and rupture

Positive moments						
A_w+A_f (cm ²) (Half total reinf.)	χ_y (/1000m)	χ_u (/1000m)	c_y (m)	c_u (m)	M_y (kNm)	M_u (kNm)
31.25	1.42	77.90	0.349	0.193	468.9	768.1
86.70	1.59	38.10	0.510	0.394	1157.2	1875.6
260.05	1.84	23.29	0.697	0.644	2990.5	4680.4

Negative moments						
A_w+A_f (cm ²) (Half total reinf.)	χ_y (/1000m)	χ_u (/1000m)	c_y (m)	c_u (m)	M_y (kNm)	M_u (kNm)
31.25	1.25	108.19	0.140	0.031	527.9	838.5
86.70	1.31	110.84	0.223	0.076	1387.0	2266.1
260.05	1.43	74.07	0.355	0.203	3837.6	6303.5

Similarly to what was observed for sections with the reinforcement near the faces, the yield curvature for the T section with positive moments is approximately half of what it is for the compact rectangular section with the same flexural capacity. For negative moments the yield curvatures are smaller, as the larger width of the flange, partially under compression, leads to lower depths for the compressive zone and slightly longer lengths for the part of the section under tensile axial strains.

The main qualitative differences to the sections with the reinforcement concentrated near the faces parallel to the bending axis occurs at rupture, that in most cases is triggered by concrete crushing and not by steel fracture. The exceptions (cases of fracture by the steel) occur for negative moments and lower amounts of flexural reinforcement, as in this cases

due to the low compressive force and large width of the flange, the depth of the compressive zone is very small, leading to the steel reaching its ultimate strain before the concrete.

The results also show that for positive moments the ultimate curvature is much smaller than for negative moments or for the compact rectangular section with similar distribution of reinforcement and flexural capacity, as the depth of the neutral axis at rupture is much higher due to the low thickness of the web.

This result serves to generalize the previous study on the T section with reinforcement concentrated near the faces of the flange and on the top of the web. It can be concluded from both studies that to design sections with high flexural ductility, compact sections are better than T sections or of other similar non compact shapes, regardless of the distribution of flexural reinforcement.

Another parameter worth mentioning is the ratio between compressive and tensile reinforcement: the reduction of this ratio would produce exactly the same effects as the distribution of reinforcement in the web, leading to less ductile sections, as it would also lead to the increase of the depth of the compressive zone at rupture.

(d) Level of Axial Force. It is known that axial forces have a negative effect on the ductility of reinforced concrete elements, as lead to an increase of the area under compression at cross section level. This obviously leads to the increase of the maximum compressive strain for a given applied curvature, triggering rupture at lower curvatures. For the purpose of providing some sensitivity to this effect, the moment-curvature diagrams for sections A and B (defined in figure 4.3) subjected to an axial force that induces a compressive stress of 40% of the design confined concrete capacity are presented in figure 4.19 and table 4.10.

Section A $N=1000^2 \times \pi / 4 \times 35 \times 0.4 \approx 11\,000\,000\text{N} = 11\,000\text{kN}$

Section B $N=1000 \times 1000 \times 35 \times 0.4 = 14\,000\,000\text{N} = 14\,000\text{kN}$

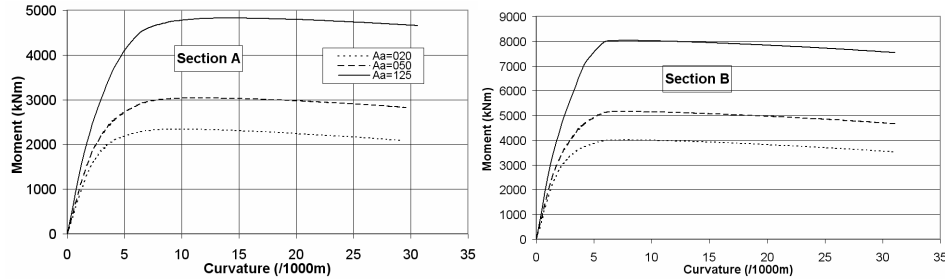


Figure 4.19. Moment curvature relationships for compressed sections

Table 4.10. Results with high axial force at yielding and rupture

Circular section (A)

Aa (cm ²)	χ_y (/1000m)	χ_u (/1000m)	c_y (m)	c_u (m)	M_y (kNm)	M_u (kNm)
20	6.515	29.337	0.546	0.511	2289.64	2085.73
50	6.311	29.792	0.535	0.503	2899.95	2824.85
125	5.978	30.625	0.516	0.490	4413.92	4655.94

Square section (B)

Aa (cm ²)	χ_y (/1000m)	χ_u (/1000m)	c_y (m)	c_u (m)	M_y (kNm)	M_u (kNm)
20	5.942	31.191	0.514	0.481	3986.47	3515.79
50	5.938	31.191	0.514	0.481	5129.27	4664.65
125	5.928	31.191	0.513	0.481	7988.07	7535.72

The main features associated to the influence of the axial force on the moment-curvature relationships can be highlighted comparing the above results with the ones for the same section but without axial force (shown in figure 4.6 and tables 4.1 and 4.2): (i) the axial force leads to the increase of the depth of the compressive zone at yielding, therefore increasing the yield curvatures, (ii) all sections fail by crushing of the concrete, as the axial force increased the area under compression, (iii) the ultimate curvatures are very similar for different amounts of flexural reinforcement because the depth of the compressive zone varies very little with the amount of flexural reinforcement; this is due to the fact that the amounts of flexural reinforcement under tensile and compressive stresses are similar and therefore any change in the amount of reinforcement almost does not change

the balance of forces taken by the steel, leading always to similar compressive forces on the concrete. In the case of the circular section (A) this only takes place because the neutral axis is near the centre of mass of the gross concrete sections, (iv) the amount of flexural reinforcement influences essentially the flexural capacity but very little the section deformation capacity, (v) the ultimate curvatures are much smaller than for similar sections without high compressive forces, and (vi) the last part of the moment curvature diagrams has a negative slope due to the large depth of the compressive zone of concrete where the effect of the descending branch of confined concrete is strongly felt. The steel strain hardening, not accounted for, would decrease or eliminate this effect that also depends on the slope of the descending branch of the constitutive relationship of confined concrete.

The above highlights very clearly the negative effects of axial forces on the ductility of reinforced concrete sections. The effect of the negative branch of the moment curvature diagrams is further discussed at the end of this chapter.

(e) Concrete Tensile Strength. The effect of the tensile strength of concrete was studied by means of analysing the example column with sections A and B. The tensile strength of concrete was assumed to have an above average value of 10% of the respective compressive strength, thus maximizing the effect of this parameter. The calculations performed were the same already performed with the example columns and described in the previous section (4.2.1). The value of δ_y is the yield displacement of the circular section, case 1. Since the yield displacement for section B is smaller than δ_y , when this displacement is imposed to the column with section B in fact a displacement higher than the yield displacement of this column is imposed on it. The steel hardening stiffness was also considered as 2% of the elastic stiffness. Thus the only difference between the models is the value of the concrete tensile strength that in the first models was $f_{ct}=0$ and in the new calculations was $f_{ct}=3.5\text{MPa}$. Figure 4.20 shows the moment-curvature relationships for the circular section highlighting the initial part of each diagram approximately up to the yield curvatures. If the full moment curvature diagrams, as shown in figure 4.6 were shown the difference would hardly be noticeable, in particular for the cases with higher amounts of flexural reinforcement. Tables 4.11 and 4.12 shows the maximum curvatures at the top and bottom sections for all the analysed cases.

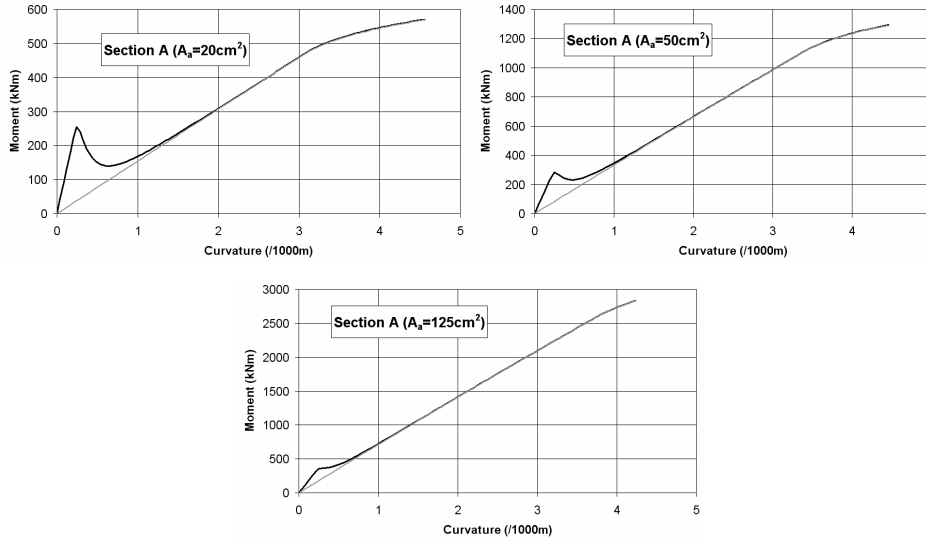


Figure 4.20. Curvature diagrams for sections A considering the concrete tensile strength

Table 4.11. Curvatures at the base section with and without concrete tensile strength [/1000m]. (section A)

Concrete with no tensile strength ($f_{ct}=0$)				Concrete with tensile strength ($f_{ct}=3.5\text{MPa}$)			
Aa (cm ²)	$\delta=\delta_y$	$\delta=2.5\delta_y$	$\delta=6\delta_y$	Aa (cm ²)	$\delta=\delta_y$	$\delta=2.5\delta_y$	$\delta=6\delta_y$
20	3.12	17.61	48.92	20	3.63	18.22	49.35
50	3.12	16.32	51.07	50	3.17	16.43	51.14
125	3.13	16.12	56.61	125	3.14	16.17	56.67

Table 4.12. Curvatures at the base section with and without concrete tensile strength [/1000m]. (section B)

Concrete with no tensile strength ($f_{ct}=0$)				Concrete with tensile strength ($f_{ct}=3.5\text{MPa}$)			
Aa (cm ²)	$\delta=\delta_y$	$\delta=2.5\delta_y$	$\delta=6\delta_y$	Aa (cm ²)	$\delta=\delta_y$	$\delta=2.5\delta_y$	$\delta=6\delta_y$
20	4.84	23.26	75.00	20	8.67	23.91	82.27
50	3.13	22.28	75.66	50	3.39	22.43	75.74
125	3.12	21.27	59.27	125	3.13	21.33	59.37

It should be noted that the analysis is monotonic and does not account for the fact that in sections in which the cracking moment is exceeded in both directions of loading all fibres have cracked (as the neutral axis moves to the compressive side) and do not resist tensile axial stresses again. The model does not account for this effect and continues to consider the concrete tensile capacity even after the cracking moment is exceeded. In the calculations performed the concrete tensile capacity was considered in all sections of the example column, leading to the overestimation of the influence of the concrete tensile strength.

The concrete tensile strength increases the stiffness of the uncracked sections, the ones with lower applied moments, near the middle height in the example columns. Therefore, for the same applied displacements between column extremities, the lower deformation of the uncracked sections must be compensated by larger deformations in the zones where sections have cracked. This effect tends to be higher if column sections are lightly reinforced, as the difference between the cracking and ultimate moment is smaller, as shown in figure 4.20 and the zone of the column with higher rigidity is a larger part of the column.

In qualitative terms the results indicate that disregarding the concrete tensile strength may lead to an underestimation of the maximum curvatures imposed to the structure. However the most relevant feature of the results is the little quantitative importance of this effect. Therefore disregarding the concrete tensile strength can be considered an acceptable approximation.

(f) *Steel Hardening Stiffness and Ultimate to Yield Stress Ratio.* Designers cannot change the steel constitutive relationship but only choose what type of steel to use, generally as a function of a nominal yield stress. However it is useful to provide some insight into the influence that other relevant parameters of steel mechanical behaviour have on the ductility of reinforced concrete elements.

At section level the steel ultimate to yield stress ratio produces an effect equivalent to a slight increase in the amount of flexural reinforcement for large imposed curvatures clearly beyond the yield curvature. The main effect on reinforced concrete elements concerns the spread of plasticity along the element's length, this is, the dimension of the plastic hinge zones (PHZ). The hardening stiffness influences the strain that is necessary to develop to mobilize the ultimate stress, as can be seen in figure 4.9. The dimension of the PHZ is an important parameter as after yielding the deformations tend to concentrate on the PHZ because of the stiffness reduction there. For a given rotation between the extremities of the PHZ, the smaller the length of the PHZ the higher will be the curvature ductility demand at the end section.

The influence of the steel hardening stiffness and ultimate to yield stress ratio was studied imposing to the example column with section A displacements of $2.5\delta_y$ and $6\delta_y$ at the top, considering three ratios between the steel hardening and elastic stiffness ($E_h/E_c = 1\%$, 2% and 5%), and two values for the ultimate to yield steel stress ratio ($\sigma_u/\sigma_y = 1.3$ and 1.2). The moment-curvature diagrams of section A considering the ultimate to yield steel stress ratio $\sigma_u/\sigma_y = 1.3$, for the three cases of area of flexural reinforcement and hardening stiffness are shown in figure 4.21. Tables 4.13 and 4.14 show the maximum curvature at the top and base sections for cases in which the prescribed displacements were achieved before rupture.

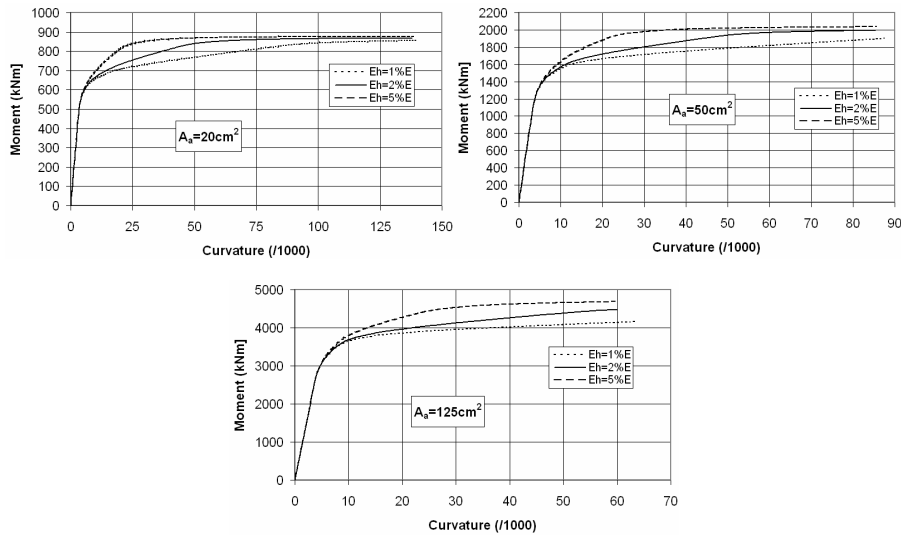


Figure 4.21. Moment-curvature diagrams for columns with different steel hardening stiffness and $\sigma_u/\sigma_y = 1.3$

Table 4.13. Maximum curvature at the base section (section A, $\delta = 2.5\delta_y$)

	$\sigma_u/\sigma_y = 1.2$			$\sigma_u/\sigma_y = 1.3$			
	$E_h/E_s = 0.01$	$E_h/E_s = 0.02$	$E_h/E_s = 0.05$	$E_h/E_s = 0.01$	$E_h/E_s = 0.02$	$E_h/E_s = 0.05$	
Case 1	20.41	17.75	14.41	Case 1	20.41	17.75	14.41
Case 2	18.69	16.30	13.62	Case 2	18.69	16.30	13.62
Case 3	18.15	16.07	13.44	Case 3	18.15	16.07	13.44

Table 4.14. Maximum curvature demand at the base section (section A, $\delta=6\delta_y$)

$\sigma_u/\sigma_y = 1.2$				$\sigma_u/\sigma_y = 1.3$			
	$E_h/E_s=0.01$	$E_h/E_s=0.02$	$E_h/E_s=0.05$		$E_h/E_s=0.01$	$E_h/E_s=0.02$	$E_h/E_s=0.05$
Case 1	62.50	104.40	---	Case 1	62.12	47.98	---
Case 2	68.21	---	---	Case 2	67.53	51.39	---
Case 3	---	---	---	Case 3	---	56.63	---

It can be observed that for $\delta=2.5\delta_y$ the steel ultimate to yield stress ratio does not change the results. This is due to the fact that the steel stress did not exceed $1.2\sigma_y$ in any case, and before this point there is no difference between both types of steel considered. Therefore this parameter is not relevant below certain levels of ductility demand.

The larger target displacement $\delta=6\delta_y$ is not achieved in some cases, as failure is triggered at lower displacements. In general the larger the steel ultimate to yield stress ratio the larger the ratio between the ultimate and yield moment, this is, the larger the length of the zone where plasticity spreads, what is a favourable effect. This can also be also illustrated by the distribution of curvatures along the height. An example is shown in figure 4.22, which shows the curvature distribution along the bottom half of the column with the reinforcement of case 2 and the intermediate value of the steel hardening stiffness $E_h=0.02E_c$ for both ultimate to yield stress ratios. The applied displacement was $\delta=5\delta_y$, in order that the column with $\sigma_u=1.2\sigma_y$ does not fail before the target displacement is reached (notice that according to table 4.14 this column fails before $\delta=6\delta_y$).

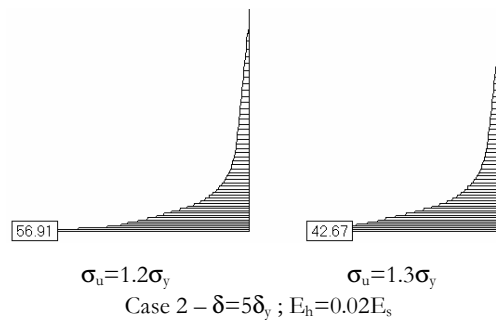


Figure 4.22. Curvature diagrams for columns with different steel hardening stiffness

The results illustrate the higher concentration of curvatures near the bottom for the case with the lower ultimate to yield stress ratio, yielding an higher curvature demand if both columns undergo the same displacement demand.

The effect of the steel hardening stiffness is not so clear. For the purpose of studying the influence of this parameter at the higher displacement levels, figure 4.23 shows the curvature diagrams along the bottom half of the example columns for a displacement of $\delta=5\delta_y$ that was reached in all cases. Case 2, with $\sigma_u=1.3\sigma_y$ was chosen as an example.

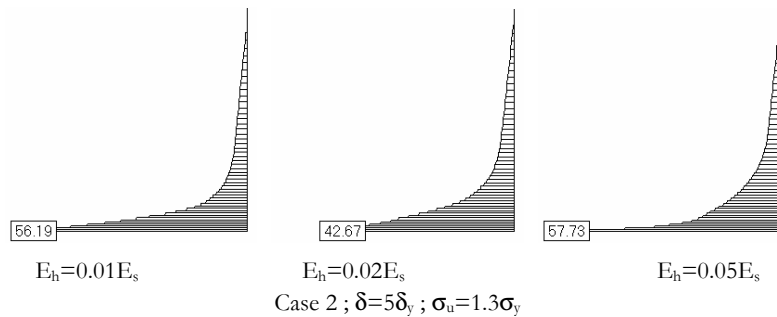


Figure 4.23. Curvature diagrams for columns with different steel hardening stiffness

The results show that the curvature demand at the base section is lower for the intermediate value of the steel hardening stiffness $E_h=0.02E_s$. A possible explanation for this is as follows: after the yield moment is reached at the extreme sections, it must increase beyond this level in order that other adjacent sections, where the moment is less than at this section, can yield. Therefore the closer the moment curvature diagram of the column cross section approaches an elastic perfectly plastic diagram the more difficult the spread of plasticity is. If the hardening stiffness is too high, the post yield stiffness in the moment curvature diagram is also high and the section reaches its ultimate moment with low increase in curvature, yielding a moment curvature diagram not too different of a elastic perfectly plastic one. In practical terms the effect of the hardening branch of the steel constitutive relationship is equivalent to a slight softening of the transition from the elastic branch to the plastic branch in the moment curvature diagram. On the other hand if the steel hardening stiffness is too low, the steel constitutive relationship tends to an elastic perfectly plastic one inducing a similar effect on the moment curvature diagram of the cross section. Both effects can be observed in figure 4.21, that indicates that with the exception of the lightly reinforced section (case 1), it is for the lowest and the highest values of the hardening stiffness that the moment curvature diagrams approach more the elastic perfectly plastic behaviour. This effect can also be influenced by the slope the

descending branch of the confined concrete constitutive relationship and by the distribution of flexural reinforcement.

It can be concluded from the above that the curvature demand at high displacements far beyond the yield level can be influenced by the shape of the steel constitutive relationship in the post-yield range. Therefore care must be taken in the simulation of this relationship. Eventually it may be concluded that in some cases the trilinear envelope is not accurate enough for this purpose.

(g) Shear Forces. The influence of high shear forces can be measured by the shear-ratio $\lambda = M/Vh$ (in which h is the cross-section dimension in the bending plane), and has the following effects:

1. it decreases the length of the PHZ and therefore the ductility and energy dissipation capacity; the reduction of the structure energy dissipation capacity is not important as it has almost no influence on the dynamic response of the soil/structure system,
2. it reduces ductility as it may trigger failure at displacements and curvatures lower than the ones the structure would withstand if it is allowed to develop its flexural capacity and deform by flexure in the non linear range. In the absence of strong axial forces the likelihood that shear may curtail a ductile flexural response of reinforced concrete elements with compact cross-section is very reduced if $\lambda > 3$. For linear elements with a linear bending moment diagram with change in curvature, this means that if $L/h > 6$ it is unlikely that relevant negative effects due to shear may occur. Since the development of flexural plastic hinges is the best ductile deformation mode possible in reinforced concrete elements, all other types of deformation in the nonlinear range and failure modes should be restricted/avoided by application of Capacity Design principles.

(h) Slope of the Post-ultimate Stress Descending Branch of the Constitutive Relationship of Confined Concrete. After the maximum stress the concrete constitutive relationship may comprise a descending branch. In this cases this descending branch has a negative effect, as it decreases the stress capacity of concrete at large strains. This leads to the increase of the depth of the compressive zone at high ductility demand, reducing the ultimate curvature χ_u . This is more relevant in sections with less compressive than tensile reinforcement or/and under high axial forces.

4.3 CONCEPTION

The conception of large underground structures in soft soils to resist earthquake actions must aim essentially at providing deformation capacity to the flexible alignments of the structure. This means that along those alignments the structure must be as flexible and ductile as possible. Obviously there are restrictions to the structural conception that

derive from the need to provide resistance to other actions. If only the resistance to earthquake actions was the purpose of the design, for instances in the case of an isolated pile in a soft soil, rubber would be a material more adequate than reinforced concrete. Therefore structural elements must have minimum dimensions necessary to provide the necessary levels of stiffness and resistance to permanent actions, live loads and other actions. However, even with this restrictions, the designer is left with many options.

For the purpose of the recommendations discussed in this section it is convenient to separate structural members in two groups:

1. main structural elements: elements whose collapse leads to unacceptable damage. Examples of these elements are the perimeter walls, columns from top to bottom of the structure, beams that transfer between opposite perimeter walls strong axial forces due to soil and water horizontal pressures.
2. secondary structural elements: elements whose collapse leads to acceptable damage. Examples of these elements are stairs, small columns that support other secondary elements, platform slabs, etc..

One of the most important criteria is to minimize the dimension of the main structural elements where plastic hinges may develop, in the plane of the flexible alignments. It was already shown that, in general, there is no interest in increasing the flexural capacity beyond what is necessary to resist to other actions but the seismic action, in these elements. In fact to increase the flexural capacity beyond this limit would contribute to increase the shear demand and the strength demand in elements intended to remain elastic. Therefore section dimensions of elements that are supposed to develop plastic hinges should be the ones strictly necessary to resist to the other actions. And since it is important to minimize section dimensions, the designers will be led to design sections with reasonably high percentages of flexural reinforcement. However it may not be advisable to design sections near the allowable upper limits of flexural reinforcement as in general the sections deformation capacity is lower than if lower percentages of flexural reinforcement are used. The designer must balance all these effects in order to maximize the elements deformation capacity. The above criteria of minimizing section dimensions in the plane of the flexible alignments may not apply in the cases of elements that are intended to remain elastic, as in these cases it may be necessary to provide these elements with a reserve strength (beyond the one necessary to resist to other actions but the seismic action) in order to avoid the formation of plastic hinges in those elements.

In the case of perimeter walls, which are subjected to high bending moments due to permanent loads and need to be provided with reasonable stiffness in the plane of flexible alignments, the designer could consider efficient to use counterforts on the perimeter walls. Even though it may be an efficient solution for the purpose of resisting

to permanent actions, yielding sections such as the one shown in figure 4.11, it is a solution that should be avoided and compact sections should be used instead. In general structural elements with large dimension in the plane of flexible alignments should be avoided. However, this is unavoidable if the width of the station varies for instances in zones away from the extremities, as exemplified in figure 4.24.

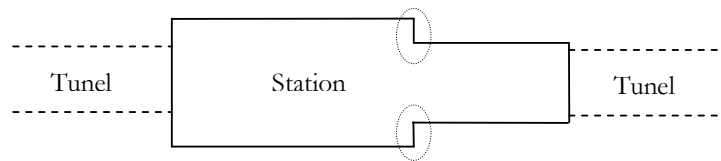


Figure 4.24. Plan of tube station of variable width

If the zone where the width of the station changes is far from rigid alignments, the part of the perimeter walls parallel to the adjacent flexible alignments may be subjected to similar imposed displacement fields. Due to the large dimension of the perimeter walls in the direction of the flexible alignments there is a probability larger than for most other elements, that the ductility demand exceeds the available ductility in those zones, pointed out in figure 4.24. Even if concrete crushing takes place in the perimeter walls, it may not necessarily lead to collapse of the rest of the structure, as perimeter walls have an excess resistance to vertical loads and some redistribution of internal action-effects may allow to maintain the resistance to soil and water pressures. But even if this optimistic perspective is what happens (it may be a bit speculative to speak about the consequences of localized failure), it would be difficult that the watertightness of the perimeter walls would not be affected, triggering large damages, difficult and lengthy to repair. Therefore it would be better to design the station avoiding changes in the width.

In the interior structure there may also be situations in which the designer may be led to design beams or columns that are supposed to develop plastic hinges with dimension more than desirable in the plane of flexible alignments. This may arise for instances if there are short spans or if elements with large cross sections are necessary to resist axial forces. Three solutions may be suggested in such situations:

1. Change the cause of that situation, for instances by changing the architecture of the station to avoid the short spans or high axial forces. However, in some cases this may be impossible or very inconvenient.
2. Increase the dimension of the element in the perpendicular direction (assuming that this is not the direction of a flexible alignment) to be able to reduce the dimension in the plan of the flexible alignment.

- To divide the element in two with half size elements on the plane of the flexible alignments, as suggested in figure 4.25. Since for short beams, as the one shown in the figure, the bending effects due to permanent loads are not very strong, it is recommended to divide the height of the beam in order to yield beams with a free span at least six times the height. Obviously the height can not be reduced excessively for practical reasons related with detailing and the need to ensure the resistance to other actions.

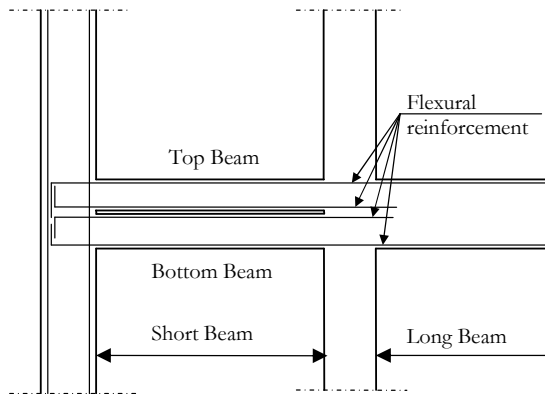


Figure 4.25. Division of short beam in two adjacent beams

Obviously the above does not apply to elements intended to remain elastic. Another very important aspect is the need to limit axial forces due to the negative effect of high compressive forces on ductility of reinforced concrete elements. Vertical axial forces on columns can be strongly reduced by eliminating the soil cover over the top slab. Therefore it is recommended that the structure runs up to the surface even if that is not strictly necessary for functional reasons. In some cases it may be possible to use the extra space for a car park, shops or other type of facilities. The soil cover contributed to reduce the available ductility of the columns of Dakai tube station, reducing the ability to withstand large relative horizontal displacements between the top and bottom sections of the columns.

Unfortunately the soil and water pressures depend on the geotechnical scenario and can not be reduced by means of the structural conception. However any soil treatment that improves soil characteristics and reduces soil pressures is positive, as it reduces the axial forces on the beams that transfer those forces between parallel perimeter walls.

The use of prestressed beams (for instances due to long spans) should be avoided to do not increase axial compression, unless it is possible to ensure that the beams will remain elastic.

Secondary structural elements and non structural elements, such as masonry walls or others, must be designed and built in such a way they do not create restrictions to the deformation of main structural elements and if possible, that they possess good deformation capacity if that is advantageous for the purpose of damage limitation. Some examples are shown in figures 4.26 to 4.28.

Figure 4.26 shows a scheme and a photo that illustrate the negative effects the stairs may have. The scheme represents a stair in the plane of a flexible alignment. An horizontal relative displacement δ is imposed as shown in the figure. While the left-hand side column freely deforms along the distance “L” between the two levels, the right-hand side column has to accommodate the imposed displacement only on its top half, as the stairs restrict the deformation below that level. Situations qualitatively similar also exist in buildings, sometimes with the consequences shown on the photo of figure 4.26. Situations of this type must be avoided, if possible locating the stairs parallel and close to rigid alignments without any support at middle height of columns.

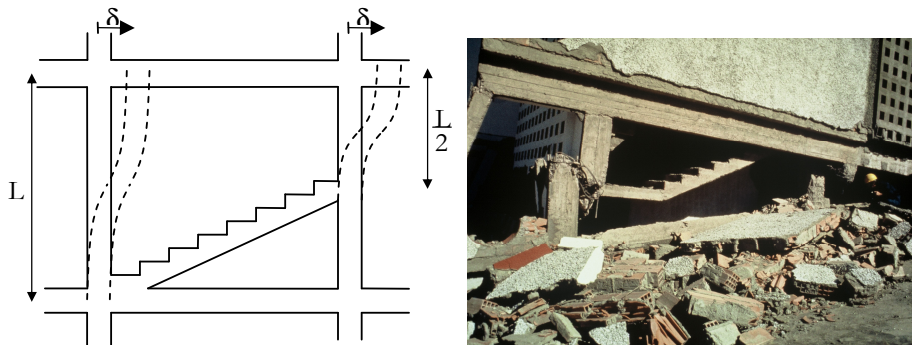


Figure 4.26. Restriction to column deformation due to stairs and potential consequences

Other type of interference may arise from non structural elements as masonry partition walls, as represented in figure 4.27.a. At the initial stages of the earthquake action, while the amplitude of the imposed relative displacements is small the masonry wall behaves as part of the structure, restricting the deformation of the columns. However for larger amplitudes of displacement the masonry will start getting damaged in some parts of the panel. If no control is kept on the type and location of damage, situations of localized damage adjacent to the columns may arise, such as the shown in figure 4.27.a. As a

consequence an artificial short column may be created. Due to its shorter length any relative horizontal displacement between the two adjacent levels will create at the end sections of the short column a ductility demand higher than expected. The problem may be worsened by the fact that those locations of the column may not be confined, as no plastic hinge is expected to develop there according to usual bare frame models that do not predict that type of damage. A possible solution would be to separate the panel from the surrounding frame along three sides filling the space left with a flexible material, as indicated in figure 4.27.b. If the separation of the structure from the masonry wall can not be executed with reliability, than it is prudent to confine the column throughout the height and be aware that the column shear and ductility demand may be higher than predicted by models that in general do not account for localized masonry failure.

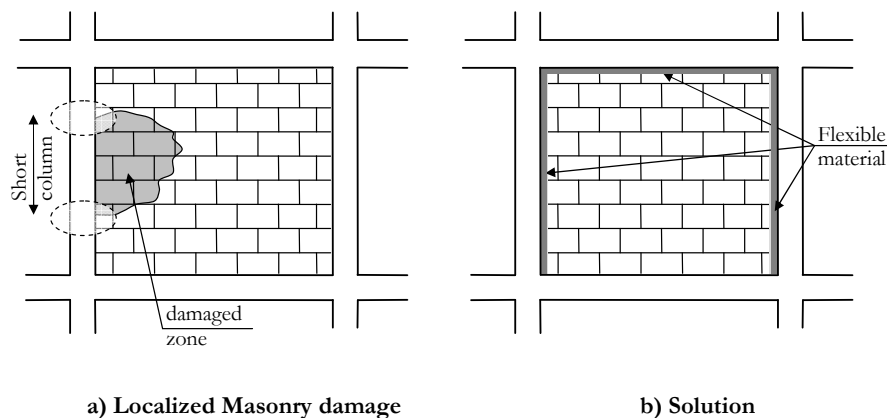


Figure 4.27. Restriction to deformation of the structure due to non structural masonry wall and possible solution

Figure 4.28 shows a similar situation. Let's assume that due to upwards water pressure on the base slab it is necessary to increase the weight of the station to avoid the tendency for uplifting. Let's assume that for that purpose the space below the platforms slabs is filled with large aggregate concrete. It is important to leave a reasonable gap between the filling material and the structural elements in order to do not reduce the deformable length of those elements, as shown in the lower part of the figure.

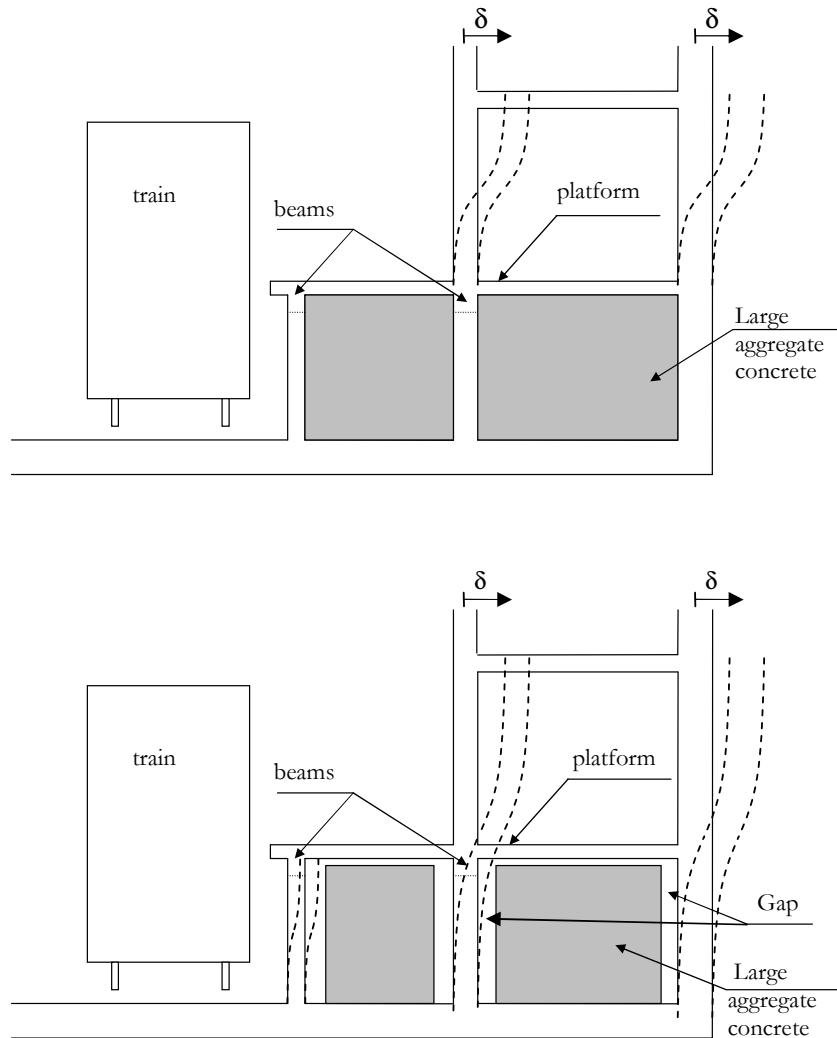


Figure 4.28. Restriction to column deformation due to stiff filling material and possible solution

The discussion in chapter 2 and in this chapter has highlighted qualitative differences between the seismic behaviour of underground structures and of structures that develop essentially above ground. These differences are reflected in differences in the design methodology, and issues usually regarded as “design” (for instances the calculation of

amounts of reinforcement for the purpose of ensuring that bending, shear and axial capacity are superior to the corresponding action-effects) become “conception” issues in the framework of the methodology proposed for the seismic analysis and design of underground structures. These issues will be discussed in the next section.

It is worth to highlight some of the main differences in what regards the seismic conception of large underground structures and seismic conception of building structures. The first difference concerns the objectives: while underground structures must be conceived essentially to be flexible and ductile, buildings are conceived to have stiffness, strength (understood as ability to transfer horizontal inertia forces to the foundations), ductility and energy dissipation capacity. This difference obviously reflects in practical aspects: for instances buildings are often conceived with structural walls and cores aiming at increasing the buildings stiffness and resistance to horizontal inertia forces. Since underground structures must be flexible to withstand the relative horizontal displacements the surrounding soil may impose, rigid elements as walls or cores should be avoided along flexible alignments. If a building structure is designed with very stiff, and eventually not very ductile elements, the ductility demand can be reduced by means of evaluating seismic action-effects using smaller q -factors than could be used for the design of more ductile structures. If a designer wants he may even decide to design the structure to withstand earthquake effects in the linear range to avoid damage, by means of adopting $q=1$. On the design of an underground structure the designer has no such option. He can not act upon the overall ductility demand using a design parameter of his choice. He is forced to design a more flexible and ductile structure, for instances by dividing a structural element in two minor adjacent elements, a solution that would not be used in buildings.

4.4 DESIGN METHODOLOGY

Regardless of the need to provide deformation capacity to the structure to resist earthquake actions, the structure has to be designed to resist to the other actions and to the effects of modes with configurations not controlled by the soil dynamic behaviour. Therefore the dimensions and amounts of reinforcement must be enough to resist to all the static actions-effects (bending and torsion moments, shear and axial forces) due to all code prescribed load combinations, including static seismic action-effects associated to those vibration modes. Anyway it should be emphasized that in well conceived structures, without significant soil covers, the effects of this modes are reduced and unlikely to condition the envelopes of static action-effects. In practical terms, this means that in such cases the seismic action is not relevant and can be disregarded at this phase. This is the first phase of design, to be performed using current design methodologies and code procedures.

The second phase regards the main purpose of the seismic design: to provide the flexible alignments of the structure with enough deformation capacity to undergo the deformation that the surrounding soil may impose on the structure without losing the resistance to permanent loads and part of the live loads. However there are limits to the deformation capacity a designer may provide to a structure. If the imposed displacements are higher than the maximum the structure may sustain, it is necessary to act in two ways: (i) maximize the structure lateral deformation capacity while maintaining its ability to sustain the permanent loads, and (ii) to treat the soil to reduce its deformability and the amplitude of the displacements imposed to the structure. The discussion that follows focus on the first objective.

It has already been shown that to resist to externally imposed displacement the structure does not need to resist horizontal inertia forces, and for ductile reinforced concrete structures the static action-effects (bending moments, shear and axial forces) associated with this action is zero for the purpose of load combinations. In order to maximize the deformation capacity of the structure the application of Capacity Design principles is fundamental, in order to choose the most adequate ductile mechanisms and ensure its maintenance during large excursions in the inelastic range in the zones of the structure chosen for this purpose. In the choice of the most adequate ductile mechanism the structural designer must account for uncertainties in the horizontal displacement field the structure may be subjected to. For instances if the vertical soil profiles vary along the perimeter of the station, with transitions between soil layers of different stiffness characteristics occurring at different heights in different locations, concentrated deformations may be imposed at different heights of the perimeter walls. In this conditions it may not be possible to control the location of plastic hinges in the perimeter walls and the most prudent approach is to design those elements allowing for the possibility of development of plastic hinges in all plausible locations, the entire height if necessary. This means that the cross-sections of the perimeter walls may need to be designed for ductility, this is, provided with adequate confinement reinforcement, throughout the height.

It is well known that according to Capacity Design principles the zones of the structure chosen to remain elastic must be provided with enough reserve strength to do not reach the yield flexural capacity or the yield or ultimate strength in any failure mode throughout the development of the chosen mechanism. This means that the resisting internal moments and forces in these zones may need to be increased relatively to the respective values resulting from the first phase of the design process. This increase must be enough to maintain the equilibrium with the ductile zones of the structure at development of the overstrength (increase in moment capacity beyond the respective design value, due to several causes, as the steel strain hardening or the increase in concrete strength due to confinement) of the respective plastic hinges. This may also have implications on the

previous phase of structural conception, has elements that are intended to remain elastic may need to be designed with larger dimensions for this purpose.

The zones chosen to develop plastic hinges must be designed for ductility. For this purpose confinement reinforcement must be provided to enhance the deformation capacity of concrete and to prevent buckling of compressive flexural reinforcement. This is a more likely phenomena in plastic hinge zones due to loss of the concrete cover and loss of stiffness of the compressive reinforcement during some stages of the development of plastic hinges due to yielding in compression and to the Bauschinger effect. Another aspect that may be important in compressive elements and elements with large amounts of tensile reinforcement is the provision of compressive reinforcement. In terms of section behaviour it helps to decrease the depth of the compressive zone, reducing the maximum compressive strains in the concrete for a given imposed curvature. The elements where plastic hinges develop need also to be designed against the possibility of failing in more brittle modes, namely in shear. For this purpose according to Capacity Design principles excess shear strength must be provided to these elements as compared to the one that results from the first design phase. The reduction of shear strength due to large crack openings must be considered in the evaluation of the shear capacity in the PHZ.

The design process is in general a process of conception, analysis and verification. The conception phase comprises the choice of materials, creation of the general layout of the structure, and choice of geometry and dimensions of structural elements including reinforcement. Knowing the structure, it is then possible to perform the analysis phase, the evaluation of the static and cinematic parameters that are more adequate to characterize the structural response to the applied actions. Therefore it includes the evaluation of the design static action-effects, moments, shear and axial forces. The last design phase, verification, consists of comparing the design and resisting static action-effects, ensuring that the former are inferior to the latter throughout the structure, and the acceptability of some cinematic action-effects. In reality this is not the usual practice in the design of reinforced concrete structures: in general codes admit the possibility of performing the analysis phase without the knowledge of the full structure but only of the general layout, geometry and dimensions of the concrete, this is, without any knowledge of characteristics and amounts of reinforcement. This derives from the fact that those characteristics are enough for the purpose of deriving a constant stiffness for linear analysis based on the elastic behaviour of gross concrete sections. As a consequence the verification phase is transformed in a calculation phase, evaluating amounts and detailing the reinforcement in order to ensure that flexural, shear and axial capacities exceed the corresponding design values obtained in the analysis phase. This is the general design practice for what was previously designated the first phase of the design methodology suggested for underground structures. However the second design phase of the proposed

methodology is qualitatively different. What is being verified is the deformation capacity. Therefore if the action is defined in terms of cinematic variables, static action-effects are unsuitable variables for the safety verification of the critical regions that undergo large inelastic deformations. Figure 4.29 can be used to illustrate this simple concept: if the design action is defined in the horizontal δ axis, for instances by the imposition of an applied displacement δ_{sd} , safety can not be assessed comparing static variables in the F axis. It must be done explicitly in terms of the cinematic variables, verifying if $\delta_{sd} \leq \delta_u$, or, in real cases, comparing other cinematic variables that define rupture, for instances in terms of ultimate strains, verifying if $\epsilon_{sd} \leq \epsilon_u$, or ultimate curvatures, verifying if $\chi_{sd} \leq \chi_u$.

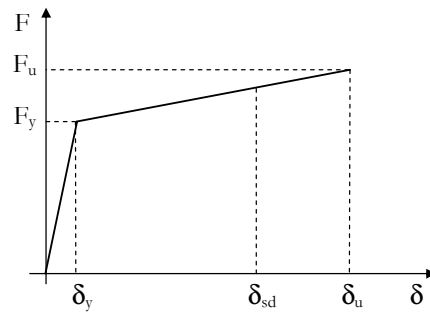


Figure 4.29. Imposed displacements on a ductile structure

Since for ductile reinforced concrete structures the ultimate values of the cinematic variables can only be reached after long incursions in the non linear (post yield) range, the evaluation of cinematic action-effects requires a physically non linear analysis of the structure. This type of analysis requires the knowledge of the amounts and detailing of reinforcement as input. Therefore, in the second phase of the proposed methodology, the amounts of flexural and confinement reinforcement to add to the reinforcement that resulted from the first design phase have to be set by the designer prior to the analysis, as part of a second conception phase. This type of analysis also requires other input variables not necessary for linear analysis: the parameters necessary to the complete definition of the monotonic stress-strain curves for steel and concrete, including the parameters associated with steel strain hardening and confinement of concrete. The verification phase that follows the non linear analysis is a real verification phase, in which the strains, curvatures or displacement demands are compared with the respective ultimate values.

Initially the application of the proposed design methodology may require an adaptation from most reinforced concrete designers as they are used to a different methodology in which the amounts of flexural reinforcement are part of the final output and not the

input for analysis. Adding to this, the amounts of confinement reinforcement are also input for analysis. To set the amounts of flexural reinforcement without the usual tools and also the amounts of confinement reinforcement, designers will need to use their sensitivity or approximate methods. For instances Capacity Design procedures, including the use of overstrength factors and equilibrium considerations based on the flexural capacity of the plastic hinges, can be used to evaluate the moment demand in sections or elements required to remain elastic; amounts of confinement reinforcement can be estimated as a function of curvature ductility demands previously derived using only cinematic considerations and the geometry of the structure. Shear reinforcement may continue to be calculated using current procedures, since avoiding shear failure is mandatory if good conception is followed and therefore no limits are established for the shear capacity in the nonlinear analysis. Thus design shear forces are part of the output of the non linear analysis and can be used to evaluate the necessary amount of shear reinforcement.

A design criteria of increasing importance, especially in developed countries, is the need to control economic losses. This is related with performance criteria, generally coupled with the type of damage that can be accepted. One of the tools that are available for the purpose of damage control in the design of structures that develop above ground is the value of the q -factor, as it can be used as a measure of the extension of the incursions in the nonlinear range. In the design of underground structures that tool is not available. There are two conception and design tools which can be used to minimize damage: (i) to conceive a flexible structure for it to yield at large displacements, and (ii) by means of the choice of the locations of plastic hinges and by avoiding types of non linear behaviour that yield damage patters more difficult and expensive to repair. If possible, the location of the plastic hinges must account for the need for access to repair and the nonlinear behaviour must be controlled by flexural yielding without interference of more brittle types of behaviour. This type of behaviour presents other advantages such as:

1. stiffness and strength degradation with increasing number of cycles at the same amplitude is less than if the non linear behaviour is influenced by shear or other modes that induce brittle types of failure.
2. the effect of the load history in the available ductility is also much smaller than if other more brittle types of failure occur. The fact that the load is cyclic can be considered more easily in the estimation of the value of the concrete ultimate strain ϵ_{cu} , rendering monotonic analysis acceptable for the evaluation of safety, in which deformation capacity is a critical parameter.
3. it is the type of nonlinear deformations and failure that can be predicted with more reliability, therefore leading to more accurate safety verifications. However it should be noticed that the evaluation of concrete ultimate strains is much less accurate than the evaluation of steel yield stresses. Since the flexural capacity is, in general, more

dependent of the steel yield stress than of the concrete ultimate strain, failure in a ductile flexural mechanism can not be predicted with the same level of accuracy that can be obtained in the evaluation of the flexural capacity for current safety verifications under applied forces.

The safety verification format used in design comprises the analysis of the overall structure using average values of material properties (stiffness) and the verification of safety at local level using design values (lower fractiles). This allows accounting for the possibility that in localised parts of a structure the material properties are below average. If this happens only in a few locations it is reasonable to assume it does not affect significantly the results of the overall structural analysis based on average stiffness properties.

In the current work the nonlinear analysis of the whole structure is based on a discretization in linear elements whose reinforced concrete sections are discretized by fibers, in what concerns the concrete, or each individual bar or groups of bars, in what concerns the steel. Therefore the same program used to perform the overall analysis also evaluates stresses and strains within each cross section, allowing performing safety verifications at section and fiber level. In this situation, that couples the overall structural analysis with the safety verifications at section level, it is necessary to decide what material properties to use.

Average stiffnesses are widely accepted as the best option to study the distribution of curvatures, displacements and static action-effects throughout the structure. The use of design constitutive relationships for concrete, to which correspond lower stiffnesses, would certainly lead to the overestimation of the deformability of the structure, therefore overestimating curvatures and displacements under applied forces. However in this case, in which the action corresponds to imposed displacement fields, the distribution of curvatures and displacements throughout the structure is not strongly affected if the stiffness of all elements is affected in the similar proportions. Therefore for the purpose of global structural analysis both average and design values are acceptable for the evaluation of the stiffness properties. Since safety verifications at local level must be performed with design values of material properties, these will be used for the analysis of the example structures analysed in the next chapter.

5. PRACTICAL APPLICATION EXAMPLE

In this section the application of the proposed methodology to an underground structure with appropriate conception (in terms of geometry and dimensions) is shown, complemented by the presentation of criteria for the “conception” of the reinforcement added (to what is necessary to resist to other actions) to increase its ductility. The application of the proposed methodology is also compared with code procedures for structures that develop above ground, namely EC 8 – Part 1, both in what regards seismic performance and economy.

The geometry of the example structure, with a conception considered adequate, is shown in figure 7.4. A reduced width of 3.80m of the exterior walls was used in the calculations. The materials chosen are steel A500 and concrete C35/45.

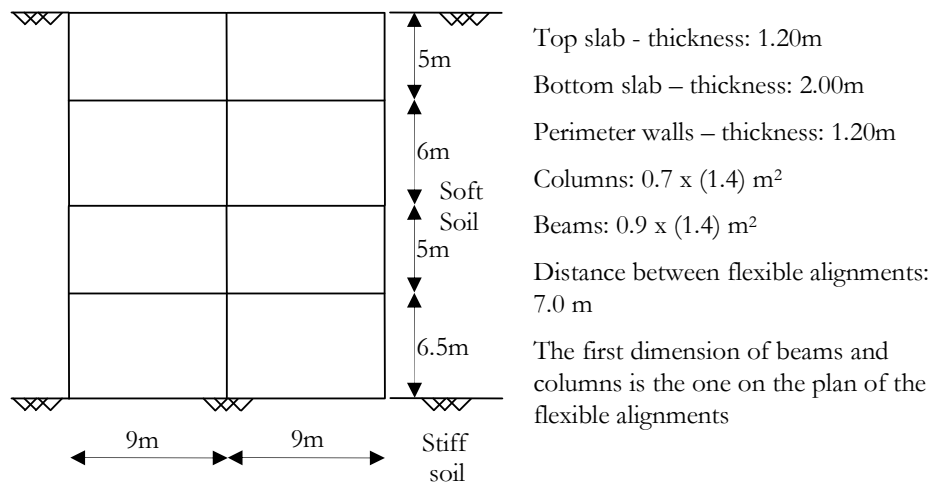


Figure 5.1. Example underground structure

The seismic action can be simulated by means of applying to the structure horizontal displacement fields with the profiles represented in figure 7.5. The profile shown in figure 7.5.a intends to represent the effect of a soil with increased stiffness with depth. The profile shown in figure 7.5.b consists of a sinusoidal variation of the displacements along the height, and corresponds to the first mode shape of a soil with constant stiffness along the height. However, it is not uncommon to find strong variations of soil stiffness along the height, for instances due to the existence of more than one soil layer. This can be simulated by a displacement profile as shown in figure 7.5.c, in which the deformations are concentrated at an intermediate soft soil layer. The examples shown next are based on the linear profile; the effects of the other profiles are discussed only qualitatively. The maximum distortion γ_{\max} is used as a measure of the deformation capacity of the structure.

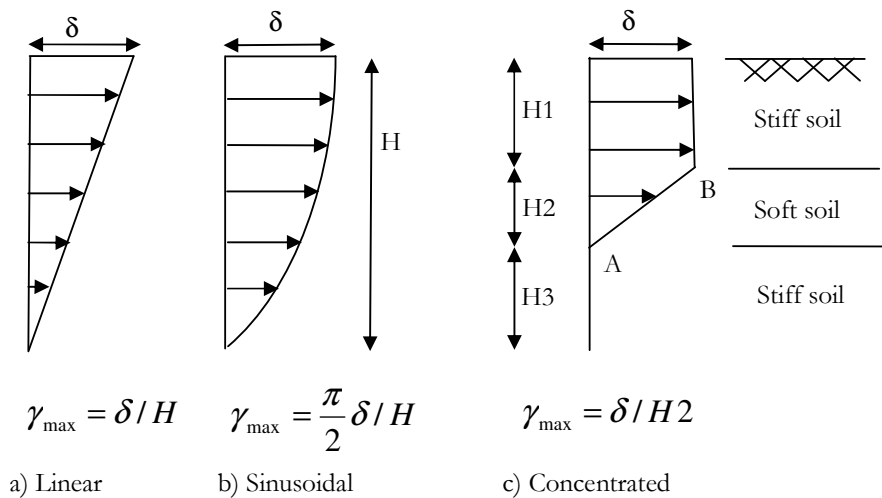


Figure 5.2. Horizontal displacement profiles

5.1 STRUCTURE DESIGNED ACCORDING TO CURRENT CODE CONCEPTS

Following current code procedures, seismic action-effects are obtained dividing the results of elastic analysis by a behaviour factor (q-factor in EC 8), a procedure that will be designated as Direct Design. Since EC8 does not cover this type of structures, an extrapolation of Part 1 will be made, as this is the most likely procedure designers will adopt. EC 8 – Part 1 (referred to as EC 8, from now onwards) considers three main Ductility Classes in seismic design: Low, Medium and High. Ductility Class Low structures are designed to resist earthquake effects essentially in the linear range and no

procedures are applied to increase ductility. EC 8 prescribes a q-factor of 1.5 for this type of structures to account for some levels of overstrength that is assumed is always available in reinforced concrete structures. Structures of Ductility Classes Medium and High are designed to resist earthquake actions by a combination of their resistance to inertia forces with their ductility and energy dissipation capacity. This represents an intermediate type of design between the one associated with Ductility Class Low and the proposed methodology. Therefore to highlight the differences to the proposed methodology the example structure is designed as a Low Ductility Class structure.

Since in the framework of Direct Design applied displacements result in internal action-effects on the structure (bending moments, shear and axial forces), the maximum displacement the structure can withstand is restricted by the maximum amounts of reinforcement that is possible to place in any structural member. Assuming $q=1.5$ and that the constant member stiffness assumed in the elastic analysis is half the stiffness of the gross concrete sections as prescribed in EC 8, the maximum allowable distortion associated with the linear profile of imposed displacements is $\gamma_{\max}=8.2 \times 10^{-3}$. The reinforcement corresponding to this distortion is shown in figure 7.6.

The explicit evaluation of the deformation capacity of this structure was evaluated by means of a static nonlinear analysis imposing the permanent loads and the linear displacement profile. It is assumed that proper detailing ensures the anchorage and effectiveness of all reinforcement, in particular confinement reinforcement after spalling of the concrete cover. The deformability of the nodes and shear deformations were disregarded, only flexural deformations were accounted for. The nonlinear behaviour of concrete and steel were simulated using the constitutive relationships for confined concrete prescribed in EC 8 – Part 2 and constitutive relationships for steel obtained from a large statistical characterization of the Tempcore steels used in Europe (Pipa, 1993). Figure 7.11 shows the constitutive relationship for steel and an example of constitutive relationships for confined concrete. Rupture was defined by the attainment of the maximum axial strain anywhere in the structure. The maximum allowable strain for steel is $\epsilon_{\max}=7.5\%$, corresponding to steel type C and for concrete it depends on the level of confinement, according to the equation prescribed in Annex C of EC 8 – Part 2.

The results of this analysis indicate that the maximum average distortion that the structure can withstand is $\gamma_{\max}=5.0 \times 10^{-3}$. Figure 7.7 shows the curvature diagrams at this situation, indicating the yield curvature at some sections and showing that flexural yielding took place at several locations. The maximum tensile strain is $\epsilon=27.8\%$, 13 times the steel yield strain ($\epsilon=2.07\%$). Note that at this stage the maximum distortion was 60% of the distortion evaluated according to EC8 (Low Ductility Class), at which the structure was supposed to be elastic. If the sinusoidal profile had been applied the

ductility demand would be higher at the lower part of the structure and it would withstand a lower relative displacement (δ) between the top and bottom slabs.

The above results show that the design with a low behaviour factor does not prevent yielding if the action is an imposed displacement field, contradicting widely held views and basic concepts of current code prescriptions for seismic design of structures that develop above ground. It also shows that extrapolating those procedures to underground structures can be unsafe, as lead to an overestimation of the structure deformation capacity.

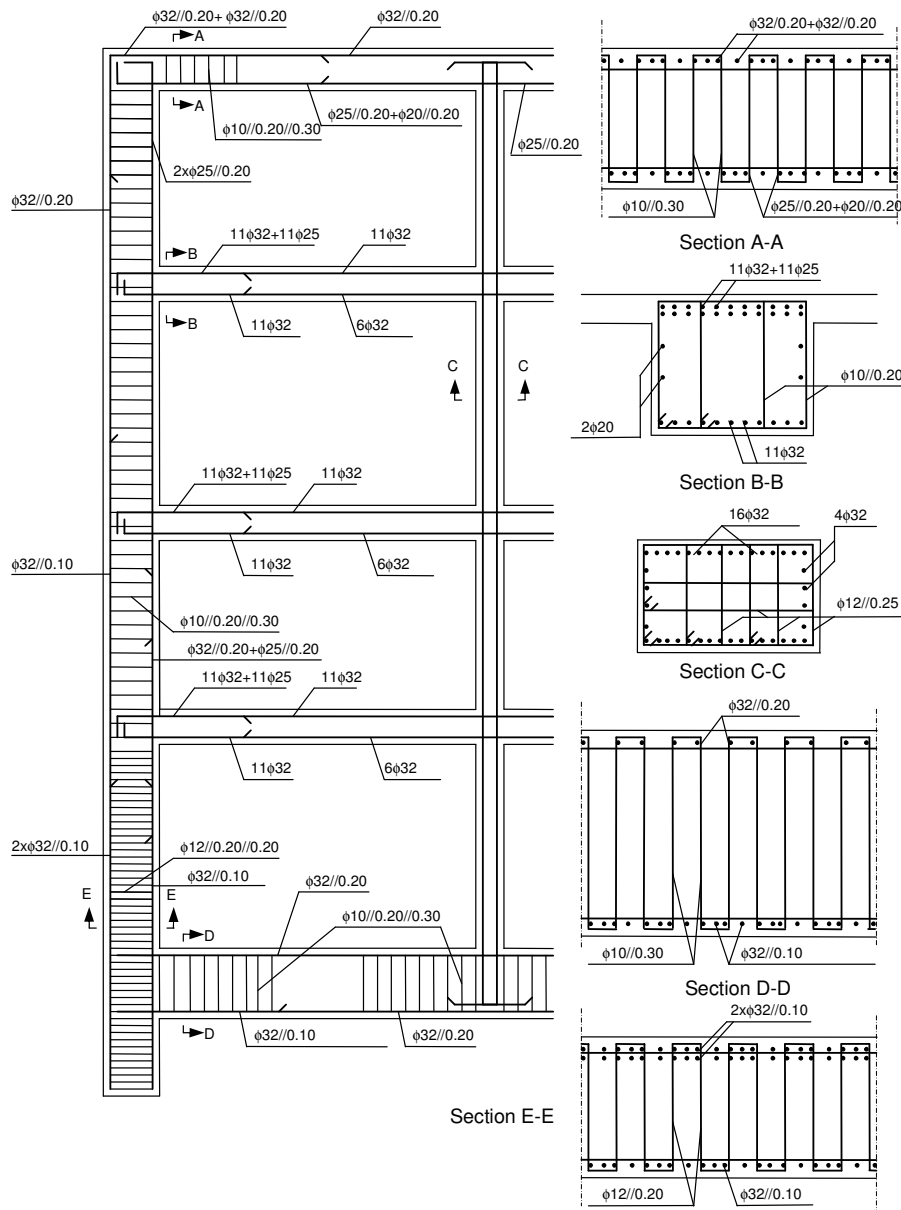


Figure 5.3. Reinforcement for maximum displacement according to Direct Design

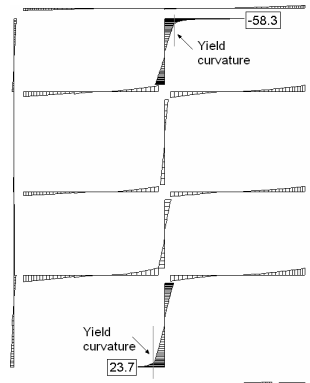


Figure 5.4. Curvature diagrams at maximum displacement – code design [/1000m]

5.2 STRUCTURE DESIGNED ACCORDING TO THE PROPOSED METHODOLOGY

In order to maximize the ductility of the structure, Capacity Design principles must be applied, as described in the next sections.

5.2.1 Choice of deformation mechanism

The number and location of plastic hinges involves in general the choice of a partial or global mechanism (structure with fewer connections than necessary to maintain equilibrium). In structures that develop above ground the mechanism can be chosen by the designer, but in an underground structure it must be compatible with the applied displacement profile. For the linear, sinusoidal or any other profile reasonably regular along the height (not the one shown in figure 7.6.c) two main global mechanisms can be foreseen, as shown in figure 7.8.

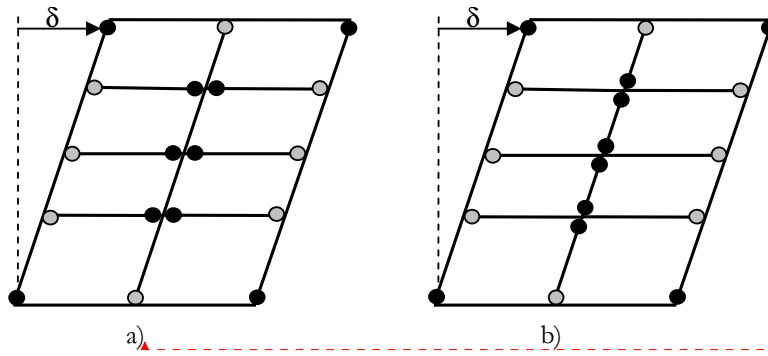


Figure 5.5. Example structure: global mechanisms

In what regards the choice of an appropriate mechanism it would be difficult to formulate standard recommendations for all cases. However some considerations can be made, as follows. In nodes where elements with very different dimensions in the plan of the flexible alignments join, it may not be possible to choose the element in which the plastic hinge will develop. That is the case where beams or columns join slabs or perimeter walls. In general it is very difficult to avoid that the hinges in the vicinity of this nodes develop in the beams or columns, as it is almost impossible to design these elements with more flexural capacity than the slabs or walls. This hinges are identified in figure 7.8 by the grey colour.

In wall-slab or beam-column connections the location of the hinges is in general a designer's choice. Some criteria to support these choices can be considered. The bottom slab is usually a very thick element with considerable flexural capacity. It is therefore easier that at the connection with perimeter walls the hinges develop at the walls. At the wall-top slab connections the dimensions of both elements usually are not too different and the designer may be able to choose where to develop the hinges, as of the point of view of performance (maximization of the global ductility) both options can be acceptable. Therefore two criteria can be used: easiness of construction and easiness of repair after a strong earthquake. The zone where the plastic hinge develops needs to be confined, what implies placing a large amount of reinforcement perpendicular to wall or slab faces to provide confining stresses in that direction. The horizontal reinforcement perpendicular to the thickness of the wall is probably easier to place than vertical reinforcement in the slabs. And since other plastic hinges develop in the perimeter walls (at the base and other locations, as will be shown later), the best options appears to be to locate the hinges in the walls. This allows maintaining the top slab elastic during strong earthquakes, avoiding the need to repair it afterwards.

Formatada: Português (Portugal)

A similar option about the location of the plastic hinges has to be done at the beam column joints. Note that the reasons why EC 8 prescribes the weak-beam/strong-column mechanism in building frames don't apply to underground structures: there is no need to avoid the soft storey mechanism since the deformation of the structure is conditioned by the surrounding soil and therefore large ductility demands and large second orders effects can not be triggered due to the soft-storey deformability. Another issue related with the choice of the hinges location at beam-column joints is the shape of the displacement profile imposed on the structure. If it is a profile similar to the one shown in figure 7.5.c, it is impossible to avoid hinging at intermediate levels of the vertical elements, as shown in figure 7.9. Note that even though in node 2 the designer can choose to locate the hinges in the beams or in the columns, in nodes 1 and 3 there is a variation of rotation between the columns converging on those nodes, which forces column hinging regardless of beam design.

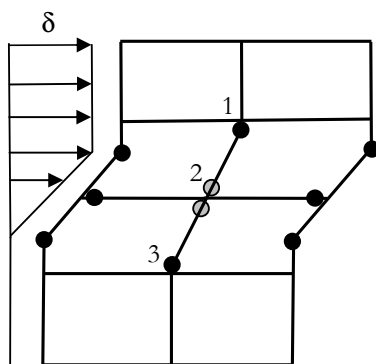


Figure 5.6. Mechanism with unavoidable hinges at intermediate locations of walls and columns

Since column hinging is unavoidable at the extremities and probably also at intermediate levels, it is the first option to consider and probably the most suitable. Another argument of practical nature in support of this option is that for the other actions the columns are essentially under axial compression, while the beams also have to withstand flexure and shear effects, leading in general to larger dimensions in the bending plan. However if the beams have similar dimensions to columns and larger aspect ratios it may be possible to provide more ductility to beams than to columns, leading to a larger deformation capacity for the structure. Another feature of behaviour highlighted in figure 7.9 is that unless the soil characteristics are very uniform in the entire vicinity of the structure yielding can take place anywhere in the perimeter walls. Therefore it may be necessary to provide confinement reinforcement throughout the perimeter walls.

Following the above discussion the example structure was designed to develop the mechanism shown in figure 7.8.b and the perimeter walls were confined at all locations in order that a reasonable curvature ductility is available at any location.

It is worth to emphasize that the different constraints to the choice of the best mechanism in underground structures as compared to building frames lead to criteria different from the ones prescribed in EC 8 for those structures.

5.2.2 Design of reinforcement

The starting point for this phase is the structure as designed to resist to all other actions but the seismic action. According to Capacity Design principles the zones chosen to remain elastic must be designed to do not yield during the development of the plastic hinges. This implies these zones must be provided with enough reserve strength for that purpose. The plastic hinge zones must be designed for ductility as well as to avoid any brittle type of failure. Considering the chosen mechanism the main implications for the different structural elements are as follows:

- perimeter walls: it is not necessary to increase the flexural capacity as hinges are expected to develop at the walls (remind that the proposed methodology is equivalent to consider $q=\infty$). It is necessary to increase the available ductility throughout the walls: for this purpose confinement reinforcement, comprising horizontal links in the direction of the wall thickness and properly anchored at the extremities around the vertical reinforcement must be provided. Figure 7.10 shows the new design of the wall cross sections.

- slabs: the design for the other actions ensures that slabs are stronger than the columns to which they are connected. However the flexural capacity may need to be increased, particularly in the extremities of the top slab, to be higher than the maximum moment at the walls hinges, in order to avoid the formation of plastic hinges at the slab extremities. For this purpose at the extremities the slab is designed for a bending moment which is $M_{Sd,slab}=\gamma_0.M_{Rd,wall}$, with both moments evaluated by the usual design procedure prescribed in EC 2. A value $\gamma_0=1.3$, as prescribed in EC 8 for column design, seems appropriate for the first iteration of the proposed design procedure. Figure 7.10 shows a longitudinal cut of the top slab.

- beams: in order to increase the ductility of the extreme sections where plastic hinges are expected to develop, confinement reinforcement must be provided at these zones. Flexural reinforcement on the lower face was also added in order to reduce the size of the compressive zone when the top reinforcement yields at beam extremities. The effectiveness of this extra reinforcement in increasing the curvature ductility can be easily

evaluated by section analysis. In what regards interior beam column joints it was decided to develop the plastic hinges in the columns. Therefore in the first iteration the flexural reinforcement on the beams in the vicinity of these nodes provide an excess flexural capacity above the sum of the moments of resistance of the columns converging at the same node of 30%, what also depends on column design. However the analysis showed this was not enough. Figure 7.10 shows the new design of the beams. The beams were provided with more transverse reinforcement at the zones plastic hinges are expected to develop to increase the ductility of confined concrete.

- columns: since the columns are essentially under axial compression for all other loads, can be designed for that purpose with the minimum amounts of flexural and transverse reinforcement. Since the columns are not intended to remain elastic there is no need to increase their flexural capacity ($q=\infty$). However flexural reinforcement may be useful to decrease the ductility demand because of the following reasons: (i) to increase column

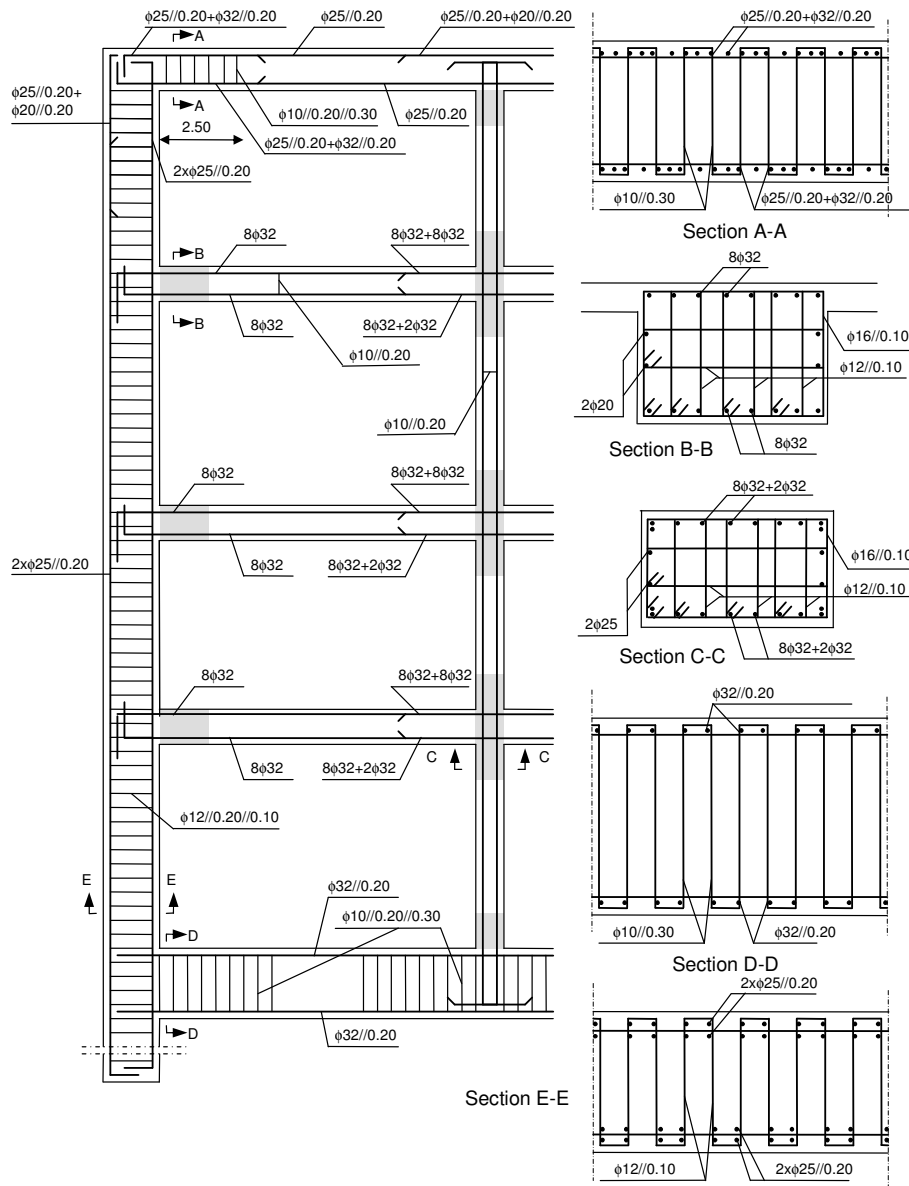


Figure 5.7. Details of design according to the proposed methodology

stiffness relatively to the beams, in order to reduce the restrictions that the beams impose to column rotations at beam-column joints, (ii) because large spacing of vertical reinforcement reduces the effectiveness of confinement, (iii) because the spacing of confinement reinforcement should be proportional to the diameter of the flexural reinforcement, therefore this should not be too small.

Besides there is the obvious need to provide confinement reinforcement in the plastic hinge zones to increase the available curvature ductility in those zones. The efficiency of the above can be evaluated by section analysis. Figure 7.11 shows the constitutive relationships for steel, confined and unconfined concrete and the moment curvature diagrams at the base of the columns before and after the increase in reinforcement, evaluated considering the axial force at maximum displacement.

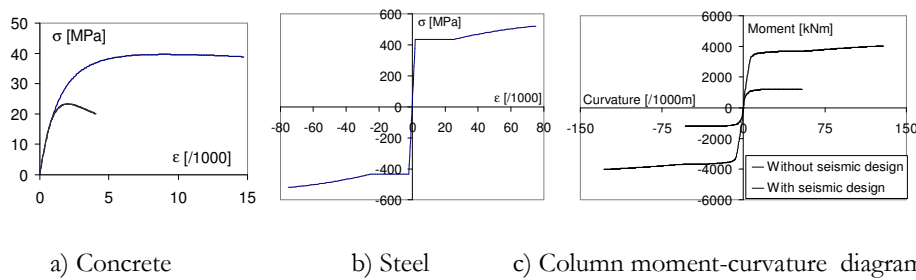


Figure 5.8. Material constitutive relationships and moment-curvature diagrams at the column base section

It should be emphasized that the process of maximizing the overall structural ductility is an iterative procedure, that starts from the structure as designed to resist to all other actions. Successive analysis and changes were done in order to improve the overall ductility. The following examples highlight this procedure: (i) at each analysis the rupture point and other locations close to rupture were identified and the possibility of increasing the available ductility at those locations was analysed; this was the case at beam extremities that initially were all designed with 6 vertical stirrups $\phi 12$, that the analysis showed were not enough to prevent rupture at the beams, limiting the overall ductility of the structure; in the final design, at the extremities the beams were designed with $6\phi 12+2\phi 16$ vertical stirrups; another change of this type was the use of external stirrups $\phi 16$ at the three lower column hinges; (ii) column flexural reinforcement was increased in order to increase its stiffness (according to the concept discussed in section 7.3 and illustrated in figure 7.3, the amount of flexural reinforcement influences the member stiffness) relatively to the beams, to reduce the ductility demand on the columns; note that the increase in column flexural reinforcement also led to an increase in beam flexural

reinforcement to avoid beam hinging but due to the curtailment of reinforcement, the stiffness of the beams increased less than the stiffness of the columns, in which there was no curtailment of flexural reinforcement; (iii) beam overstrength at beam-column joints was increased far above the initial value of $\gamma_0=1.3$, because the balance between beam moments on both sides of the nodes changed in the non-linear range increasing the moment demand.

The above is qualitatively different from current elastic analysis in which the designer knows the exact procedure that must be followed. The design for ductility leaves the designer with much more freedom but demands more knowledge and capacity to anticipate the potential seismic behaviour of the structure in order to decide at each iteration what are the most adequate changes to the design that resulted from the previous iteration.

5.2.3 Results

The non linear analysis of the structure designed according to the proposed methodology showed it could withstand a distortion of $\gamma_{\max}=14.6 \times 10^{-3}$, corresponding to an horizontal relative displacement between top and bottom of the structure of $\delta=32.9\text{cm}$. Figure 7.12 shows the curvature diagrams at this stage.

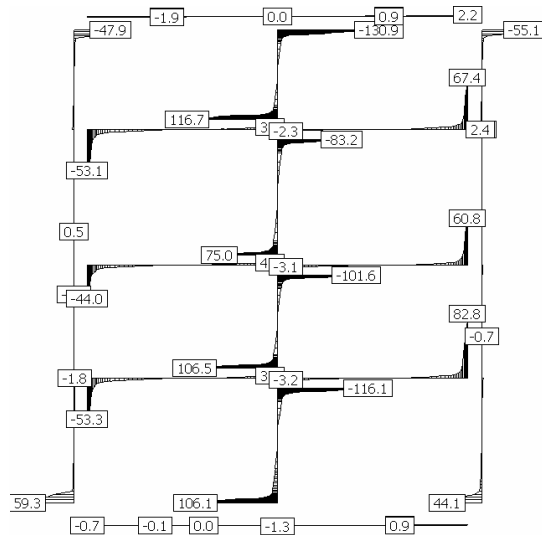


Figure 5.9. Curvatures at maximum displacement - proposed methodology [/ 1000m]

The comparison of this results with the ones of the structure designed according to current code concepts $\gamma_{\max}=5.0 \times 10^{-3}$ shows the superior seismic performance of the structure designed according to the proposed methodology. The comparison between the curvatures at maximum displacement for both structures (figures 7.7 and 7.12) highlights the reasons for this difference: the higher ductility of the structural elements and the efficient exploration of that ductility throughout the structure designed according to the proposed methodology. A full comparison of costs can not be done as the structure was not fully defined, neither was the constructive process. However, in terms of materials most of the difference regards the amount of steel in the perimeter walls. The proposed methodology leads to the use of less flexural reinforcement, but needs large amounts of confinement reinforcement, leading to almost equal total amounts of steel spent in the perimeter walls. In the slabs the proposed methodology leads to moderate savings, as the flexural reinforcement is conditioned essentially by the minimum levels prescribed in EC2. In beams and columns the general trend is similar to that observed in the perimeter walls, with some savings for the design of the columns according to the proposed methodology. The above indicates that in general the design according to the proposed methodology does not has a significant influence on the overall costs, and may even lead to slight savings in some elements.

6. SUMMARY AND CONCLUSIONS

During earthquakes underground structures do not have to resist to horizontal inertia forces, as structures that develop essentially above ground, but only to withstand the displacements the soil imposes on them without losing the capacity to resist to permanent actions. Therefore reinforced concrete structures must be designed to be flexible and ductile. For instances large underground reinforced concrete structures, such as tube stations, should be designed in the transverse direction with elements whose dimensions must be the ones strictly necessary to resist to other actions but the seismic actions. Stiff elements, such as counterforts or short beams should be avoided, as well as large soil covers. The interference of secondary or non-structural elements with the deformation of the main structure should be avoided.

The structure must be designed by stages: first for all load combinations whose main variable action is not the seismic action; second for the seismic action. Since there are no inertia forces (equivalent to consider the behaviour factor infinite) the designer must choose a suitable deformation mechanism and apply Capacity Design principles, this is, to design the potential plastic hinge zones for ductility and the remaining zones with excess strength to remain elastic. An application example is shown. The proposed procedure tends to lead to considerable savings in flexural reinforcement but more confinement reinforcement. In general terms it leads to structures with better seismic performance than the extrapolation of of code procedures derived for structures that develop above ground, that may lead to unsafe underground structures. Therefore it is recommended that EC8 covers explicitly the seismic design of underground structures.

REFERENCES

- CEB [1983] Bulletin 161 “Response of reinforced concrete critical regions under large amplitude reversed actions”, Lausanne, Switzerland
- EC 2 [2004] Design of concrete structures- Part 1-1: General rules and rules for buildings, EN 1992-1-1, Brussels
- EC 8 [2005] Design of structures for earthquake resistance – Part 1: General rules, seismic action and rules for buildings, EN 1998-1, Brussels
- EC 8 [2005] Design of structures for earthquake resistance – Part 2: Bridges, EN 1998-2, Brussels
- EC 8 [2004] Design of structures for earthquake resistance – Part 5: Foundations retaining structures and geotechnical aspects, EN 1998-5, Brussels
- Gomes, R.C. [1999] “Behaviour of underground structures under seismic actions” MSc thesis, IST, Lisbon, Portugal
- Hashash, Y.M.A., Hook, J.J., Schmidt, B. [2000] “Seismic design and analysis of underground structures” A state-of-the-art Report sponsored by the International Tunneling association, Working Group N°2
- Ishibashi, I. & Zhang, X. [1993] Unified dynamic shear moduli and damping ratios of sand and clay. *Soils and Foundations*, *JSSMFE*, vol. 33, n.1: 182-191.
- Iwatate, T., Kobayashi, Y., Kusu, H., Rin, K., [2000] “Investigation and shaking table tests of subway structures of the Hyogoken-Nanbu earthquake” *12th World Conference Earthquake Engineering*, paper 1043, New Zeleand.
- Pipa, [1993], “Ductility of reinforced concrete elements under cyclic actions. Influence of the reinforcement mechanical characteristics” (in Portuguese), PhD thesis, IST, Lisbon.